# NON-LINEAR ADAPTIVE CONTROL OF SQUIRREL CAGE INDUCTION MACHINES USED IN WIND ENERGY CONVERSION SYSTEMS

A thesis submitted to the Division of Graduate Studies of the Royal Military College of Canada by

Zhan Shi, PEng, Lieutenant-Navy

In Partial Fulfillment of the Requirements for Masters degree of Electrical Engineering

June 11, 2017

# Contents

# List of Figures

# List of Tables

# List of Nomenclature

TABLE 1: List of Nomenclature

| | |
|---|---|
| $R_s$ | stator winding resistance |
| $R_r$ | rotor winding resistance |
| $L_{ls}$ | stator leakage inductance |
| $L_{lr}$ | rotor leakage inductance |
| $L_m$ | magnetizing inductance |
| $J$ | moment of inertia |
| $\theta$ | orientation angle |
| $\theta_r$ | rotor orientation angle |
| $\theta_{sl}$ | slip angle |
| $\lambda_{qs}$ | stator $q$ flux |
| $\lambda_{ds}$ | stator $d$ flux |
| $\lambda_{qr}$ | rotor $q$ flux |
| $\lambda_{dr}$ | rotor $d$ flux |
| $I_{qs}$ | stator $q$ current |
| $I_{ds}$ | stator $d$ current |
| $I_{qr}$ | rotor $q$ current |
| $I_{dr}$ | rotor $d$ current |
| $\omega_r$ | rotor electrical speed |
| $\omega_s$ | stator flux speed |
| $\omega_{sl}$ | slip speed |
| $V_{ds}$ | $d$ input voltage |
| $V_{qs}$ | $q$ input voltage |
| $a$ | system parameter |
| $\hat{a}$ | estimated system parameter |
| $\tilde{a}$ | parameter error |
| $u$, $v$, $z$ | new coordinate systems |
| $A$ | system matrix |
| $B$ | input matrix |
| $A_s$ | linearized system matrix |
| $K$ | feedback gain |
| $V$ | Lyapunov's canadidate function |
| $X_r$ | rotor reactance |
| $X_s$ | stator reactance |
| $X_m$ | magnetizing reactance |
| $X_{ls}$ | stator reactance |
| $P_m$ | mechanical power |
| $\omega_m$ | mechanical speed |
| $T_m$ | mechanical torque |
| $\eta$ | augmented error |
| $e$ | error augmentation |
| $z$ | adaptive gain |

# List of Abbreviations

TABLE 2: Abbreviations and Acronyms

| | |
|---|---|
| SCIG | squirrel cage induction generator |
| PMSG | permanent magnet synchronous generator |
| DFIG | doubly fed induction generator |
| PID | proportional integral derivative |
| PI | proportional integral |
| WECS | wind energy conversion systems |
| FOC | field oriented control |
| DTC | direct torque control |
| BESS | battery energy storage system |
| PWM | pulse width modulation |
| MPPT | maximum power point tracking |
| MPE | maximum power extraction |
| LM | loss minimization |
| DFOC | direct field oriented control |
| IFOC | indirect field oriented control |
| MRAC | model reference adaptive control |
| WFNN | wavelet fuzzy neural network |

# Abstract

Electric machines are used for the conversion of energy in most industrial, commercial and residential applications. They are essential elements in wind turbines that convert the mechanical energy of the wind into electrical energy. The squirrel cage induction machine is used in wind turbines because of its numerous advantages. It is robust, simple in design and affordable compared to other alternatives such as doubly-fed induction machines and permanent magnet synchronous generators.

An adequate control system is necessary for wind turbines to extract the maximum wind energy and to adapt electric power to the load. Various industrial control systems are used for wind turbines that use the induction machine. This includes the field oriented control method that uses PI controllers and the direct torque control method which uses hysteresis controllers.

The main drawback of conventional control systems for wind power generators is the deterioration of transient and steady state performances with the change of operating conditions. Due to the unpredictable nature of wind speed, such vast changes in operating points are inevitable. The stabilization time for the control system can be long. The steady state errors are not always zero. The deterioration of performance is due to several simplifying assumptions while designing the controller. One assumption is the local linearization of the nonlinear structure of the induction machine and the uncertainty of the machine parameters with the change in operating points.

This thesis proposes a non-linear adaptive control algorithm for a wind turbine energy conversion system that uses an induction machine. The structure and equations of the control system will be obtained from the nonlinear model of the machine. The state feedback linearization method will be used for the design. An adaptation module will be included to ensure that the system stability is sensitive of parameter variation.

The control system will be tested in simulation using Simulink Power systems Toolbox in Matlab. Different wind conditions will be considered to validate the system performance.

# Résumé

Les machines électriques sont utilisées pour la conversion d'énergie dans la plupart des applications industrielles, commerciales et résidentielles. Ce sont des éléments essentiels dans les éoliennes qui transforment l'énergie mécanique du vent en énergie électrique. La machine à induction de cage d'écureuil est utilisée dans les éoliennes en raison de ses nombreux avantages. Il est robuste, de conception simple et abordable par rapport à d'autres solutions de rechange, telles que les machines à induction doublement alimentées et les générateurs synchrones à aimants permanents.

Un système de contrôle adéquat est nécessaire pour que les éoliennes puissent extraire l'énergie éolienne maximale et adapter l'alimentation électrique à la charge. Divers systèmes de contrôle industriels sont utilisés pour les éoliennes qui utilisent la machine à induction. Cela inclut la méthode du flux orienté qui utilise les contrôleurs PI et la méthode de contrôle direct du couple qui utilise des contrôleurs d'hystérésis. Le principal inconvénient des systèmes de contrôle conventionnels pour les générateurs d'énergie éolienne est la détérioration des performances transitoire et en régime permanent avec le changement de conditions de fonctionnement. En raison de la nature imprévisible de la vitesse du vent, de tels changements importants dans les conditions de fonctionnement sont inévitables. Le temps de stabilisation pour le système de contrôle peut être long. Les erreurs en régime permanent ne sont pas toujours nulles. La détérioration de la performance est due à plusieurs hypothèses simplifiées lors de la conception du contrôleur. Une hypothèse est la linéarisation locale de la structure non linéaire de la machine à induction et l'incertitude des paramètres de la machine avec la variation des points d'opération.

Cette thèse propose un algorithme de contrôle adaptatif non linéaire pour un système de conversion d'énergie éolienne utilisant une machine à induction. La structure et les équations du système de contrôle seront obtenues à partir du modèle non linéaire de la machine. La méthode de linéarisation par retour d'état sera utilisée pour la conception. Un module d'adaptation sera inclus afin de s'assurer que la stabilité du système est sensible aux variations de paramètres. Le système de contrôle sera testé en simulation à l'aide du logiciel de simulation SimPowerSystems de Matlab. Différentes conditions de vent seront considérées pour valider les performances du système.

# Chapter 1

# Introduction

With the increase in environmental concerns, more resources has been dedicated to utilization of renewable energy sources. The technology to harness wind energy as a renewable energy source to generate electricity has developed very rapidly in recent years. Given the finite nature of fossil fuel and the difficulties with offshore oil extraction, renewable energy sources like wind energy is the way of the future. Many viable wind energy generating units are already available in the industry. Various configurations and topology of wind energy systems are available.

Although wind energy is a clean, abundant, and renewable energy source, it is random and unpredictable. Due to the unpredictability of wind velocity, current technology have only scratched the surface in maximizing the efficiency in achieving the full potential of energy conversion and delivering it to end users. [2] [5].

This evolution of maximizing the efficiency of wind energy systems can be seen in the transition of variable speed wind turbine generators from fixed speed wind turbine systems. In the past five years, there has been huge improvements in variable speed wind turbine systems in terms of efficiency in energy conversion. As a result, more innovative and sophisticated development in control techniques have been realized. Less components are required, greater energy is extracted and less cost overall in production and maintenance of components.

Variable speed wind systems are not only able to deliver from 20 to 30 percent more energy than constant power systems, they also reduce the stress imposed on the transmission system of the plant [6]. Many different types of machines can be used for power generation. So far three main types of generators have proven to be the most viable options to be used

for this purpose namely doubly-fed induction generators (DFIG), permanent magnet synchronous generators (PMSG), and squirrel cage induction generators (SCIG). There are several advantages and disadvantages to each type of generator. [5]

DFIG requires only $30\%$ of the rated power. This means that the desired variable-speed range is $\pm 30\%$ around the rated turbine speed. However the DFIG must utilize slip-rings, brush and gear box. Given the additional components in DFIG, the failure rate and maintenance cost dramatically increases. This impacts on the system stability [6]. In the case of the PMSG, the rotor uses a permanent magnet without external excitation. The system model is greatly simplified. The generation system can be directly coupled to the wind turbine without additional transmission system. The noise during operation is greatly reduced, reliability and efficiency is improved [6]. The downside of PMSG is the increase production cost of the generator due to the cost of permanent magnet material [7].

The third most popular option is the SCIG. The SCIG is much more robust than both the DFIG and PMSG. SCIG does not utilize brushes and slip rings, it has stable performance and rugged in structure. It has lower cost in production and maintenance, and operates at full speed range. The disadvantage of SCIG is that the system has a non-linear structure which makes the designing of the controller more difficult. Furthermore, given that SCIG operates at full speed range, this large variation in operating points can increase the uncertainty in system parameters. This poses additional challenges for the design of a controller.

# Chapter 2

# Related Work

There has been much research and experiments done to improve the performance of wind energy systems in the past ten years. It is agreed upon by most main stream power electronic experts working in this area that the most optimal configuration for Wind Energy Conversion Systems (WECS) involves a wind turbine, generator (Permanent Magnet Synchronous Generator PMSG, Double Fed Inducton Generator DFIG or Squirrel Cage Induction Generator SCIG) and back-to-back converters supplying to the grid.

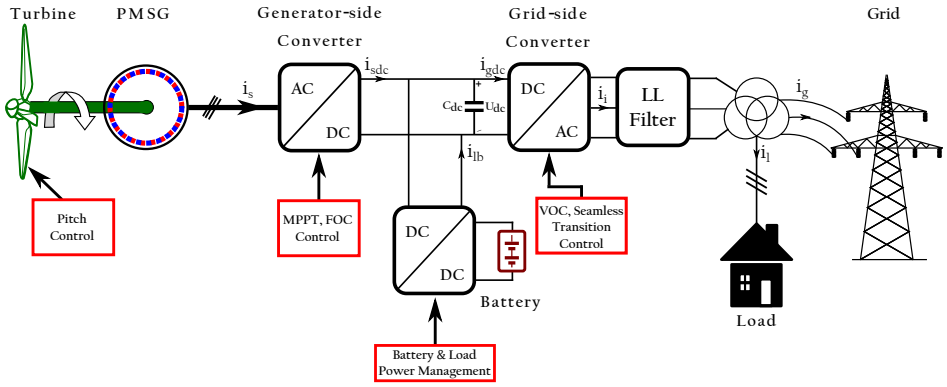


FIGURE 2.1: generic wind energy system [1]

Given the major components of the system, many improvements has been done to each major component in order to improve the system as a whole. It is important that any new method to improve the system efficiency will be weighed in light of maximum benefit with the minimum cost. The method proposed in this thesis will improve the performance of the wind energy system by implementing a new control algorithm. The algorithm can be installed in existing off-the-shelf systems without any alteration in hardware.

Many configurations of WECS exist, this ranges from the type of generator, the controller and the type of power electronics that are used. The most common generators used in the industry are SCIG, DFIG and PMSG. Each generator has its advantages and disadvantages. The most popular controllers used in industry has been Field Oriented Control (FOC) and Direct Torque Control (DTC). Both FOC and DTC are fairly developed methods. In the following section, the advantages of different types of generator and control methods will be discussed.

This section can be divided into the following subsections:

1. Comparison of the different types of generators used in WECS. The advantages and disadvantages of each generator will be discussed and why the SCIG will be used as the generator to develop the control algorithm in this thesis.

2. The more traditional types of controllers (ie, DTC, FOC etc.) used for WECS will be analysed. The strength and limitations of these generators will be discussed.

3. Nonlinear control algorithms will be discussed (ie, input-output linearization, backstepping, etc.). In addition how these newer control algorithms will improve upon the limitations of traditional controllers.

4. Adaptive control algorithm will be discussed. The adaptive control will attempt to solve the problem of uncertainty of system parameters which causes deterioration in terms of performance for nonlinear control algorithms and traditional controllers (DTC and FOC) on their own addresses.

The flow of this sections will be the discussion of choice of generator to be used for the modelling of the control algorithm. Which will be followed by the strength and limitations of traditional controllers such as DTC and FOC. Once the limitations of the traditional controllers are identified, newer nonlinear control algorithms such as input-output linearization are discussed. The improvements of the nonlinear controllers and how they improve upon the traditional controllers will be analysed in detail. The last section of this chapter will be the analysis of adaptive control algorithm and how they address the problem of uncertainty of system parameters.

## 2.1 Generator Types

There are three main types of generators commonly used in WECS; DFIG, SCIG and PWSG. Through out the development of wind energy conversion technology, fixed speed WECS were the first topologies used in the early to the late 90's. SCIG were the generators of choice for fix speed systems. There were many short comings with fix speed systems. They were less than 1kw and cannot operate in the full range of wind speeds [8]. Currently almost all WECS are variable speed systems. The advantage of variable speed system is that it can operate over a wide range of speeds thus extracting the maximum energy from the wind. Given the variable speed systems, generators like DFIG and PMSG are used because they are easy to control. However, with the advancement of more sophisticated control systems, SCIG is starting to make a resurgence for wind energy systems applications.

#### Doubly Fed Induction Generators

Currently DFIG are the most common used generators in the wind industry. The most common configuration is to have the stator terminals of the generator connected directly to the grid and the rotor connected to converters. A transmission gearbox is necessary to compensate for the vast difference in speed ranges between the wind turbine and the generator [8]. The converters used are usually of the variable frequency back-to-back AC/DC/AC voltage source. The converter set up usually consists of two insulated-gate bipolar transistor (IGBT) converters. One for the rotor side and one for the grid side. The two converters are connected via a DC link. The purpose of the converters is to decouple the grid frienquency and the mechanical rotor frequency which in turn allows for variable speed operation [9].

Advantages of DFIG

- Mechanically and electrically simpler than other generator types. This simplicity also enables less complicated control drives [8]
- Converter rating is only 25%-30% of the generator [8]
- Has a wide range of operating speeds, up to 30% of synchronous speed
- Converters connecting to the rotor compensates the reactive power and ensures smooth grid integration

- High efficiency and energy yield [8]

Disadvantages of DFIG

- Gearboxes are still a necessity due to the large different between the turbine and generator, since a multiple pole DFIG with low speed is not yet technically available
- The necessity of gearboxes results in mediocre reliability and reduced longevity due to bearings and gear faults [8]

**Squirrel Cage Induction Generator**

Traditionally SCIG are used in fix speed WECS. It operates in very limited ranges of wind speeds through a gearbox transmission system. The only speed variations are a result of the rotor slip [8] [10]. The construction of SCIG is very robust and low in maintenance cost, only maintenance is the bearings and lubrication. The rotor is constructed from metallic bars which are very resistant to vibration and dirt. Some SCIG are used in variable speed WECS in conjunction with full-scale power electronic converters to take advantage of the robust and low cost aspect of SCIG [8]. To extract more power from the wind, pitch angle regulation is traditionally used. Recently more sophisticated controllers have been investigated in order to enable higher efficiency of SCIG in variable speed systems.

Advantages of SCIG

- Simplicity and robust in construction
- Rotor bars are very resistant to vibration and dirt
- Fully decoupled from the grid for variable speed applications [8]
- SCIG WECS is able to avoid short circuit power from the grid, the control system limits any fault current from the grid side converter going into the system [8]

disadvantages of SCIG

- Two full scale converters are required for operation

**Permanent Magnet Synchronous Generator**

Previously the advantages and disadvantages of SCIG and DFIG have been discussed. For DFIG and SCIG, the turbines spins at much lower speeds than the operation speed of the generator, high speed multi-stage gearboxes are necessary for operation. The unique feature of a WECS based on PMSG is that it is direct-driven. It does not require a gearbox for operation. Multi-stage gearboxes have been proven to be less reliable than manufacture rating , as a result requires replacement from 5 to 7 years in operation [8].

Advantages of PMSG

- Lower maintenance cost due to absence of gearbox
- Improved reliability due to absence of gearbox, ie, maintenance of gears and bearings which causes most of faults
- Lower weight
- High efficiency and energy conversion

disadvantages of PMSG

- Much higher cost than DFIG and SCIG, material required for the permanent magnet is very costly
- Greater size, the outer diameter of PMSG is much larger than gear-driven SCIG
- Newer technology, lower maturity in development
- Increased mass and weight can reach critical proportions especially for WT above 3MW [8]

**Generator Comparison**

Many comparisons of the three generators have been done in research [8]. Some have done comparisons regarding the variable speed and fixed speed systems. Others compared fixed speed SCIG with direct drive PMSG systems [8]. Research shows that each generator excels in specific applications than others. Given the market penetration of each type of generator, it is reasonable to assume that future trends in the wind energy industry will continue to develop and improve upon the more established

technologies, ie, PSMG, SCIG and DFIG.

It is worth mentioning some obvious differences between the three generators. The outer diameter of the PMSG is almost twice that of the geared-driven SCIG; however the length of the PMSG is much shorter than SCIG. Considering the total dimension of the two generator systems and given the fact that most SCIG and DFIG will require multi-stage geared transmission systems [8], the overall weight of both WT may have no big difference [8]. In addition, the PMSG system has on average 1.6% higher efficiency than fix speed SCIG systems at 3 MW rated power. Given that the PMSG is variable speed operation, it can produce more than 10-15% enery than fixed-single speed systems [8].

Considering the market penetration, most turbine systems in industry leans towards DFIG and SCIG with multi-stage gearbox. The most popular generator in operation is still DFIG and SCIG. However, SCIG have decreases in use over the last decade and have been taken over by variable speed systems like DFIG. The direct drive systems involving PMSG have been steadily increasing in the market. It's been shown without a doubt that the direction of research in WECS is focused towards variable speed systems due to reduced mechanical stress and increased power conversion [8]. The utilization of multi-stage gear driven DFIG with IGBT is sill the most dominant configuration in current market. The main advantage of DFIG is that only 30% of the generator power goes to the power converters which will have substantial cost advantages even with the decrease in cost of converters and power electronics [8].

Given all the advantages of DFIG, it however suffers from large peak currents during grid related faults [8]. Variable speed SCIG with full-scale power converters are completely detached from the grid is not susceptible to the same problems as DFIG [8]. The development of more sophisticated control systems may give rise to a resurgence of variable speed SCIG systems and become more attractive option in the future. When selecting purely based on overall efficiency, reliability and availability, the direct-driven PMSG systems out performs the other two systems because of the absence of the gearbox [8]; this is crucial for offshore wind energy applications when land and space hindrance is not an issue, and replacement of components are less viable. However when size and cost are considered PMSG is not the best option [8].

Given all the considerations it seems that both DFIG and PMSG have

the best performance [8]. However, SCIG has the most potential for improvement. The only reason DFIG and PMSG outperforms SCIG is that SCIG can only operate in limited speeds, which decreases its ability to efficiently extract wind energy in a wide operating range [8]. This limitation is mostly due the controller used to control the generator. Huge improvements have been done to improve the efficiency of SCIG operation in wider wind-speed operations. Controllers such as FOC and DTC have shown great improvements in power generation efficiency [8]. Both FOC and DTC still have many limitations due to the complexed nonlinear structure of SCIG and parameter variation during operation; which as a result causes deterioration of the total system performance [8]. Therefore, a controller which addresses the nonlineariarities of the SCIG and the uncertainty of system parameters can potentially have huge impacts in bringing back the SCIG given its many other advantages.

## 2.2 Direct Torque Control

Direct Torque Control (DTC) was originally developed to control high performance motors that required precision in torque and speed with fast response in dynamic conditions. DTC can easily be adjusted for generators. During this section of the literature review, the basic principle will be discussed along with some of its applications and followed with a criticism of its limitations. The idea of DTC is that by keeping the stator flux $\lambda_s$ constant while the rotor flux $\lambda_r$ is almost constant over a large operating range, one can control the torque by controlling the angle ($\theta_t$) between the two flux vectors [2].

The stator flux vector $\vec{\lambda}_s$ is a function of the stator voltage $\vec{v}_s$. The stator voltage $\vec{v}_s$ can be controlled by modulation through a PWM rectifer. If the correct stator voltage $\vec{v}_s$ is modulated, the desired stator flux vector $\vec{\lambda}_s$ is created as a result. By controlling the stator flux vector one can control the orientation angle between the stator flux vector and the rotor flux vector, thus controlling the torque.

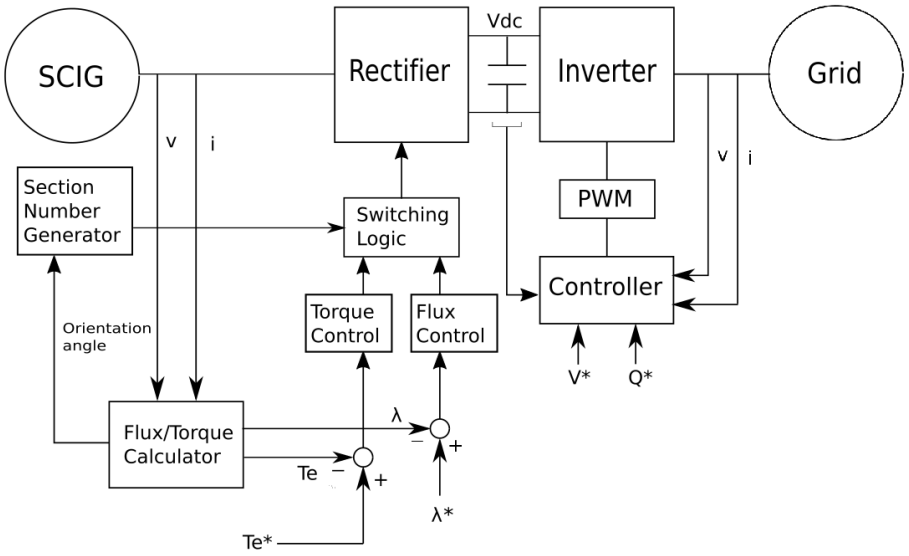


FIGURE 2.2: DTC block diagram

Shown in figure 2.2 is a generic block diagram of DTC. The reference torque $T_e^*$ is generated from Maximum Power Point Tracking (MPPT). The MPPT scheme is a way to determine the optimal generator reference

to extract the most energy for a specific wind speed, MPPT will be discussed in detail in later sections. $T_e^*$ is compared with the actual electromagnetic torque $T_e$ calculated by the Flux/Torque calculator, the error signal is passed to the torque hysteresis controller. The reference stator flux $\lambda_s^*$ is compared with the stator flux calculated by the Flux/Torque calculator, the resultant error is passed to the flux hysteresis controller. The output from the torque hysteresis controller and the flux hysteresis controller will cause the switching logic component to produce the appropriate voltage reference vectors ($\vec{v}_s^*$) to the rectifier, the rectifier then produces the required stator voltage.

The inherent assumption in using predetermined look up table to produce an output to correct a system is that the designer knows the system parameters and they are constant in operations. The design of DTC are based on known models where the parameters are identified in order to derive the look up tables. If the system parameters are uncertain or varying with time, there is no guarantee that DTC will stabilize the system.

A paper published in 2015 proposed a configuration for WECS [11], the system was to optimize the efficiency of power generation during dynamic wind conditions. The system consists of SCIG with battery energy storage system (BESS). The controller used for the generator side is direct torque control (DTC) controller, operating with maximum power point tracking algorithm (MPPT) to maximize wind energy conversion. The generator is connected to the grid via back-to-back converters. The addition to this generic set up is a BESS to ensure that DC voltage of the DC bus stays constant during variation of wind speed. The active and reactive power of the grid side converter is controlled by a voltage oriented controller [11].

The DTC controller utilized in [11] calculates the flux and the torque of the generator using the stator currents and voltages. The calculated torque and flux is compared to the reference torque and reference flux. The reference torque is derived from MPPT scheme, which calculates the optimum torque for a given wind speed to extract the maximum amount of power from the wind. The reference flux is kept at a constant rated flux. The error signals of both the torque and the flux is then fed as inputs to two hysteresis comparators. The hysteresis can produced several outputs depending on where the error signal lies on the hysteresis band. The outputs of the hysteresis comparators will trigger an action based on prearranged look up tables. The look up tables contains the voltage vectors

that is to be modulated by the PWM converter to produce the necessary voltage to drive the torque and the flux of the generator to match the reference values.

The BESS is a very useful addition to the system, it has the advantage of supplying to the grid when wind turbine generator is not generating enough power, and being charged when the wind turbine generator is generating surplus power. Having the capacity to store power in batteries improves the stability of power generation, allowing for the control of power grid voltage and frequency, and provide compensation of active and reactive power to the power grid [11]. The battery is connected to the DC bus via DC-DC (buck/boost) converters, the converter is controlled by two switches. The error between the DC voltage and the reference DC voltage is the input to a PI controller. The output of the PI controller becomes the reference value for DC current, which is then compared to the actual current, the resultant error becomes the input for a second PI controller. The output of the second PI controller will determine the switching sequence which will regulate the DC voltage [11].

The proposed topology was implemented in a simulation. The simulation was conducted based on a MPPT scheme. The MPPT scheme determines the optimal rotor speed of the generator required at specific wind speeds in order to extract the maximum power from the wind. This speed is used as the reference speed that the generator will attempt to track. The range of wind speed that was simulated ranged from $2m/s$ to $12m/s$. The results shows that the controller tracks the reference trajectory quite well, for step increases of $150rad/s$ rotor speed it took the generator $0.3s$ to converge to steady-state [11]. In reality changes in wind condition will be a gradual change, so a step change is a much aggressive change in reference value which means that the tracking capability in reality will have much better performance than in simulation.

Given the simulation results, the proposed system topology is a huge improvement from fixed-speed WES. However there are few issues that has still yet being addressed. One being that the performance was assessed by simulation only, the designer of the system has no explicit knowledge of how the individual components of the system effect each other. The second issue being that when PI controllers are used, the tuning of the gains used in PI controllers are mostly done by trial error, this is due to the limited knowledge of the behavior of a non-linear system. The problem of the trial and error method is that it is by nature empirical,

even though the system is tested with mass samples of operating conditions, one can never guarantee that the system will always be stable under all conditions. Furthermore, PI controllers are used for linear systems and the system parameters are assumed to be constants with respect to time. This is not true in reality. Parameters such as resistance, inductance vary depending on temperature, frequency and saturation. PI controllers are highly sensitive to parameter variation, which further increases the chance for system instability.

To summarize the fundamental principle of DTC, the reference torque and flux are establish by MPPT and operating specifications. Once the reference torque and flux values are known, they are compared with the actual torque and flux of the generator. The error between the actual values torque and flux and the reference torque and flux becomes the input to the controller. The hysteresis controllers act as a limiter to determine if the input error signals fall between a given range. When the input error signal falls outside of that range, a set of predetermined outputs are produced. The outputs in this case are the voltage vectors which will produce the new torque and flux which is closer to the reference torque and flux.

## 2.3 Field Oriented Control

Another popular controller used for SCIG in WECS applications is field oriented control (FOC). Along with DTC, FOC is the most developed and commercially available controller on the market. FOC is based on the use of PID controllers to control the flux and the torque of a generator. FOC is different from DTC in that it decouples the flux and the torque components through the use of field orientation. In this subsection of the literature review, the fundamental principle of field oriented control will be discussed along with some of its applications in recent research papers followed by critiques of its limitations.

The difficulty in older control methods for SCIG such as scalar control is that the torque of SCIG is expressed as a function of the flux; the two variables are thus coupled. Its difficult to independently controlling the torque or flux accurately because they are coupled. The fundamental principle behind FOC is the decoupling of the torque and flux components of the generator. The decoupling is done using field orientation. The coordinate system transformation converts a three phase system to a two phase system (figure 2.3). The $dq$ transformation is crucial in decoupling the relationship between flux and torque. Once the coordinate system is in $dq$, the $d$ components controls the flux, the $q$ component controls the torque. The $dq$ coordinate system appears same as DC machines where the flux and torque can be controlled independently. $dq$ transformation is used in both FOC and other nonlinear control algorithms which will be discussed in later sections.

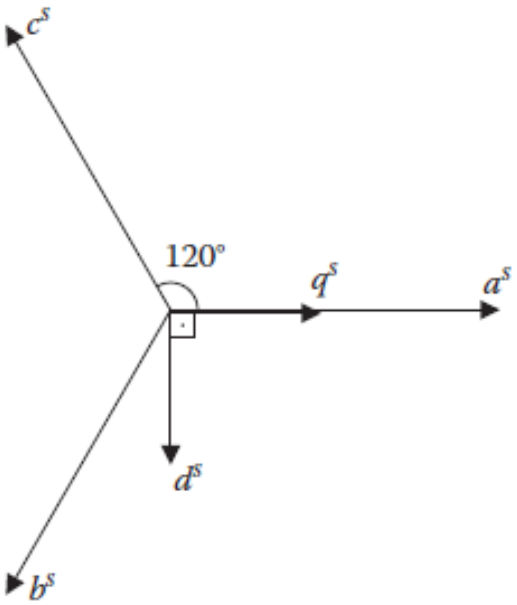


FIGURE 2.3: abc to dq coordinate transformation [2]

The three phase system is typically referred to as $abc$ coordinate system, the two phase system is typically referred to as $dq$ coordinate system. The $q$ axis is typically aligned with one of the rotating reference frames. When the $dq$ axis is aligned with the stator flux, this is referred to as the synchronous reference frame. When the $dq$ axis is aligned with the rotor speed, this is referred to as the rotor reference frame. Depending on the application, one of the reference frames are chosen as means to simplify the computation.

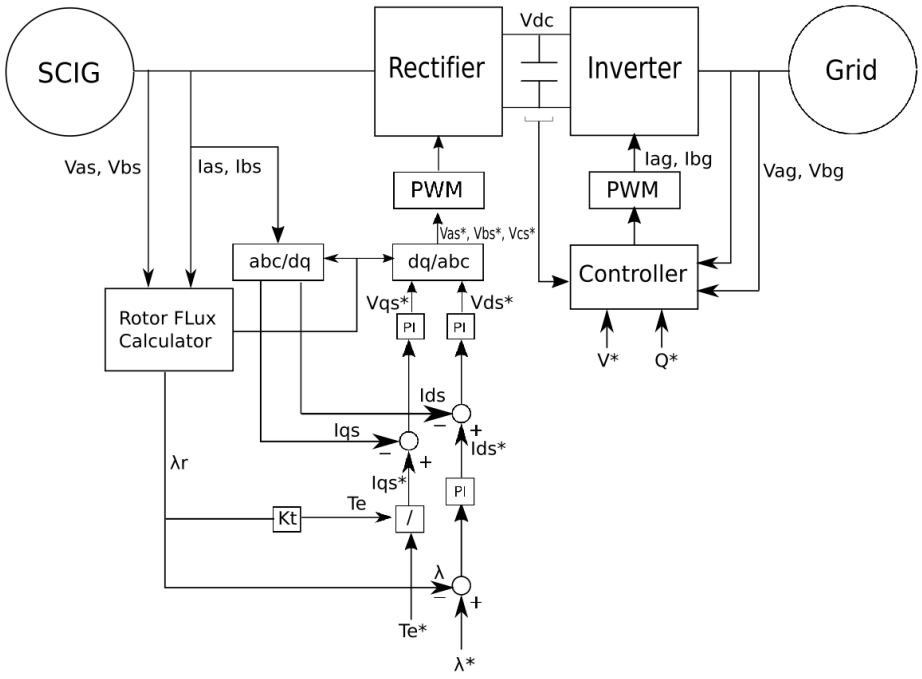


FIGURE 2.4: direct field oriented control

Illustrated in figure 2.4 is a block diagram of a generic direct field orientated control system. There are several key components that warrant some detailed discussion, not only are they crucial to field oriented control using PI controllers, they are also important when non-linear control techniques are introduced later.

The $dq$ rotor components can be calculated using the relationship between flux, stator current and system parameters. Once the components of the rotor flux are known, the rotor flux vectors magnitude and orientation angle can be calculated using equation (**??**).

The rotor flux can be calculated using the stator flux and system parameters $L_r$, $L_m$, $i_{ds}$ and $i_{qs}$; this is under the assumption that $L_r$ and $L_m$ are known, this again is not accurate in reality which can present errors in estimating the rotor flux orientation angle resulting in reduce precision in control.

Field orientated control system has three control loops, the most outer loop is the rotor flux loop. The reference rotor flux $\lambda_r^*$ is compared with the actual rotor flux $\lambda_r$ that was calculated. The resultant error is processed

by a PI controller to produce the reference $d$ component of the stator current $i^*_{ds}$. $i^*_{ds}$ is then used as the reference signal for the second control loop, $i^*_{ds}$ is compared with the actual $i_{ds}$ to produce an error signal that is processed by another PI controller to produce the $d$ component of the stator voltage $v^*_{ds}$. In the third loop, the reference torque $T^*_e$ is derived from the maximum power point tracking scheme (MPPT), the MPPT is a scheme that is designed to give a desired torque given a specific speed in order to extract the most power/energy from the wind source. Once $T^*_e$ is known, $i^*_{qs}$ can be calculated. $i^*_{qs}$ is then compared with the measured $i_{qs}$ to produce an error signal, the error signal is fed to another PI controller to produce $v^*_{qs}$. Once $v^*_{ds}, v^*_{qs}$ and $\theta_f$ are known, $v^*_{as}, v^*_{bs}$ and $v^*_{cs}$ can be calculated. This 3-phase voltage signal is then modulated with a PWM and rectifier.

As one may observe, there are three PI controllers used in the conventional FOC structure, one is nested inside the other. Although PI controllers are widely used in this application, its easy to see that the structure is far from optimal. When PI controllers are utilized to control a highly nonlinear model such as that of an induction machine, its very difficult to tune the PI controller accurately. PI controller in these applications are mostly tuned via trial and error [12] [13] [14], or based on a linearized model about some steady-state operating point. Once the operating point changes, the gains for the PI controllers has to be re-tuned, this can be achieve by several ways such as a look up table depending on the desired rotor speed.

FOC depends heavily on knowing the system parameters and assuming they are constant with respect to time. In reality system parameters are either uncertain or vary with respect to temperature and other factors. Thus a more secure and reliable control technique is warranted to ensure stability and good performance for such application. A recent paper in IEEE journal in 2015 proposed an algorithm for maximum power extraction with a strategy for optimal efficiency of WECS [15]. The control strategy proposed to extract the maximum power from wind energy in different wind conditions and to optimize the efficiency of the induction generator. This is done using a maximum power extraction (MPE) controller on the generator side and a Loss Minimization (LM) controller to minimized the generator electric loss. The controllers determines the optimal $d$ and $q$ components of the stator current through optimal condtions in order to achieve fast dynamic response.

The two major control components in the system setup that is being proposed is generator side controller and the grid side controller. The generator side controller uses field oriented control (FOC) scheme which has two control loops, hence the MPPT for maximum power extraction and LM search controller. For FOC the most common input is the reference rotor speed ($\omega_r$) of the generator which is derived from the MPPT scheme. The MPPT scheme is used for tracking the product of $I_{ds}$ and $\omega_r$ which is analogous to generator output power [15].

Within the FOC scheme, there are two different variations, direct and indirect FOC. The method which was discussed in [15], direct FOC was used. The difference between the two methods is how the orientation angle is obtained in order to perform the field orientation. In direct field oriented control (DFOC) the orientation angle $\theta_f$ is the inverse tangent of the ratio between the rotor flux components in the dq axis: $\theta_f = tan^{-1}(\lambda_{qr}/\lambda_{dr})$. The rotor fluxes are functions of the stator flux and stator current. The stator flux measurement is not always possible depending on the structure and size of the induction machine. Therefore indirect FOC method was devised to estimate the orientation angle.

Another paper was published in 2014 [13] proposed a control scheme for SCIG in WECS. It uses indirect field orientation control (IFOC). The principle behind IFOC is that the orientation angle can be estimated by taking the integral of the rotor electromagnetic angular speed $\theta_f = \int(\omega_r + \omega_{sl})dt$, the rotor electromagnetic frequency is the sum of the slip angular speed $\omega_{sl}$ and the rotor angular $\omega_r$ speed. $\omega_r$ can be measured and $\omega_{sl}$ can be estimated as a function of system parameters and the stator current. The downside of IFOC is that anytime an integration is done, the accuracy of the result depends on the level of noise of the signal that is been integrated. In many cases a filter has to be implemented to cancel out the noise in the signal which imposes on the system components and calculation. In general the performance of IFOC is comparable to the performance of DFOC.

Many improvements have been attempted to enhance the accuracy of torque control of FOC in dynamic operating conditions. One improvement is the elimination of flux sensor in DFOC or position sensor in IFOC, this is done by estimating the rotor flux using terminal quantities. The classic way of doing this is rotor flux orientation, however when estimating the rotor flux, the rotor resistance and leakage inductance is used. The rotor resistance and the leakage inductance are assumed to be constant

during design, in reality these assumptions are false. System parameters vary with temperature and operating speed. One technique that was used in a paper published in 2015 in the IEEE journal suggested field orientation with respect to a different reference frame [12]. In this paper, the FOC method used stator flux orientation as opposed to the classic rotor flux orientation. By using stator flux orientation, only the stator resistance is used to estimate the stator flux which is still sensitive to temperature variation, however a compensation block can be added in the model. Stator flux orientation reduces the effect of parameter variation but it does not eliminate it. To truly eliminate all parameter variation, adaptive control techniques must be used.

FOC can be implemented in conjunction with the techniques that are used in other components mentioned previously in other papers, for example in [13] a system was proposed using IFOC for the SCIG reinforced by a BESS in order to keep the frequency and voltage constant during the variation of the loads and wind speeds [13], a dc-dc converter is used between the DC bus and the battery to keep the DC bus voltage constant; the point here is that for each component the control technique can be changed to enhance the overall performance of the WECS

The combination of components and control schemes used both papers mentioned above [13, 15] are the most cutting edge method to date, it is the most tried and true control scheme in terms of maximizing the power transfer from wind to electrical energy while taking advantage or a wide range of wind speeds. They utilize a SCIG which has all the advantages previously mentioned. However, in the FOC of the SCIG, PI controllers are used, which presents the same problem as most of the other related developments. Anytime PI controllers are used to control a system which has a nonlinear structure. The PI controller are tuned by trial and error, or the gains of the PI controller are calculated based on a linearized model of the nonlinear system about some operating point. The issue with this approach is that whenever trial and error method has been used to tune a PI controller to control a nonlinear system, there can never been guarantee of system stability especially when the system parameters are not constant.

## 2.4 Input-Output Feedback Linearization Method Applied to SCIG

Nonlinear controllers are relatively newer than traditional PID based controllers and hysterisis controllers such as FOC and DTC. Unlike FOC and DTC, nonlinear controllers considers the nonlinear structure of the system and utilizes certain techniques to provide a greater stability capability and greater control for the transient response. Once such nonlinear control techniques is input-output linearization [16].

The fundamental concept of input-output linearization is based on a coordinate transformation technique and pole placement technique. When a system is nonlinear in the case of SCIG, a coordinate transformation can be applied to derive a new set of state variables such that the new state equations are linear. Once the new state equations are obtained, pole placement technique can be applied to derive a feedback gain to ensure the poles of the system have negative real parts. When the pole of the system have negative real parts, the system stability is guaranteed. The advantage of input-output linearization is that once the feedback gain is applied, the system is stable over the entire operating range, which could not be said for methods such as FOC and DTC. The feedback gains can be tuned to produce the desired transient response.

A research paper was publish in 2002 on the topic of adaptive speed control for induction motors using input-output linearization [17]. The control algorithm proposed in the paper is a combination of input-output linearization and least-square method. The goal of this algorithm is to produce an adaptive speed controller for an induction machine that is stable and robust to parameter variations and external disturbances. The motivation of this research paper was to improve upon the existing input-output linearization control technique which degrades in performance when the parameters change in operation. The adaptive algorithm used is a composite adaptive algorithm based on the integral cost function minimized by the least-square method. The novelty in this paper was that the proposed algorithm was able to provide good speed tracking performance for SCIG that is insensitive to some system parameters and load torque disturbance without the need to estimate them. Computer simulations where done and provided results with good speed tracking and load regulating responses.

An improvement was done in [17] in a paper that was published in

2003 [16]. The proposed algorithm in [16] utilized input-output linearization to compensate for magnetic saturation. The algorithm consists of input-output linearization with adaptive control applied to the rotor resistance. The adaptive law was derived using Lyapunov's theory. Further development of input-output linearization has been analysed and applied to SCIG in [18] in 2006. The author adopted the traditional input-output linearization technique on a SCIG. The state variables used were the currents in $\alpha\beta$ coordinate system, the flux in $\alpha\beta$ coordinate system and the rotor speed. The outputs chosen were the flux in $\alpha\beta$ coordinate system and the rotor speed. The inputs of the system are the stator voltages in $\alpha\beta$ coordinate system. The coordinate transformation was applied and new inputs were obtained.

The author realized the relative degree of the system was less than the order of the system, therefore there exists internal dynamics. When a given system has internal dynamics, it must be made sure that the internal dynamics are stable before proceeding forward. The internal dynamics can be proven to be stable by finding the zero dynamics. If the zero dynamics are stable then the internal dynamics are stable, which was what the author of [18] did.

Once the input-output linearization was applied simulations were conducted. The results showed very promising performance in terms of controlling the speed of the generator. In [18] an identification procedure was developed for the rotor resistance and the load torque variations. However, the rotor resistance was assumed to be constant with regard to speed. This assumption is not true in reality, the variation of speed can have great influence in the temperature of the rotor which effects the resistance of the rotor. To achieve the same results in reality, an adaptive method for the system parameters is needed.

Another paper that was published in 2015 that addressed the problem of parameter variation, specifically the rotor resistance [19]. In [19] two methods were compared, adaptive input-output linearization and adaptive sliding mode control. The adaptive input-output linearization method was the same as in [18], however the parameter for rotor resistance was expressed as an estimate of its actual value. The error for the rotor resistance is the difference between the estimated value and the actual rotor resistance. Lypunov's stability theory and Barbalats lemma were used in the adaptive algorithm so that the estimated value approaches the real rotor resistance value. The adaptive technique used in [19] is known

as indirect adaptive control.

The sliding mode controller in [19] used the same state-space model as the adaptive input-output linearization technique. A switching surface was derived, by utilizing the Mamdani type fuzzy system the global control law can be calculated. One the global control law is obtained, Lyapunov's candidate function was used to produce an estimation of the switching gain for the sliding mode observer.

The two methods were implimented in Matlab to conduct simulations. Both techniques were adequate in controlling the output of the generator. However each technique has its advantages and disadvantages in terms of stability and robustness. The adaptive input-output linearization controller gave good result controlling the speed and the flux with fast and accurate response. However the result is heavily dependant upon the knowledge of other system parameters such as the stator resistance, magnetizing inductance etc. Only the rotor resistance is insensitive to variation. When the other system parameters are unknown or varying with speed, the accuracy of the result cannot be guaranteed.

The advantage of sliding mode control is that the performance is insensitive to parameter variation and external disturbances; in this sense it out-performs the adaptive input-output linearization controller. However sliding mode control has an essential inconvenience which is the chattering due to discontinuities [19]. The discontinuities can be compensated by adopting a thick boundary layer around the sliding surface. Both control techniques provides ideas for a nonlinear control algorithm with adaptive parameter attributes.

Overall the input-output technique combine with adaptive control algorithm seems promising. The feedback linearization component is very powerful in altering the state-space structure of a SCIG, giving it greater range of stability. Once input-output linearization is applied to a nonlinear system. The system can be controlled like a linear system, all the linear system control theories such as pole placement technique can be applied. Input-output linearization is also compatible with many adaptive control techniques, especially algorithms utilizing Lyapunov's stability theory to estimate a system parameter.

## 2.5 Back-stepping Method Applied to SCIG

Back-stepping is another popular nonlinear control technique. Like input-output linearization, the back-stepping method requires a state-space representation of the system. In addition, the state-space representation must have a specific form called the feedback form [20]. Due to this restriction, its application is more limited than input-output linearization. However, when the form of the state-space representation permits the use of back-stepping, it is a very powerful control method.

Fortunately the SCIG model does conform to the structure requirements of back-stepping, as a result many variations adaptive back-stepping controllers has been proposed as a viable methodology for SCIG. The fundamental concept of back-stepping is the relevant state variables of the machine are selected recursively as virtual control inputs for lower dimension subsystems of the overall system. Each back-stepping stage results in a new virtual control design from the preceding design states. When the recursive control process ends, a feedback design for the original desired input results, which achieves the design objective [21].

The research using back-stepping technique goes back as early as 2007. A paper was published which proposed a back-stepping control algorithm to control an induction machine using sensorless recurrent neural observer [21]. Before the back-stepping technique was applied, the required structure has to exist. First a neural observer is devised, by using the neural model the block strict feedback decomposition is applied to create a series of lower order equations. Once the decomposition is implemented the required structure is achieved and ready to have back-stepping technique applied to it.

Several research works were done to enhance the performance of back-stepping controller for induction machines. One such paper conducted a comparative study between a rotor flux oriented control and non-linear back-stepping control of a five-phase induction machine [20]. From the more popular IM controllers like indirect field oriented control (IFOC), DTC and nonlinear back-stepping control, this paper conducts a comprehensive comparison between IFOC and back-stepping control. Back-stepping offers high performance in terms of accurate and quickness of repsonse in both steady-state and transient response. The performance of

back-stepping remains consistent even in the presence of parameter variations. Backstepping method can also incorporate adaptive control, it ensures that the system is asymptotically stable in the context of Lyapunov's stability theory [20]. However, performance is not the only criteria to select a controller. In the comparison, different advantages and disadvantages were compared such as stability properties, achievable dynamic performances, online computational effort, possibilities of controller design and the complexity of their implementation [20].

The results from [20] are as the following, in terms of possibilities of controller design, IFOC which is based on PI controllers has restricted dynamics where as in back-stepping which is based on system model, achieved much improved dynamic performance because the parameters of the controller in closed-loop are determined. In terms of complexity of implementation and tuning, IFOC is much easier to implement and design, the complexity of implmentation and tuning of back-stepping is much greater. In terms of stability properties, IFOC and back-stepping utilizes different methods to stabilize a system. IFOC uses pole compensation technique where back-stepping utilizes Lyapunovs stability theory. Both methods are able to stabilize the system however back-stepping provides a faster convergence rate. In terms of control dynamics, back-stepping achieved better dynamics than IFOC in terms of rise time and settling time of the drive speed. In summary, back-stepping overall provides superior performance compared to IFOC. However the draw back of back-stepping is in the complexity of implementation and tuning [20].

Other variations and nuances of back-stepping control has been researched in the same year. Once such research paper proposed a novel adaptive fuzzy back-stepping control scheme for induction machines with unknown model, uncertain load-torque and nonlinear friction [22]. A fuzzy logic system was employed to conduct online approximations regarding uncertain nonlinear variables combined with adaptive back-stepping which constructs the control and adaptive law. Simulations were conducted to test the effectiveness of the propose controller in [22] to test its ability to converge the tracking error and maintain the boundedness of all closed-loop signals, Lyapunov's adaptation technique were adopted to guarantee the stability of the system. The results have shown that the proposed controller provided a more accurated representation of an induction machine by adopting a non-linear model of frictions, and the controller was robust to uncertain system conditions and variables [22].

In summary, there has been numerous research done in constructing a nonlinear control algorithm using the adaptive back-stepping method. The results of proposed algorithms were able to provide wide range of system stability that is robust regarding to system parameter variations. Adaptive back-stepping can be implemented in conjunction with other techniques such as sliding-mode observers and fuzzy logic controllers. The only disadvantage with adaptive back-stepping is the complexity of the formulation and implementation. The complexity of calculation increases exponentially with higher order systems.

## 2.6 Model Reference Adaptive Control (MRAC)

Another nonlinear controller used as induction machine drive is model reference adaptive control (MRAC). The idea of MRAC is to design an ideal system model as a reference. Use the reference model and compare its behavior to the actual model and derive an error in behavior. The error between the reference model and the actual system is used as an input to the controller. The controller which produces the input to the actual system so that it behaves like the reference model.

Research has been done on MRAC in papers such as [23]. In this paper a neural network speed controller based on online back propagation method built on direct MRAC has been proposed to control an induction machine. The contribution of this paper is that it proposes a new error function which is used for the dynamic back progagation algorithm [23]. The error function will adjust the parameters of the neural network speed controller and minimize the error between the reference model and actual model. The proposed algorithm was implemented in simulation, the results show that the proposed controller is able to track the reference speed and robust again load disturbances. However, the algorithm does not address the issue of varying system parameters.

An improvement on MRAC drives are discussed in [24]. Most MRAC controllers prior have used the static model of an induction machine as the reference model, which results in unsatisfactory transient performances. The algorithm proposed in [24] utilizes a reference model derived from the dynamic model of the induction machine, as a result attempt to improve the real-time control of the transient response. During the design and implementation of the proposed algorithm an integrated flux field-oriented control system is designed and simulated. The results show that the controller was successful in tracking the reference signal both in steady-state and transient response, and its an improvement upon the static reference model MRAC.

Another research paper was published in 2009 [25]. In this paper several augmentations were adopted for the standard MRAC controller. First a sensorless speed control scheme based on MRAC was proposed. A robust MRAC algorithm was chosen for speed control. The speed is estimated from model reference adaptive system algortihm based on reactive power calculations [25]. In conjunction a compensated indirect rotor flux oriented control scheme was used. A Kalman filter observer was used to

avoid oscillations on rotor speed esimation that appear from asymmetries of the main and auxiliary winding [24]. The robust MRAC was chosen for tuning of the parameters of the control law. The results from simulation shows good operation in a wide speed range, the proposed algorithm can represent an alternative for traditional variable speed drives.

Given the other nonlinear control algorithms MRAC is one of many options for induction machine drive. One of the conditions as to which control to chose is how well the controller performs when the system parameters are uncertain. A paper was published that specifically tackles the problem of parameter identification [26]. The algorithm proposed in [27] attempts to identification of all system parameters. The theory of the parameter identification algorithm is based on robust MRAC that is applied to induction machine model. The input for the identification algorithm is the stator current, the estimated system parameters will provide better performance given its a more realistic representation of the electric machine in operation. The number of system parameters to be identified are five in total. The main contribution of the proposed algorithm is to provide an automatized method to obtain all given system parameters without any previous test and derivative filters. Simulations were conducted and the results are shown that the parameters obtained described adequate performance of the machine. Although robust MRAC is a via means for induction machine drive, the formulation of the reference model presents more complexity than other nonlinear adaptive controllers.

## 2.7 Adaptive Nonlinear Control Methods

In the previous subsections of the literature review, various nonlinear adaptive control algorithms has been discussed. Comparison of nonlinear adaptive control and conventional controllers (FOC and DTC) have been conducted in computer simulations. It has been demonstrated in simulation that nonlinear adaptive control has greater performance in terms of range of stability, sensitivity to parameter variation and system perturbation. In addition, adaptive control techniques provides a systematic approach for automatic on-line tuning of the system parameters which convention controllers do not. As a result of the adaptive component of the controllers, it is able to achieve and maintain greater level of performance when the system parameters are unknown or change in time. It is therefore strategic to compare the different nonlinear adaptive controls.

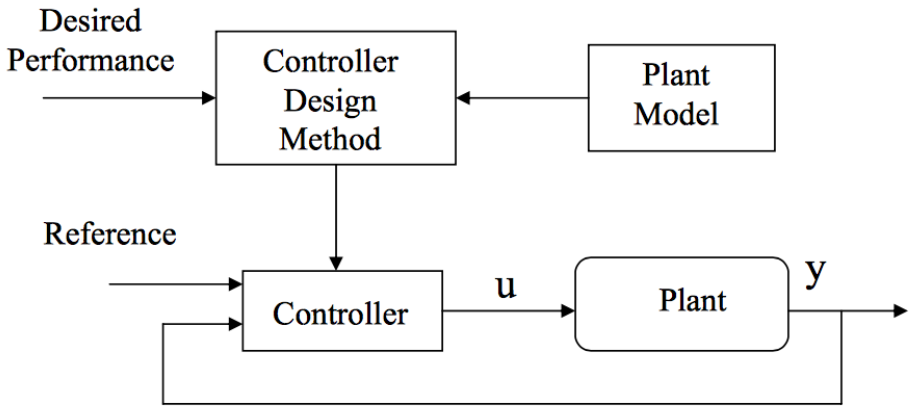


FIGURE 2.5: Model Based Control Design [3]

In figure 2.5, a scheme of a model based control design is illustrated. The principle of model based control design is that there is an ideal plant model. The controller design method takes plant model and the desired performance to produce the controller. The controller then takes the reference desired performance, the output of the actual plant to produce the inputs to the plant. The model based control design is used when the designer knows the behavior of the plant, and the designer also has the adequate criteria for the controller design. In addition, the parameter of the model is assumed to be constant.

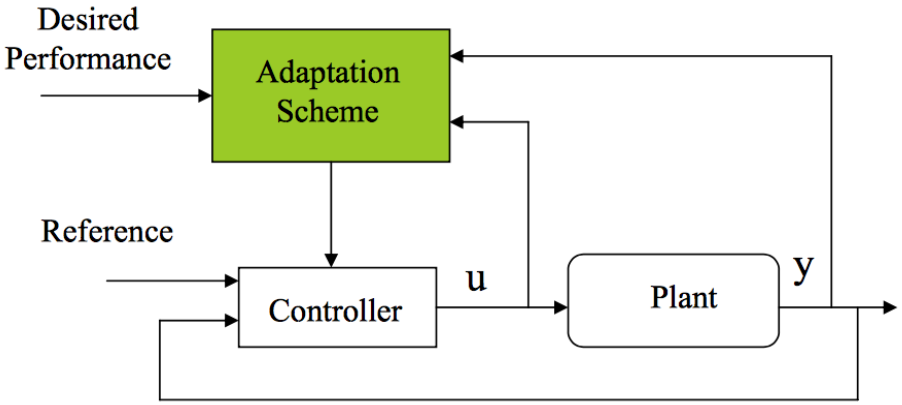


FIGURE 2.6: Adaptive Control Structure [3]

The basic scheme for the adaptive control structure is shown in figure 2.6. The adaptive control structure does not require system model. The Adaptation scheme takes the output of the plant, the output of the controller and the desired performance to modify the controllers parameters. The controller then takes the output from the adaptation scheme then produces the input to the plant. In the case of SCIG in WECS, the goal of this thesis is to improve the performance of the generator.

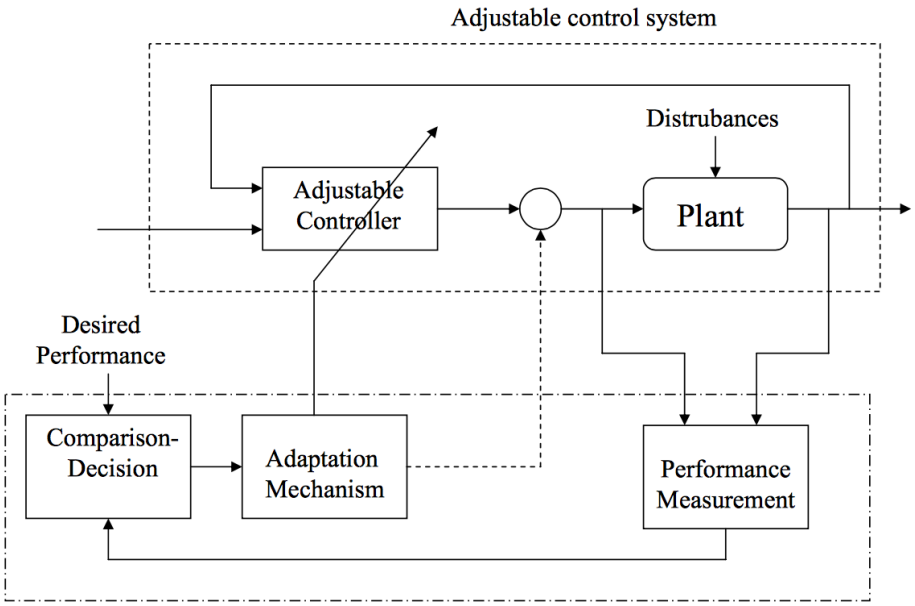


FIGURE 2.7: Adaptation Scheme [3]

A more detailed adaptation scheme is illustrated in figure 2.7. The nonlinear adaptive control scheme can be seen in two subcomponents. The adjustable control system, and the adaptation scheme. The adjustable control system provides the input direct to the plant to produce the desired outcome. The adaptation scheme will provide adjustments to the controller based on the variation of the performance measurements and the desired performance, which as a result provides sensitivity to parameters variation. In comparison to conventional feedback control systems such as FOC and DTC, the adaptive control system will provide the additional elimination of the effect of parameter variations where as the conventional feedback control only eliminates the effect of system disturbances. The adaptive control system can be further divided into two sub-categories, direct adaptive control and indirect adaptive control.

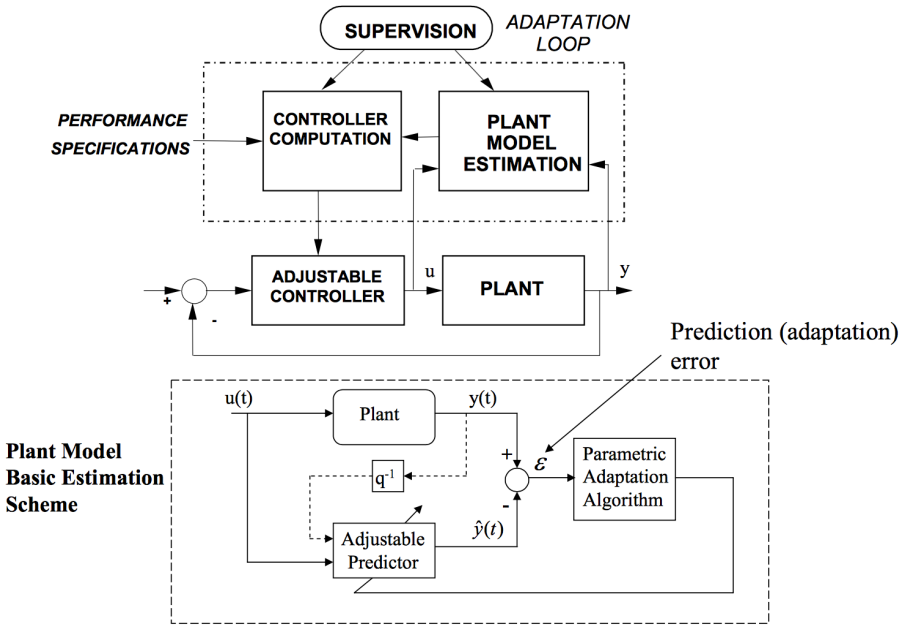


FIGURE 2.8: Indirect Adaptive scheme [3]

The difference between direct and indirect adaptive control is the way the adaptive component is achieved. In figure 2.8 an indirect adaptive control scheme is illustrated. The adaptive loop consists of the plant model estimation and the controller computation. The key to indirect adaptive control lies within the plant model estimation scheme. The plant model estimation scheme consists of the parametric adaptation algorithm and the adjustable predictor, these two components actually predicts the

real values of the system parameters which the controller requires to control the plant. Indirect adaptive control is useful when the information of the parameters are required, as well as stabilization of the system output.

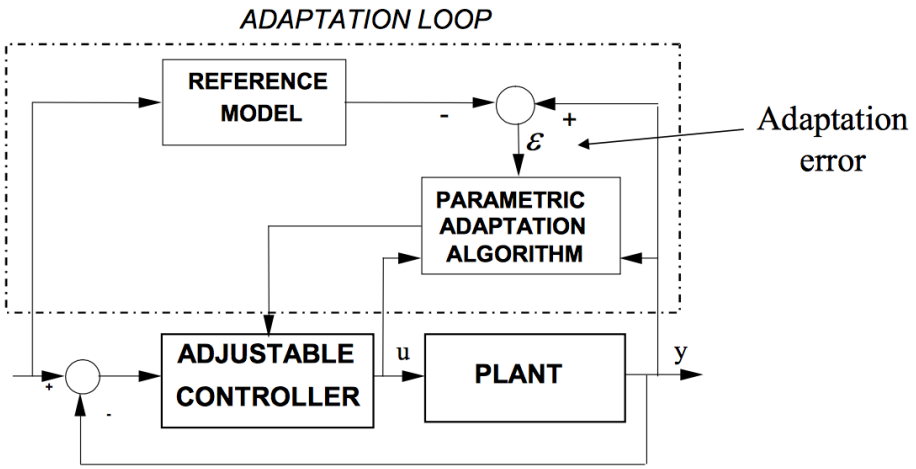


FIGURE 2.9: Direct Adaptive scheme [3]

In direct adaptive control, the adaptation loop only proposes estimation for parameters as a means to control the plant output. The values for parameter estimation are not meant to be equal to the real value of system parameters. Shown in figure 2.9 is an illustration of direct adaptive control. The adaptation loop for direct adaptive control is very different from that of indirect adaptive control. The Parametric adaptation algorithm takes the plant output, the controller output and the adaptation error as inputs. The product of the parametric adaptation will be one of the inputs to the adjustable controller, enabling the stability of the plant.

To choose the scheme of adaptive control for this thesis will depend upon which the control algorithm will attempt to achieve. Since the goal is to improve upon the conventional controllers given unknown system parameters or varying system parameters, it is certain that adaptive control will have to be utilized. The ideal system performance however is unknown in the beginning, therefore difficult to construct an ideal system model. Given that the goal is to control the output of the system, and estimations of the system parameters is not needed, direct adaptive control is the preferred method.

# Chapter 3

# Identification of System Parameters

The heart of the problem which causes the rise of many development in control theory regarding energy transfer machines such as the SCIG, is the uncertainty of the system parameters. Traditionally the system parameters of SCIG were obtained using the lock rotor test and the no load test. The locked-rotor test and no-load test will be discussed in the following sections in order to identify the limitations of these tests to justify the need for adaptive control.

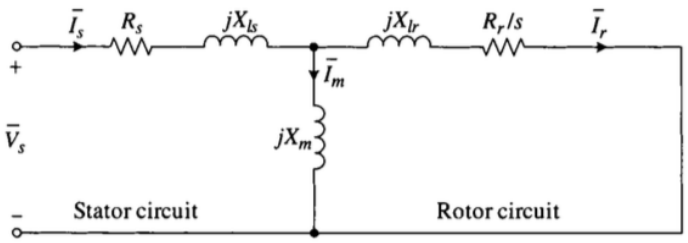


FIGURE 3.1: No-Load test Equivalent Circuit [4]

Figure 3.1 shows the simplified equivalent circuit of a SCIG in synchronous reference frame. The portion of the circuit that contains $R_s$, $X_{ls}$ and $X_m$ represents the stator. The portion of the circuit containing $X_{lr}$ and $R_r/s$ represent the rotor. The equivalent circuit will be used to derive most of the the methodology for both the no-load test and the locked-rotor test.

## 3.1 No-load test

During no load test, the rotor rotates with a speed very close to synchronous speed. Balanced voltages are applied to the stator terminals at the rated frequency. the rotor is free from any mechanical load which means the slip is very low. Current, voltage and power measured at the motor input [28]. The term $R_r/s$ can be written in two components:

$$\frac{R_r}{s} = R_r + \frac{R_r(1-s)}{s} \tag{3.1}$$

$R_r(1-s)/s$ becomes very large. The current will take the path of the least resistance and avoid the path containing $X_r$ and $R_r$. Only the stator circuit is left.

The measurements that are taken for the no-load test are $I_s$, $V_s$ and the no-load input power $P_{NL}$. The value of $R_s$ is determined from the no-load dissipated power [28]:

$$\begin{aligned} P_{NL} &= 3I_s^2 R_s \\ R_s &= P_{NL}/(3I_s^2) \end{aligned} \tag{3.2}$$

The rotor resistance can be derived from equation (3.2). The no-load impedance $Z_{NL}$ can be derived from the ratio of no-load voltage $V_s$ and the stator current $I_s$:

$$\frac{V_s}{I_s} = Z_{NL} = \sqrt{R_s^2 + (X_{ls} + X_m)^2} \tag{3.3}$$

From equation (3.3) the sum of the stator reactance and the magnetizing reactance can be obtained:

$$X_{ls} + X_m = \sqrt{Z_{NL}^2 - R_s^2} \tag{3.4}$$

The values of $X_{Ls}$ and $X_m$ cannot be determined by no-load test alone. The stator leakage reactance $X_{ls}$ will be determined by locked-rotor test, which will be used to determine the magnetizing reactance [28].

## 3.2 Locked Rotor Test

During locked rotor test the rotor is locked to prevent rotation, balanced voltages are applied to the stator terminals at $25\%$ of the rated frequency.

The voltage is gradually increased until the rated current is reached. Current, voltage and power are measured at the motor input.

The slip for the blocked rotor is unity which means the term $R_r(1 - s)/s$ in equation (3.1) becomes zero and the resistance of the rotor branch in the equivalent circuit becomes very small. As a result of the small resistance of the rotor resistance the current in the rotor branch is much larger than the excitation branch such that the excitation branch can be neglected [28].

If the excitation branch is neglected the stator current will equal to the rotor current $I_s = I_r$. The rotor resistance can be found using the current measurement $I_s$ and the dissipated power measurement $P_{LR}$:

$$P_{LR} = 3I_{LR}^2(R_s + R_r) \tag{3.5}$$

Using the ratio of the measured current and the voltage $V_s$, the locked-rotor impedance $Z_{LR}$ can be found:

$$\frac{V_{LR}}{I_s} = Z_{LR} = \sqrt{(R_s + R_r)^2 + (X_{ls} + X_{lr})^2} \tag{3.6}$$

The sum of the stator and rotor reactance can be found:

$$X_{ls} + X_{lr} = \sqrt{Z_{LR}^2 - (R_s + R_r)^2} = X_{LR} \tag{3.7}$$

Once the sum of the rotor reactance and stator reactor is obtained, some assumptions has to be made at this point. The actual distribution of the total leakage reactance between the rotor and the stator is typically unknown, the assumptions one has to make is based on empirical equations for different classes of motors/generators. Electrical machines are generally broken into four classes:

Class A SCIG: chracterized by normal starting torque, high starting current, low operating slip, low rotor impedance, good operating characteristics at the expense of high starting current, common applications include fans, flows and pumps [28].

Class B SCIG: characterized by normal starting torque, low starting current, low operating slip, higher rotor impedance than class A, good general purpose motor with common applications being the same as Class

A [28].

Class C SCIG: characterized by high starting torque, low starting current, higher operating slip than classes A and B, common aplpications include compressors and conveyors [28].

Class D SCIG: characterized by high starting torque, high starting current, high operating slip, inefficient operation efficiency for continuous loads, common applications are characterized by and intermittent load such as a punch press [28].

Given the classification of machines, an empirical system is used to assign distributions to rotor and stator reactance.

| | |
|---|---|
| Class A | $X_{ls} = 0.5X_{LR}$, $X_{lr} = 0.5X_{LR}$ |
| Class B | $X_{ls} = 0.4X_{LR}$, $X_{lr} = 0.6X_{LR}$ |
| Class C | $X_{ls} = 0.3X_{LR}$, $X_{lr} = 0.7X_{LR}$ |
| Class D | $X_{ls} = 0.5X_{LR}$, $X_{lr} = 0.5X_{LR}$ |
| Wound rotor | $X_{ls} = 0.5X_{LR}$, $X_{lr} = 0.5X_{LR}$ |

Using the above empirical formulas [28], the values for $X_{ls}$ and $X_{lr}$ can be determined. Once the value for $X_{ls}$ is determined, the magnetization reactance can be determined from the relationship obtained from the no-load test:

$$X_m = \sqrt{Z_{NL}^2 - R_s^2} - X_{LS} \tag{3.8}$$

## 3.3 Limitations of System Parameter Identification Techniques

In the previous sections, the basic principles of no-load test and locked-rotor test are discussed. There are few limitations with these methods. First, it may not be possible to conduct the tests that are mentioned. Depending on the size of the generator, many of them can be quite large which is the case for wind-turbine energy conversion system. The generators usually already installed on site. No-load and locked-rotor test may not be possible to be conducted on already installed generators [29, 30].

Induction generator themselves are very robust and require very little maintenance. Usually it is the controllers that are updated with more advanced and efficient controllers. Many manufacturers will keep the parameters confidential, therefore the parameters are not known, so the only way to tune the controllers is to use parameters of similar generators, this can introduce errors for obvious reasons.

Some manufacturer for induction generators may no longer exist, yet the generators are still in use, its virtually impossible to know the system parameters, the only ways to find the system parameters will be to conduct the no-load test and locked-rotor test which will require disassembling or rearranging the turbine-generator system. Sometimes this alteration may not be feasible [31].

In the perfect scenario when the no-load test and the locked-rotor test are conducted, there are some inherent assumptions with the test that can cause errors in tuning of controllers. As discussed in the previous section, the distribution of the rotor and the stator reactances can not be accurately known. Their distribution is decided by empirical equations. The rotor and stator inductances is therefore an assumption, there is no way to know the accuracy of these assumptions. In the generator model used for the simulation in this thesis, the stator and rotor reactances are each assumed to be $50\%$ of the total sum, which is calculated in the locked-rotor test. There is no guarantee that this assumption is accurate.

The equivalent circuit used in the no-load and locked-rotor test does not take into account of the different losses that occur in a real generator system, such as windage, friction and core losses [32]. Additional measurements of the DC resistance of the stator windings is required.

The moment of inertia is another important system parameter used to calculated the mechanical torque. To calculate the moment of inertia requires accurate dimensions of the object and the density of the object. For the rotor of a induction machine, the dimensions are very complex and the density is uneven due to difference in material. It is very difficult to calculate the density distribution of the rotor. Estimations and assumptions has to be made to obtained the moment of inertia of the rotor. When the specifications are given for a SCIG, one has to keep in mind that the moment of inertia is not completely accurate.

One other phenomenon which can effect the resistance of any conductor is skin effect. The distribution of current in AC is not uniform across the cross section of the conductor. The current density is greatest near the surface of the conductor. The current flow mostly on the surface of the conductor, between the surface and a level called skin depth. The skin depth decreases with the increase in frequency of the current. This could effect both the rotor and stator resistance especially when one of the control inputs is the stator frequency, so depending on the method of control the stator resistance can be uncertain as well [28].

The advantages of adaptive control is that it by-passes the difficulty of parameter identification. Depending on the type of adaptive control, direct or indirect, the output of the system will be controlled to approach the desired value regardless of what the parameters are.

The idea of adaptive non-linear control for SCIG is not a new concept. There has been algorithms developed previously as a solution to the uncertainty of one system parameter namely rotor resistance [31]. The reason why rotor resistance has always been the parameter which adaptive control was used is due to its large variation as result of Ohmic heating. Ohmic heating causes the resistance of a conductor to vary dramatically as result of temperature change. The temperature of the rotor increases so much in operation that the resistance value can vary more that $100\%$.

The contribution of the adaptive control algorithm proposed in this thesis not only provides an answer to the variation of rotor resistance, but for all other system parameters. The accuracy of the system parameters are irrelevant. Once the controller is installed, it will provide estimations for the system parameters in order to control the desired output of the generator.

# Chapter 4

# Solution Strategy

## 4.1 Problem Description

As mentioned in the previous section, there are many control techniques used to improve the overall performance of a SCIG WECS. The majority of the SCIG controllers mentioned in recent research involves some variation of field orientation scheme, field orientation controllers are the most effective way to achieve high precision and fast response to control the torque and the flux of a SCIG. The major flaw with the existing FOC schemes is that they use PI controllers to control a nonlinear system. The tuning of these PI controllers are mostly done by trial and error or the gains are calculated based on a model of the generator that is optimized about some operating point.

The disadvantage with the FOC approach is that one can never guarantee the stability of the system neither can one prove that the tune gains are the most optimal gains. Furthermore, once the gains are tuned to control the system at a specific operating point, if the operating point deviates as is the case when the wind speed is unpredictable and has a large variance, the gains of the PID controllers will have to be re-tuned.

Another issue with using only PI controllers is that PI controllers are highly sensitive to variations of system parameters. The system parameters cannot be assumed to be constant, in reality they change with variation of operating point. Values like resistance fluctuates with temperature with significant magnitude such that the original model of the system no longer accurately describes its behavior.

The solution to address the limited range of system stability and uncertainty of system parameters must be a control scheme that is not simply based on a linearized approximation of the model but the actual nonlinear model itself. This way one can guarantee the stability of the generator verses simply showing that it is stable under certain conditions through trial and simulations. To solve the problem of uncertain system parameters, an adaptive control technique must be used in conjunction with the nonlinear control scheme to mitigate the deterioration of the control method when system parameters change with different operating points.

Many different techniques are available to design a controller for nonlinear systems, such as input-output linearization, adaptive back-stepping, model reference adaptive control etc. Which technique is used depends on the structure of the nonlinear model and the goal that the controller is trying to achieve. In the following section one can observe very quickly that the input-output linearization method is well suited for the SCIG model.

The goal of input-output linearization is to provide a feedback to the input such that the nonlinear terms in the system model are canceled. Once the nonlinear terms of the model are canceled the new system model appears to be linear which is much easier to control. The simplest way to control the new linear system is the pole placement technique to ensure system stability. The first step in designing the input-output linearization controller is to have a state-space model representation of the SCIG. Since we are taking advantage of the field orientation method, the state variables will be the rotor flux in $dq$ coordinate system, the stator currents in $dq$ coordinate system and the rotor speed.

Input-Output linearization technique will be used in conjunction with direct adaptive control method. The adaptive control will enhance the controller, making it more robust and resistant to parameter variation. Adaptive non-linear controllers have been designed for SCIG before, but only for certain system parameter, the rotor resistance $R_r$, stator resistance $R_s$ and the torque $T_m$ [18]. The contribution of the controller proposed in this thesis will be to make all system parameters adaptive. The Input-Output adaptive controller will be compared to the performance of FOC to verify its usefulness.

It is important in the following sub sections to establish some auxiliary methodologies such as field orientation and maximum power point tracking (MPPT) scheme to give the controller a context in which it is developed. It is also important to give a background of FOC using PID controllers to reveals some of its inadequacies which the proposed nonlinear adaptive controller will attempt to compensate.

### 4.1.1 Maximum Power Point Tracking Scheme

The goal that the proposed controller is trying to achieve is to capture the maximum power at different wind speeds by adjusting the speed of the generator.

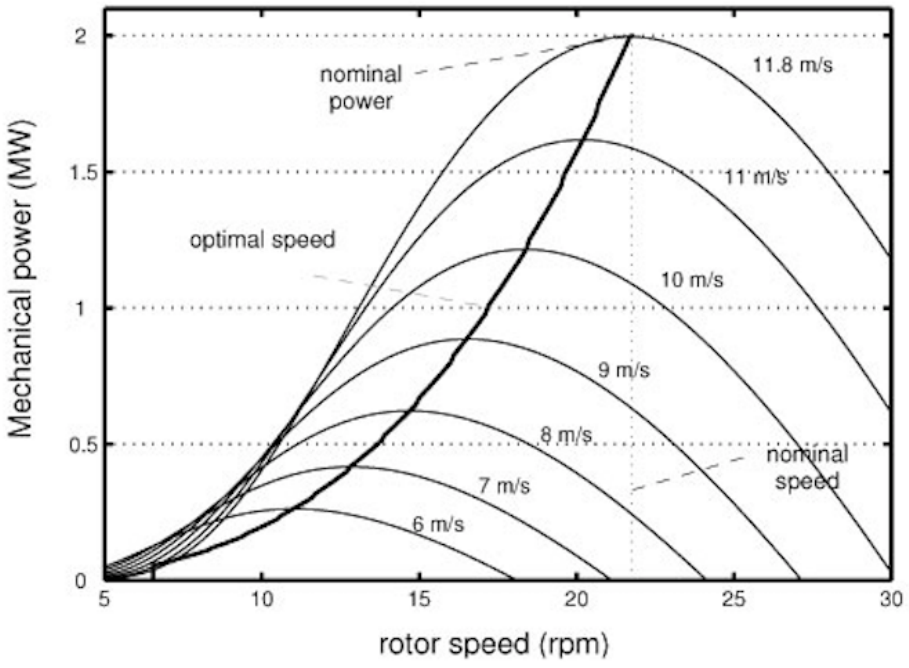


FIGURE 4.1: maximum power point tracking (Mechanical Power $P_m$ vs Rotor Speed $\omega_r$) [2]

Shown in figure 4.1 is a typical maximum power point tracking (MPPT) scheme, it shows the typical characteristics of a wind turbine operating at different wind speeds. $P_m$ is the mechanical power and $\omega_m$ is the mechanical speed. For a specific wind speed, a given power curve expresses the

power extracted by the turbine at different generator mechanical speeds. To extract the maximum power from the wind at different wind speeds, the turbine speed must be controlled and adjusted to operate at all the maximum power points (MPP). [2]

$$P_m \propto \omega_m^3 \tag{4.1}$$

When all the MPP are connected, one can observe the relationship between power $P_m$ and mechanical speed $\omega_m^3$ to be given in equation (4.1).

$$P_m = T_m \omega_m \tag{4.2}$$

The expression for power $P_m$ as a function of torque $T_m$ is given in equation (4.2). Thus torque as a function of the mechanical speed is given by equation (4.3).

$$T_m \propto \omega_m^2 \tag{4.3}$$

Knowing the relationship between power, torque and speed, there are three different ways to control a generator; power control, speed control and torque control. Regardless of the type of control used, the core idea remains the same, that is to control via stator voltage to keep the generator speed at a desired value such that the maximum power is harvested from the wind.

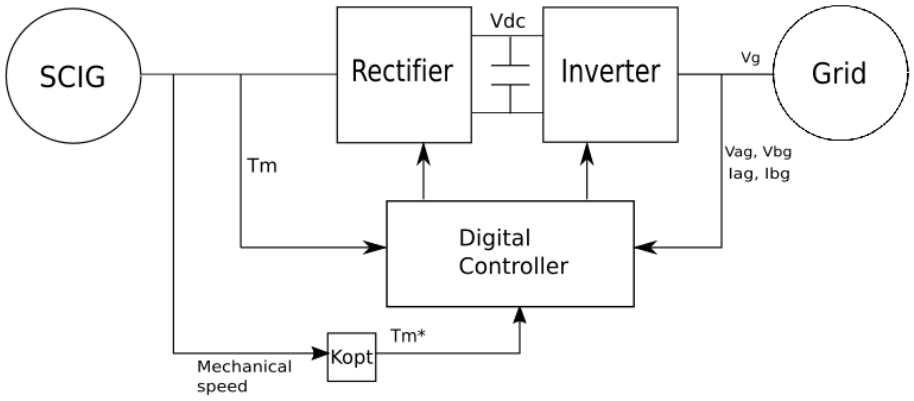


FIGURE 4.2: torque control

In figure 4.2 is a block diagram composed of all the major components of a generic squirrel cage induction generator (SCIG) wind energy system (WES), the control technique that will be proposed in this thesis will be utilizing the MPPT scheme discussed earlier. The wind speed is used to develop the desired generator speed to capture the maximum power from the wind; this will be done by calculating the required voltage that is to be modulated by the rectifier as input to the generator stator.

## 4.2 Controller Design

In this section the theoretical derivation for the adaptive control algorithm is discussed. The derivation will involve the input-output linearization technique as well as the adaptive control algorithm utilizing Lyapunov's stability theorem.

### Modelling of the SCIG

In this section of the controller design, the modelling of the SCIG will be discussed. The modelling of any controller design is the most crucial part, by settling up the structure of the system model appropriately, the design calculations can be simplified. First the appropriate governing system equations must be identified. Using the governing system equations, the appropriate state-space model can be derived [2].

Let us define the following state variables:

1. Define $\lambda_{ds}$ and $\lambda_{qs}$ as the $dq$ components of the stator flux
2. Define $\lambda_{dr}$ and $\lambda_{qr}$ as the $dq$ components of the rotor flux
3. Define $I_{ds}$ and $I_{qs}$ as the $dq$ components of the stator current
4. Define $I_{dr}$ and $I_{qr}$ as the $dq$ components of the rotor current
5. Define $\omega_r$ as the rotor speed
6. Define $\omega_s$ as the synchronous speed, where $s\omega_s = \omega_s - \omega_r$ and $s$ is the slip of the generator

$$\begin{aligned}
\dot{\lambda_{ds}} &= -R_s \cdot I_{ds} + \omega_s \cdot \lambda_{qs} + V_{ds} \\
\dot{\lambda_{qs}} &= -R_s \cdot I_{qs} - \omega_s \cdot \lambda_{ds} + V_{qs} \\
\dot{\lambda_{dr}} &= -R_r \cdot I_{dr} - s \cdot \omega_s \cdot \lambda_{qr} \\
\dot{\lambda_{qr}} &= -R_r \cdot I_{qr} - s \cdot \omega_s \cdot \lambda_{dr}
\end{aligned} \tag{4.4}$$

In equation (4.4) are the system dynamics of a SCIG. These dynamic equations can be found in most textbooks such as [2].

$$\begin{aligned}
\lambda_{ds} &= L_s \cdot I_{ds} + L_m \cdot I_{dr} \\
\lambda_{qs} &= L_s \cdot I_{qs} + L_m \cdot I_{qr} \\
\lambda_{dr} &= L_m \cdot I_{ds} + L_r \cdot I_{dr} \\
\lambda_{qr} &= L_m \cdot I_{qs} + L_r \cdot I_{qr}
\end{aligned} \tag{4.5}$$

In equation (4.5) are the flux equations of a SCIG. These equations will be used in conjunction with the system dynamic equations to derive the final system model [2].

$$\begin{aligned}
\dot{\omega_r} &= \frac{P}{J} \cdot [T_e - T_m] \\
T_e &= (3L_m P)/(2L_r)(\lambda_{ds} I_{qs} - \lambda_{qs} I_{ds})
\end{aligned} \tag{4.6}$$

The torque equation is given in equation (4.6). $T_m$ is the mechanical torque and $T_e$ is the electrical troque. The nonlinearities of equation (4.7) comes from the nonlinear relationship between the flux and current in the electrical torque equation. The torque equation will be a crucial part of the system modelling to control the speed and torque of the SCIG.

$$\begin{aligned}
\dot{I_{ds}} &= a_1 I_{ds} + \omega_s I_{qs} + a_3 \lambda_{dr} + a_4 \lambda_{qr} \omega_s - a_4 \omega_r \lambda_{qr} + a_5 V_{ds} \\
\dot{I_{qs}} &= -\omega_s I_{ds} + a_1 I_{qs} - a_4 \omega_r \lambda_{dr} + a_3 \lambda_{qr} + a_5 V_{qs} \\
\dot{\lambda_{dr}} &= a_8 \lambda_{dr} + \omega_s \lambda_{qr} - \omega_r \lambda_{qr} + a_6 I_{ds} \\
\dot{\lambda_{qr}} &= a_8 \lambda_{qr} - \omega_s \lambda_{dr} + \omega_r \lambda_{dr} + a_6 I_{qs} \\
\dot{\omega_r} &= a_7 I_{qs} \lambda_{dr} - a_7 I_{ds} \lambda_{qr} - a_2
\end{aligned} \tag{4.7}$$

The system model is derived in equation (4.7) presents the five state variables that are relevant in the control technique to follow. The parameters are derived from the parameters of the generator in equation (4.8).

$$
\begin{aligned}
D &= 1/(L_r L_s - L_m^2) \\
a_1 &= -DL_r R_s - R_r L_m^2 D/(L_r) \\
a_2 &= PT_m/J \\
a_3 &= DL_m R_r/L_r \\
a_4 &= DL_m \\
a_5 &= DL_r \\
a_6 &= R_r L_m/L_r \\
a_7 &= 3P^2 L_m/(2JL_r) \\
a_8 &= -R_r/L_r
\end{aligned}
\tag{4.8}
$$

Now the system model is attained, the next step is to define the inputs and outputs of the system.

**Feedback Linearization Theory**

Since the SCIG is a fairly complex system with many of the state variables interacting with each other, a MIMO control scheme should be adopted. The feedback linearization method is well documented in many text books. The following section is taken from [33].

Consider the following MIMO system equation (4.9):

$$
\begin{aligned}
\dot{\bar{x}} &= f(\bar{x}) + g(\bar{x})\bar{u} \\
\bar{y} &= h(\bar{x})
\end{aligned}
\tag{4.9}
$$

Where $\bar{x} \in \mathbb{R}$ is the state vector. $\bar{u} \in \mathbb{R}^m$ is the vector of $m$ inputs $u_i$ ($i = 1, ..., m$). $\bar{y} \in \mathbb{R}^m$ is the vector of $m$ outputs $y^i$ ($j = 1, ..., m$). $f$ and $g$ are smooth vector and matrix field, respectively. $h$ is the smooth vector function [33].

The input-output linearization method for MIMO systems requires the differentiating of the outputs $y_j$ until at least one of the inputs appears.

Consider $L_f h$ and $L_g h$ the Lie derivatives of $h(\bar{x})$ with repsect to $f(\bar{x})$ and $g(\bar{x})$, where $L_f h = \frac{\partial h}{\partial x} f$ and $L_g h = \frac{\partial g}{\partial x} f$ [33]

$\dot{y}_j$ can be written as

$$\dot{y}_j = L_f h_j + \sum_{i=1}^{m} (L_g, h_j) u_i \tag{4.10}$$

If $L_g, h_j(x) = 0$ for all $i$, then no inputs appears and one has to differentiate again. Assume that $y_i$ needs to be differentiated $r_j$ times before at least one input appears [33], then

$$y_j^{(r_j)} = L_f^{r_j} j_j + \sum_{i=1}^{m} L_{g_i} L_f^{r_j - 1} h_j u_i, (j = 1, ..., m) \tag{4.11}$$

Equation 4.11 can be written into matrix for as

$$\begin{bmatrix} y_1^{(r_1)} \\ \vdots \\ y_m^{(r_m)} \end{bmatrix} = \begin{bmatrix} L_f^{r_1} h_1(x) \\ \vdots \\ L_f^{r_m} h_m(x) \end{bmatrix} + E(x) \begin{bmatrix} u_1 \\ \vdots \\ \bar{u}_m \end{bmatrix} \tag{4.12}$$

where the $m \times n$ matrix $E(x)$ is the referred to as the decoupling matrix for the MIMO system. It has the following expression

$$E(x) = \begin{bmatrix} L_{g_1} L_f^{r_1 - 1} h_1 & \cdots & L_{g_m} L_f^{r_1 - 1} h_1 \\ \vdots & \ddots & \vdots \\ L_{g_1} L_f^{r_m - 1} h_m & \cdots & L_{g_m} L_f^{r_m - 1} h_m \end{bmatrix} \tag{4.13}$$

Equation 4.12 can be linearized by choosing the control input vector $u$ as follows

$$\bar{u} = -E^{-1} \begin{bmatrix} L_f^{r_1} h_1(x) \\ \vdots \\ L_f^{r_m} h_m(x) \end{bmatrix} + E^{-1} \begin{bmatrix} v_1 \\ \vdots \\ v_m \end{bmatrix} \tag{4.14}$$

where $\bar{v}$ is the new input vector that is yet to be determined.

The closed loop equation of the system is obtained by substituting equation (4.14) into equation (4.12) to get

$$\begin{bmatrix} y_1^{(r_1)} \\ \vdots \\ y_m^{(r_m)} \end{bmatrix} = \begin{bmatrix} v_1 \\ \vdots \\ v_m \end{bmatrix} \tag{4.15}$$

The input-output relationship given by equation (4.15) is not only linear but also decoupled [33].

Note that $r_1, ..., r_m$ are called the relative degree of the system and the scalar $r = r_1 + ... + r_m$ is called the total relative degree of the system. In the case where the total relative degree of the nonlinear system is smaller than the order of the system $(n)$, the system has some internal dynamics which cannot be seen from the output. There are no internal dynamics when the total relative degree is equal to $n$ [33].

**Defining Input and Outputs**

The inputs of the system are:

$$\begin{bmatrix} u_1 \\ u_2 \\ u_3 \end{bmatrix} = \begin{bmatrix} V_{ds} \\ V_{qs} \\ \omega_s \end{bmatrix} \tag{4.16}$$

The outputs of the system are:

$$\begin{bmatrix} y_1 \\ y_2 \\ y_3 \end{bmatrix} = \begin{bmatrix} h_1(\bar{x}, a) \\ h_2(\bar{x}, a) \\ h_2(\bar{x}, a) \end{bmatrix} = \begin{bmatrix} \lambda_{dr}^2 + \lambda_{qr}^2 \\ \omega_r \\ \lambda_{qr} \end{bmatrix} \tag{4.17}$$

The choices for the inputs are simple, the voltages ($V_{ds}$ and $V_{qs}$) are what drives the generator and given the stator voltages one still needs to know the synchronous speed, hence $\omega_s$ is the third input. The choice of outputs are more complicated and worth explaining in detail. The goal of field orientation is to control the flux and torque separately, therefore the $\lambda_{dr}$ will approach the rated flux, which is given as the flux magnitude. $\lambda_{qr}$ is to be approaching zero. Therefore, the flux magnitude $\sqrt{\lambda_{dr}^2 + \lambda_{qr}^2}$ must

be one of the control variables, $\lambda_{dr}^2 + \lambda_{qr}^2$ is chosen because it will achieve the same goal and also simplify calculations. $\lambda_{qr}$ will be controlled to approach zero, therefore it is another output. The rotor speed of the generator will be controlled to track the reference desired speed, therefore $\omega_r$ will be the third output.

The outputs $y_1$ and $y_2$ are chosen based on the assumption that the rotor flux can be measured. There are sensors can be used to measure the flux, however the flux sensors are very expensive. The solution in industry is to use flux observers to estimate the flux. Due to the limit time available for this thesis, the flux observer was not implemented.

**Coordinate transformation**

To apply input-output linearization and adaptive control, there has to be a change in coordinate system, consider the new coordinate system below:

$$\begin{bmatrix} z_1 \\ z_2 \\ z_3 \\ z_4 \\ z_5 \end{bmatrix} = \begin{bmatrix} y_1 \\ \dot{y_1} \\ y_2 \\ \dot{y_2} \\ y_3 \end{bmatrix} = \begin{bmatrix} h_1(\bar{x}, a) \\ L_f h_1(\bar{x}, a) \\ h_2(\bar{x}, a) \\ L_f h_2(\bar{x}, a) \\ h_3(\bar{x}, a) \end{bmatrix} \tag{4.18}$$

The new states $z$ can be explicitly expressed in terms of the original states $x$ as:

$$\begin{aligned} z_1 &= \lambda_{dr}^2 + \lambda_{qr}^2 \\ z_2 &= 2a_8\lambda_{dr}^2 + 2a_6 I_{ds}\lambda_{dr} + 2a_8\lambda_{qr}^2 + 2a_6 I_{qs}\lambda_{qr} \\ z_3 &= \omega_r \\ z_4 &= a_7 I_{qs}\lambda_{dr} - a_7 I_{ds}\lambda_{qr} - a_2 \\ z_5 &= \lambda_{qr} \end{aligned} \tag{4.19}$$

To obtain the dynamics of the new system, the derivatives of the new state $z$ is taken:

$$
\begin{aligned}
\dot{z}_1 =& 2\lambda_{dr}\dot{\lambda}_{dr} + 2\lambda_{qr}\dot{\lambda}_{qr} \\
\dot{z}_2 =& 4a_8\lambda_{dr}\dot{\lambda}_{dr} + a_6\dot{I}_{ds}\lambda_{dr} + 2a_6 I_{ds}\dot{\lambda}_{dr} \\
& + 4a_8\lambda_{qr}\dot{\lambda}_{qr} + 2a_6\dot{I}_{qs}\lambda_{qr} + 2a_6 I_{qs}\dot{\lambda}_{qr} \\
\dot{z}_3 =& \dot{\omega}_r \\
\dot{z}_4 =& a_7\dot{I}_{qs}\lambda_{dr} + a_7 I_{qs}\dot{\lambda}_{dr} - a_7\dot{I}_{dr}\lambda_{qr} - a_7 I_{dr}\dot{\lambda}_{qr} \\
\dot{z}_5 =& \dot{\lambda}_{qr}
\end{aligned}
\tag{4.20}
$$

Once the derivatives of $I_{ds}$, $I_{qs}$, $\lambda_{dr}$, $\lambda_{qr}$ and $\omega_r$ are subsituted into equation (4.20). The following equations are achieved

$$
\begin{bmatrix} \dot{z}_1 \\ \dot{z}_2 \\ \dot{z}_3 \\ \dot{z}_4 \\ \dot{z}_5 \end{bmatrix} = \begin{bmatrix} z_2 \\ f_{z_2}(x,\bar{a}) \\ z_4 \\ f_{z_4}(x,\bar{a}) \\ f_{z_5}(x,\bar{a}) \end{bmatrix} + B \cdot G(\bar{x},\bar{a}) \begin{bmatrix} u_1 \\ u_2 \\ u_3 \end{bmatrix}
\tag{4.21}
$$

where

$$
\begin{aligned}
f_{z_2}(x,\hat{a}) =& [4\hat{a}_8^2(\lambda_{dr}^2 + \lambda_{qr}^2) + 2\hat{a}_3\hat{a}_6(\lambda_{dr}^2 + \lambda_{qr}^2) + 6\hat{a}_6\hat{a}_8(I_{ds}\lambda_{dr} + I_{qs}\lambda_{qr}) \\
& + 2\hat{a}_1\hat{a}_6(I_{ds}\lambda_{dr} + I_{qs}\lambda_{qr}) + 2\hat{a}_6^2 I_{ds}^2 + 2\hat{a}_6^2 I_{qs}^2 + 2\hat{a}_6 I_{qs}\omega_r\lambda_{dr} \\
& - 2\hat{a}_6 I_{ds}\omega_r\lambda_{qr} - 4\hat{a}_4\hat{a}_6\omega_r\lambda_{dr}\lambda_{qr}] \\
f_{z_4}(x,\hat{a}) =& [\hat{a}_1\hat{a}_7 I_{qs}\lambda_{dr} - \hat{a}_7\hat{a}_4\omega_r\lambda_{dr}^2 + \hat{a}_7\hat{a}_8 I_{qs}\lambda_{dr} - \hat{a}_7\omega_r I_{qs}\lambda_{qr} - \hat{a}_1\hat{a}_7 I_{ds}\lambda_{qr} \\
& + \hat{a}_4\hat{a}_7\omega_r\lambda_{qr}^2 - \hat{a}_7\hat{a}_8 I_{ds}\lambda_{qr} - \hat{a}_7\omega_r I_{ds}\lambda_{dr}] \\
f_{z_5}(x,\hat{a}) =& [\hat{a}_8\lambda_{qr} + \omega_r\lambda_{dr} + \hat{a}_6 I_{qs}]
\end{aligned}
\tag{4.22}
$$

and

$$
G(\bar{x},\bar{a}) = \begin{bmatrix} -\hat{a}_4\hat{a}_7\lambda_{qr} & \hat{a}_5\hat{a}_7\lambda_{dr} & -\hat{a}_4\hat{a}_7\lambda_{qr}^2 \\ \hat{a}_5\hat{a}_7\lambda_{dr} & -\hat{a}_5\hat{a}_7\lambda_{qr} & -\hat{a}_4\hat{a}_7\lambda_{qr}^2 \\ 0 & 0 & -\lambda_{dr} \end{bmatrix}
\tag{4.23}
$$

and

$$B = \begin{bmatrix} 0 & 0 & 0 \\ 1 & 0 & 0 \\ 0 & 0 & 0 \\ 0 & 1 & 0 \\ 0 & 0 & 1 \end{bmatrix} \tag{4.24}$$

In order to linearized the system the inputs $u$ must be the following

$$\begin{bmatrix} u_1 \\ u_2 \\ u_3 \end{bmatrix} = G(\bar{x}, \bar{a})^{-1} \cdot \left\{ \begin{bmatrix} v_1 \\ v_2 \\ v_3 \end{bmatrix} - \begin{bmatrix} f_{z_2}(x, \hat{a}) \\ f_{z_4}(x, \hat{a}) \\ f_{z_5}(x, \hat{a}) \end{bmatrix} \right\} \tag{4.25}$$

In order for equation (4.25) to be possible $G(\bar{x}, \bar{a})$ must be invertable, which means the determinant of the matrix $G(\bar{x}, \bar{a})$ must be zero which is the case. When equation (4.25) is substituted in to equation (4.21), the following equations are derived

$$\begin{bmatrix} \dot{z}_1 \\ \dot{z}_2 \\ \dot{z}_3 \\ \dot{z}_4 \\ \dot{z}_5 \end{bmatrix} = \underbrace{\begin{bmatrix} 0 & 1 & 0 & 0 & 0 \\ 0 & 0 & 0 & 0 & 0 \\ 0 & 0 & 0 & 1 & 0 \\ 0 & 0 & 0 & 0 & 0 \\ 0 & 0 & 0 & 0 & 0 \end{bmatrix}}_{A_{new}} \begin{bmatrix} z_1 \\ z_2 \\ z_3 \\ z_4 \\ z_5 \end{bmatrix} + \underbrace{\begin{bmatrix} 0 & 0 & 0 \\ 1 & 0 & 0 \\ 0 & 0 & 0 \\ 0 & 1 & 0 \\ 0 & 0 & 1 \end{bmatrix}}_{B_{new}} \begin{bmatrix} v_1 \\ v_2 \\ v_3 \end{bmatrix} \tag{4.26}$$

It can be seen in equation (4.26) that the new system after the coordinate change, is in fact a linear system.

Before choosing the feedback gain to stabilized system, the system in equation (4.26) must be controllable; the controllability matrix of the system must have full row ranks, which is the case for equation (4.26). Once the system is proven to be controllable, the classical pole-placement technique can be applied. Let $v = -Kz$, chose $K$ such that $A_{new} - B_{new}K$ is Hurwitz, the system stability is therefore guaranteed.

**Adaptive Control Algorithm**

In the previous section, the input-output feedback linearization method was discussed. In this section, the adaptive control component will be introduced in conjuntion with the input-output linearization technique.

In this section, the accent hat $\hat{a}$ or $\hat{z}$ denotes the estimation of the actual value of a parameter or a state variable, the accent tilde $\tilde{a}$ or $\tilde{z}$ denotes the error between the estimation $\hat{a}$ or $\hat{z}$ and the actual value of $a$ or $z$, ie. $\tilde{a} = a - \hat{a}$ or $\tilde{z} = z - \hat{z}$. Given these notations, the state equations obtained previously (equation (4.19)) can be written as thus

$$\begin{aligned}
\hat{z}_1 &= \lambda_{dr}^2 + \lambda_{qr}^2 \\
\hat{z}_2 &= 2\hat{a}_8\lambda_{dr}^2 + 2\hat{a}_6 I_{ds}\lambda_{dr} + 2\hat{a}_8\lambda_{qr}^2 + 2\hat{a}_6 I_{qs}\lambda_{qr} \\
\hat{z}_3 &= \omega_r \\
\hat{z}_4 &= \hat{a}_7 I_{qs}\lambda_{dr} - \hat{a}_7 I_{ds}\lambda_{qr} - \hat{a}_2 \\
\hat{z}_5 &= \lambda_{qr}
\end{aligned} \tag{4.27}$$

To obtain the dynamic equations of the new coordinate system with the adaptive component, the derivatives of $\hat{z}$ states must be taken

$$\begin{aligned}
\dot{\hat{z}}_1 =& 2\lambda_{dr}\dot{\lambda}_{dr} + 2\lambda_{qr}\dot{\lambda}_{qr} \\
\dot{\hat{z}}_2 =& 2\dot{\hat{a}}_8\lambda_{dr}^2 + 4\hat{a}_8\lambda_{dr}\dot{\lambda}_{dr} + 2\dot{\hat{a}}_6 I_{ds}\lambda_{dr} + 2\hat{a}_6\dot{I}_{ds}\lambda_{dr} + 2\hat{a}_6 I_{ds}\dot{\lambda}_{dr} \\
& + 2\dot{\hat{a}}_8\lambda_{qr}^2 + 4\hat{a}_8\lambda_{qr}\dot{\lambda}_{qr} + 2\dot{\hat{a}}_6 I_{qr}\lambda_{qr} + 2\hat{a}_6\dot{I}_{qs}\lambda_{qr} + 2\hat{a}_6 I_{qs}\dot{\lambda}_{qr} \\
\dot{\hat{z}}_3 =& \dot{\omega}_r \\
\dot{\hat{z}}_4 =& \dot{\hat{a}}_7 I_{qs}\lambda_{dr} + \hat{a}_7\dot{I}_{qs}\lambda_{dr} + \hat{a}_7 I_{qs}\dot{\lambda}_{dr} - \dot{\hat{a}}_7 I_{ds}\lambda_{qr} - \hat{a}_7\dot{I}_{ds}\lambda_{qr} \\
& - \hat{a}_7 I_{ds}\dot{\lambda}_{qr} - \dot{\hat{a}}_2 \\
\dot{\hat{z}}_5 =& \dot{\lambda}_{qr}
\end{aligned} \tag{4.28}$$

Taking equation (4.28) and substituting the derivative of the original state variables, the new state equations can be expressed in the following way:

$$
\begin{aligned}
\dot{\hat{z}}_1 =& f_{z_1}(x,\hat{a}) + g_{z_1}(x,\hat{a},u) + \Omega_{z_1}(x,\dot{\hat{a}}) + \Psi_{z_1}(x,u,\hat{a},\tilde{a}) \\
\dot{\hat{z}}_2 =& f_{z_2}(x,\hat{a}) + g_{z_2}(x,\hat{a},u) + \Omega_{z_2}(x,\dot{\hat{a}}) + \Psi_{z_2}(x,u,\hat{a},\tilde{a}) \\
\dot{\hat{z}}_3 =& f_{z_3}(x,\hat{a}) + g_{z_3}(x,\hat{a},u) + \Omega_{z_3}(x,\dot{\hat{a}}) + \Psi_{z_3}(x,u,\hat{a},\tilde{a}) \\
\dot{\hat{z}}_4 =& f_{z_4}(x,\hat{a}) + g_{z_4}(x,\hat{a},u) + \Omega_{z_4}(x,\dot{\hat{a}}) + \Psi_{z_4}(x,u,\hat{a},\tilde{a}) \\
\dot{\hat{z}}_5 =& f_{z_5}(x,\hat{a}) + g_{z_5}(x,\hat{a},u) + \Omega_{z_5}(x,\dot{\hat{a}}) + \Psi_{z_5}(x,u,\hat{a},\tilde{a})
\end{aligned}
\tag{4.29}
$$

Details on derivation see equation (6.1) and equation (6.2) can be found in the Annex section on page 119. Functions $f_z(x,\hat{a})$ can be seen as the system equations and $g_z(x,\hat{a},u)$ can be seen as the input equations. Given $f_z(x,\hat{a})$ and $g_z(x,\hat{a},u)$ are derived, in subsequent derivations one will see that $\dot{\hat{z}} = f_z(x,\hat{a}) + g_z(x,\hat{a},u)$ will undergo a coordinate transformation and become a linear system. $\Omega_z(x,\dot{\hat{a}})$ and $\Psi_z(x,\tilde{a})$ are the adaptive components and will be driven to zero by the adaptive control technique.

Define $\dot{\hat{z}} = f_z(x,\hat{a}) + g_z(x,\hat{a},u)$, let $g_z(x,\hat{a},u) = G(\bar{x},\hat{a})\bar{u}$

Chose the new inputs $\bar{v}$ to be

$$
\begin{bmatrix} v_1 \\ v_2 \\ v_3 \end{bmatrix} = \begin{bmatrix} f_{z_2}(x,\hat{a}) \\ f_{z_4}(x,\hat{a}) \\ f_{z_5}(x,\hat{a}) \end{bmatrix} + B \cdot G(\bar{x},\hat{a}) \begin{bmatrix} u_1 \\ u_2 \\ u_3 \end{bmatrix}
\tag{4.30}
$$

where

$$
\begin{aligned}
f_{z_2}(x,\hat{a}) =& [4\hat{a}_8^2(\lambda_{dr}^2 + \lambda_{qr}^2) + 2\hat{a}_3\hat{a}_6(\lambda_{dr}^2 + \lambda_{qr}^2) + 6\hat{a}_6\hat{a}_8(I_{ds}\lambda_{dr} + I_{qs}\lambda_{qr}) \\
& + 2\hat{a}_1\hat{a}_6(I_{ds}\lambda_{dr} + I_{qs}\lambda_{qr}) + 2\hat{a}_6^2 I_{ds}^2 + 2\hat{a}_6^2 I_{qs}^2 + 2\hat{a}_6 I_{qs}\omega_r\lambda_{dr} \\
& - 2\hat{a}_6 I_{ds}\omega_r\lambda_{qr} - 4\hat{a}_4\hat{a}_6\omega_r\lambda_{dr}\lambda_{qr}] \\
f_{z_4}(x,\hat{a}) =& [\hat{a}_1\hat{a}_7 I_{qs}\lambda_{dr} - \hat{a}_7\hat{a}_4\omega_r\lambda_{dr}^2 + \hat{a}_7\hat{a}_8 I_{qs}\lambda_{dr} - \hat{a}_7\omega_r I_{qs}\lambda_{qr} - \hat{a}_1\hat{a}_7 I_{ds}\lambda_{qr} \\
& + \hat{a}_4\hat{a}_7\omega_r\lambda_{qr}^2 - \hat{a}_7\hat{a}_8 I_{ds}\lambda_{qr} - \hat{a}_7\omega_r I_{ds}\lambda_{dr}] \\
f_{z_5}(x,\hat{a}) =& [\hat{a}_8\lambda_{qr} + \omega_r\lambda_{dr} + \hat{a}_6 I_{qs}]
\end{aligned}
\tag{4.31}
$$

and

$$G(\bar{x},\hat{a}) = \begin{bmatrix} 2\hat{a}_6\hat{a}_5\lambda_{dr} & 2\hat{a}_6\hat{a}_5\lambda_{qr} & 2\hat{a}_6\hat{a}_4\lambda_{dr}\lambda_{qr} \\ -\hat{a}_5\hat{a}_7\lambda_{qr} & \hat{a}_5\hat{a}_7\lambda_{dr} & -\hat{a}_4\hat{a}_7\lambda_{qr}^2 \\ 0 & 0 & -\lambda_{dr} \end{bmatrix} \tag{4.32}$$

and

$$B = \begin{bmatrix} 0 & 0 & 0 \\ 1 & 0 & 0 \\ 0 & 0 & 0 \\ 0 & 1 & 0 \\ 0 & 0 & 1 \end{bmatrix} \tag{4.33}$$

The control law can be written as

$$\begin{bmatrix} u_1 \\ u_2 \\ u_3 \end{bmatrix} = G(\bar{x},\hat{a})^{-1} \cdot \left\{ \begin{bmatrix} v_1 \\ v_2 \\ v_3 \end{bmatrix} - \begin{bmatrix} f_{z_2}(x,\hat{a}) \\ f_{z_4}(x,\hat{a}) \\ f_{z_5}(x,\hat{a}) \end{bmatrix} \right\} \tag{4.34}$$

The control law expressed in equation (4.34) can only be implemented if the matrix $G(\bar{x},\hat{a})$ is invertable. As mentioned before $G(\bar{x},\hat{a})$ is invertable because its determinant is zero. Another assumption is that all the variables involved in equation (4.31) are measurable. All variables are measureable in equation (4.31), however typically in industry the rotor flux vectors are estimated using adaptive rotor flux observer [34].

By substituting equation (4.34) into equation (4.29), we get

$$\begin{aligned} \dot{\hat{z}}_1 &= \hat{z}_2 + \Omega_{z_1}(x,\dot{\hat{a}}) + \Psi_{z_1}(x,\tilde{a}) \\ \dot{\hat{z}}_2 &= v_1 + \Omega_{z_2}(x,\dot{\hat{a}}) + \Psi_{z_2}(x,\tilde{a}) \\ \dot{\hat{z}}_3 &= \hat{z}_4 + \Omega_{z_3}(x,\dot{\hat{a}}) + \Psi_{z_3}(x,\tilde{a}) \\ \dot{\hat{z}}_4 &= v_2 + \Omega_{z_4}(x,\dot{\hat{a}}) + \Psi_{z_4}(x,\tilde{a}) \\ \dot{\hat{z}}_5 &= v_3 + \Omega_{z_5}(x,\dot{\hat{a}}) + \Psi_{z_5}(x,\tilde{a}) \end{aligned} \tag{4.35}$$

The state equation in equation (4.35) is composed of a linear $5^{th}$ order system plus an adaptive component:

$$\dot{\hat{z}} = [A]\hat{z} + [B_{adapt}]v + \Omega\dot{\hat{a}} + \Psi^T\tilde{a} \tag{4.36}$$

The individual components in equation (4.36) are:

$$\dot{z} = \begin{bmatrix} \dot{z}_1 \\ \dot{z}_2 \\ \dot{z}_3 \\ \dot{z}_4 \\ \dot{z}_5 \end{bmatrix}, v = \begin{bmatrix} v_1 \\ v_2 \\ v_3 \end{bmatrix}, \dot{\hat{a}} = \begin{bmatrix} \dot{\hat{a}}_1 \\ \dot{\hat{a}}_2 \\ \dot{\hat{a}}_3 \\ \dot{\hat{a}}_4 \\ \dot{\hat{a}}_5 \\ \dot{\hat{a}}_6 \\ \dot{\hat{a}}_7 \\ \dot{\hat{a}}_8 \end{bmatrix}, \tilde{a} = \begin{bmatrix} \tilde{a}_1 \\ \tilde{a}_2 \\ \tilde{a}_3 \\ \tilde{a}_4 \\ \tilde{a}_5 \\ \tilde{a}_6 \\ \tilde{a}_7 \\ \tilde{a}_8 \end{bmatrix}$$

$$[A] = \begin{bmatrix} 0 & 1 & 0 & 0 & 0 \\ 0 & 0 & 0 & 0 & 0 \\ 0 & 0 & 0 & 1 & 0 \\ 0 & 0 & 0 & 0 & 0 \\ 0 & 0 & 0 & 0 & 0 \end{bmatrix}, [B_{adapt}] = \begin{bmatrix} 0 & 0 & 0 \\ 1 & 0 & 0 \\ 0 & 0 & 0 \\ 0 & 1 & 0 \\ 0 & 0 & 1 \end{bmatrix}$$

$$\Omega = \begin{bmatrix} 0 & 0 & 0 & 0 & 0 & 0 & 0 & 0 \\ 0 & 0 & 0 & 0 & 0 & 2(I_{ds}\lambda_{dr} + I_{qs}\lambda_{qr}) & 0 & 2(\lambda_{dr}^2 + \lambda_{qr}^2) \\ 0 & 0 & 0 & 0 & 0 & 0 & 0 & 0 \\ 0 & -1 & 0 & 0 & 0 & 0 & I_{qs}\lambda_{dr} - I_{ds}\lambda_{qr} & 0 \\ 0 & 0 & 0 & 0 & 0 & 0 & 0 & \end{bmatrix}$$

$$\Psi^T\tilde{a} = \begin{bmatrix} \Psi_{z_1}^T \\ \Psi_{z_2}^T \\ \Psi_{z_3}^T \\ \Psi_{z_4}^T \\ \Psi_{z_5}^T \end{bmatrix} \tag{4.37}$$

Given equation (4.36), first we are to stabilize the first portion of the equation:

$$\left[A\right]\hat{z} + \left[B\right]v \tag{4.38}$$

chose $v = -K_1\hat{z}$

In control theory a linear system is said to be stable if its poles have negative real parts, let $p$ be a vector containing negative and real numbers. Compute a state-feedback matrix $K_1$ such that the eigenvalues of $A - B \cdot K_1$ are those specified in the vector $p$. This is the classical pole placement method.

Once the poles have been chosen and the gain $K_1$ is obtained, the linear portion of the system $f(\hat{z}, \hat{a})$ is stable.

To design the adaptive law, let $\bar{e}$ be the error augmentation, and $\bar{\eta}$ be the augmented error such that:

$$\begin{aligned} \dot{\bar{e}} &= A_s\bar{e} + \Omega\dot{\hat{a}} \\ \bar{\eta} &= \hat{z} - \bar{e} \end{aligned} \tag{4.39}$$

Where $A_s$ is such that:

$$A_s = A - B \cdot K_1 \tag{4.40}$$

Given equation (4.39) and equation (4.40), equation (4.36) becomes:

$$\dot{\hat{z}} = A_s\bar{\eta} + \Psi^T\tilde{a} + \dot{\bar{e}} \tag{4.41}$$

The adaptation law can be derive by using Lyapunov stability theorem. let $V$ be the Lyapunov candidate function:

$$V = \bar{\eta}^T P\bar{\eta} + \tilde{a}^T\Gamma^{-1}\tilde{a} \tag{4.42}$$

Such that

$\Gamma > 0$

Let the Lyapunov equations be

$$\begin{aligned} A_s^T P + PA_s &= -Q \\ Q &> 0 \end{aligned} \tag{4.43}$$

Therefore $P > 0$, and $V > 0$

In order for the system to be stable, the derivative of the Lyapunov function must be semi-negative definite:

$$\dot{V} = -\bar{\eta}^T Q\bar{\eta} + 2\tilde{a}^T(\Psi P\bar{\eta} - \Gamma^{-1}\dot{\hat{a}}) \tag{4.44}$$

If one chose $\dot{\hat{a}} = \Gamma\Psi P\bar{\eta}$ then $\dot{V} = -\bar{\eta}^T Q\bar{\eta}$, $\dot{V}$ is thus semi-negative definite, the system is stable. In summary, the Control law is:

$$\begin{bmatrix} u_1 \\ u_2 \\ u_3 \end{bmatrix} = G(\bar{x}, \hat{a})^{-1} \cdot \left\{ \begin{bmatrix} v_1 \\ v_2 \\ v_3 \end{bmatrix} - \begin{bmatrix} f_{z_2}(x, \hat{a}) \\ f_{z_4}(x, \hat{a}) \\ f_{z_5}(x, \hat{a}) \end{bmatrix} \right\} \tag{4.45}$$

The adaptive law is:

$$\begin{aligned} \dot{\hat{a}} &= \Gamma\Psi P\bar{\eta} \\ \bar{\eta} &= \hat{z} - \bar{e} \\ \dot{\bar{e}} &= A_s\bar{e} + \Omega\dot{\hat{a}} \\ \bar{e}(0) &= 0 \end{aligned} \tag{4.46}$$

In summary, this section of the thesis provides the theoretical techniques to obtain the control law equation (4.45) and the adaptive law equation (4.46). The control law is responsible for transforming a nonlinear system into a linear system to which pole placement method can be applied. The adaptive law enables the controller to be sensitive to change in parameter. With the combination of the control law and the adaptive law, the system stability is guaranteed.

**Implementation of Input-Output Linearization and Adaptive Law**

Given the theory of input-output linearization and adaptive control established in the previous section, the next step is to establish a structure which the theory can be implemented:

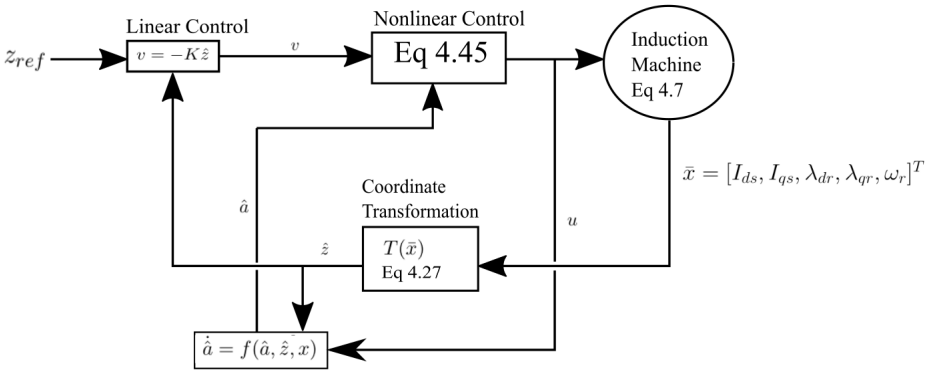


FIGURE 4.3: Full block diagram

Displayed in figure 4.3, there are four major blocks which represents the four major components of the entire system required to demonstrate the effectiveness of proposed control algorithm. The system is composed of the induction machine model, a coordinate transformation block, the adaptive control block and the controller itself. Each of the individual blocks will be discuss in detail.

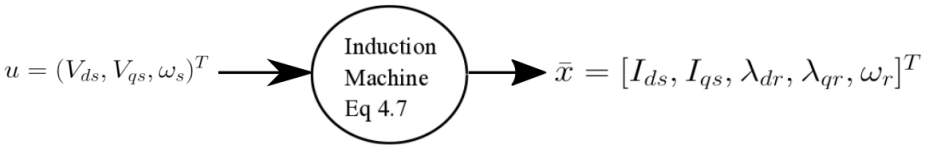


FIGURE 4.4: Induction Machine Block

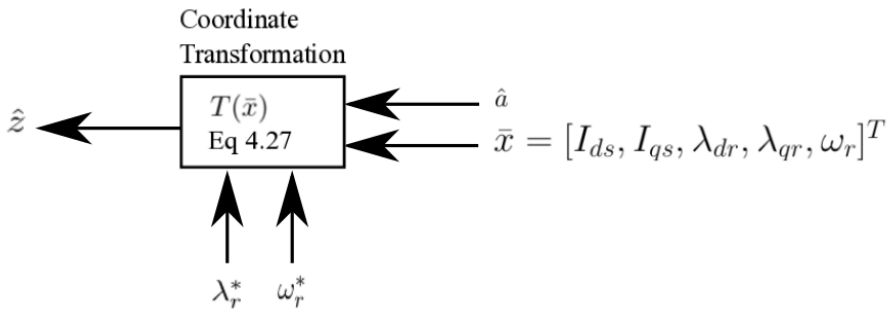


FIGURE 4.5: Coordinate Transformation Block

In figure 4.5 is shown the Simulink block that is used in simulation. The inputs of this block are the reference mechanical speed $\omega_r^*$, reference rotor flux $\lambda_r^*$, the estimated system parameters $a_{estimate}$ ($\hat{a}$) and the state variables calculated in the induction machine block in figure 4.4. The rotor flux reference is set to the rated rotor flux. The mechanical speed reference $\omega_r^*$ is the variable that the proposed controller is intended to control. By using the coordinate transformation equations in equation (4.27), the new coordinate system is obtained which is the output for the block named gamma estimate.

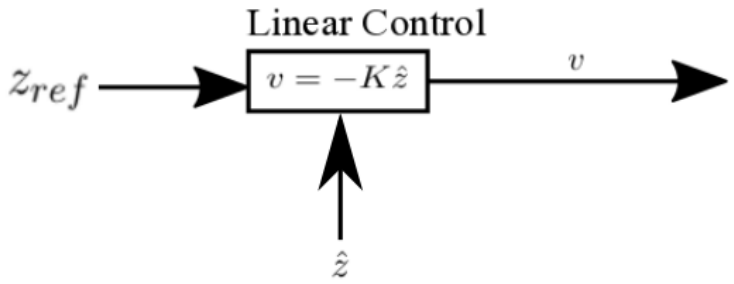


FIGURE 4.6: Feedback Gain

Once the feedback gain is implemented into the simulation model. The linear system portion denoted in equation (4.38) will have guaranteed stability. Note that $z_{ref}$ comes from the original reference states $\lambda_r^*$ and $\omega_r^*$ which is transformed in $z$ coordinates shown by figure 4.5.

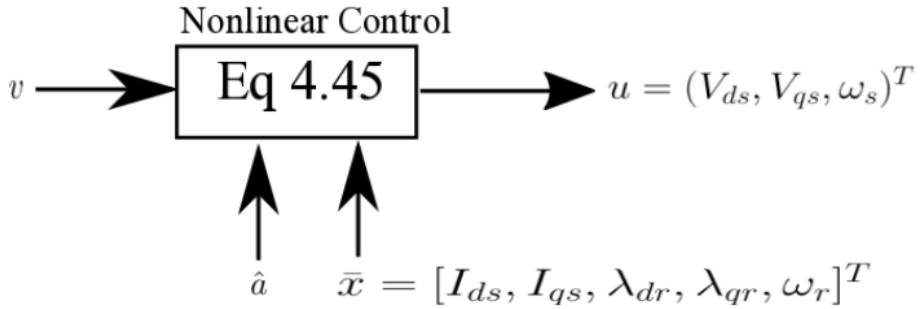


FIGURE 4.7: Controller Block

Shown in figure 4.7 is the block which encapsulates equation (4.45). It was established that the new inputs $v_1$, $v_2$ and $v_3$ were introduced in equation (4.30) to stabilize the induction machine system in order to apply pole placement technique to ensure system stability. After the system is stabilized through feedback block (figure 4.6), the new inputs has to be converted back to the original system inputs $V_{ds}$, $V_{qs}$ and $\omega_s$ which is the purpose of the controller block.

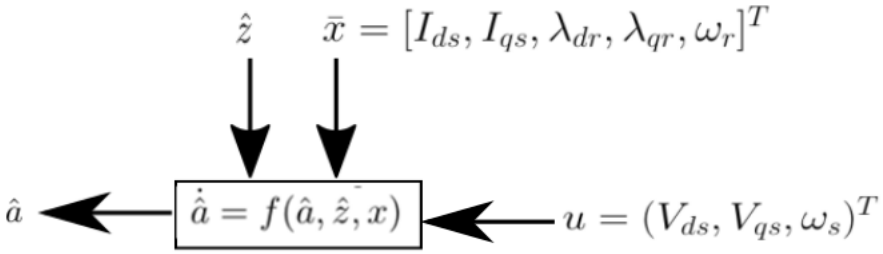


FIGURE 4.8: Adaptive Law Block

The block shown in figure 4.8 covers equation (4.46). The adaptive law block takes as inputs the states generated by the induction machine model in figure 4.4. The new states in the new coordinate system ($\hat{z}$) generated by the coordinate system transformation block in figure 4.5. Within the adaptive law block there are three other blocks that function collectively to achieve the adaptive law.

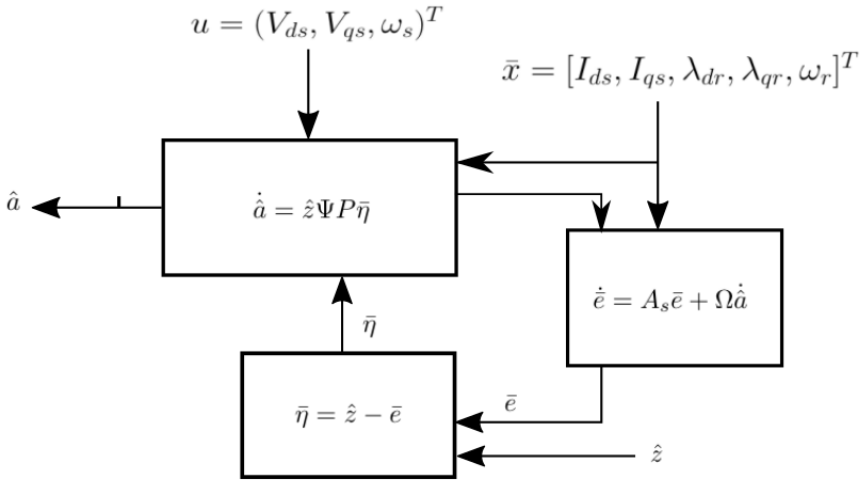


FIGURE 4.9: Adaptive Law Block Subroutines

In figure 4.9, it can be seen how the three subroutine blocks work together to achieve the direct adaptive law. The three subroutine blocks are $e$ which represents the error augmentation, $\eta$ which represents the augmented error and $\dot{\hat{a}}$ block which represents the adaptive law discussed in page 67 on adaptive algorithm.

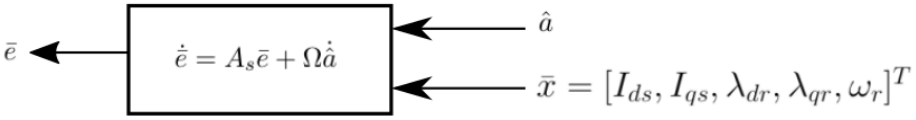


FIGURE 4.10: Error Augmentation Block

The error augmentation block in figure 4.10 calculates the first part of equation (4.39) where $\dot{\bar{e}} = A_s\bar{e} + \Omega\dot{\hat{a}}$, which is a first order differential equation. The initial condition of $e$ is set as zero. $A_s$ is the stabilized system matrix, $\Omega$ is the matrix established in equation (4.37).

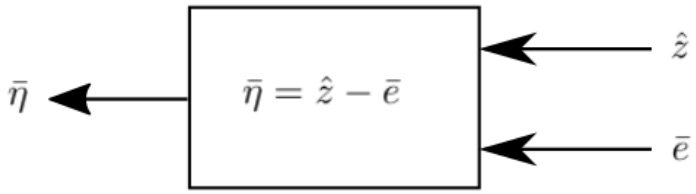


FIGURE 4.11: Augmented Error Block

Once the error augmentation $e$ has been achieved, the augmented error $\eta$ can be calculated in figure 4.11 where $\bar{\eta} = \hat{z} - \bar{e}$.

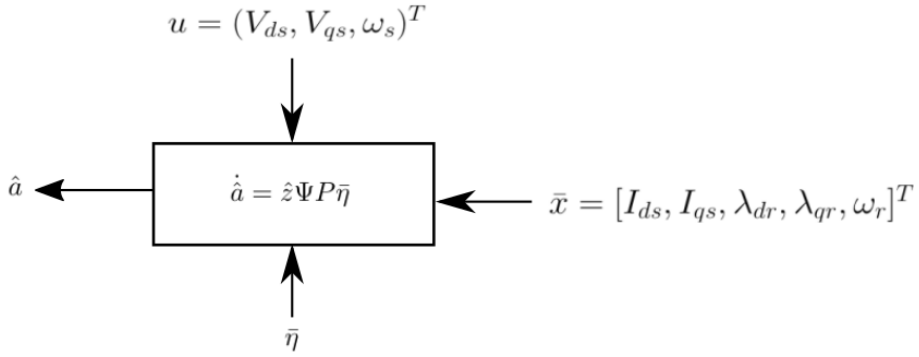


FIGURE 4.12: Parameter Estimation Block

Shown in figure 4.12 is a block that encapsulates the calculation required to find the estimation of the system parameters $a_1$ to $a_8$. The equations is derived previously in equation (4.46) where $\dot{\hat{a}} = z\Psi P\bar{\eta}$. $P$ is not to be confused with the number of pole pairs, $P$ is a positive real number. The matrix $\Gamma$ can be a positive real number of a diagonal matrix consisting of positive real number. $\Gamma$ is the gain that is used for the adaptive law. In order to tune the gain for individual system parameters which there are eight ($a_1$ to $a_8$), a diagonal matrix is used. The individual numbers on the diagonal dictates the adaptive gain for each system parameter.

$$\Gamma = \begin{bmatrix} \Gamma_1 & 0 & 0 & 0 & 0 & 0 & 0 & 0 \\ 0 & \Gamma_2 & 0 & 0 & 0 & 0 & 0 & 0 \\ 0 & 0 & \Gamma_3 & 0 & 0 & 0 & 0 & 0 \\ 0 & 0 & 0 & \Gamma_4 & 0 & 0 & 0 & 0 \\ 0 & 0 & 0 & 0 & \Gamma_5 & 0 & 0 & 0 \\ 0 & 0 & 0 & 0 & 0 & \Gamma_6 & 0 & 0 \\ 0 & 0 & 0 & 0 & 0 & 0 & \Gamma_7 & 0 \\ 0 & 0 & 0 & 0 & 0 & 0 & 0 & \Gamma_8 \end{bmatrix} \tag{4.47}$$

# Chapter 5

# Simulation Results

To establish the context of the test simulations, WECS setup of the simulation will be based on a setup illustrated in figure 5.1

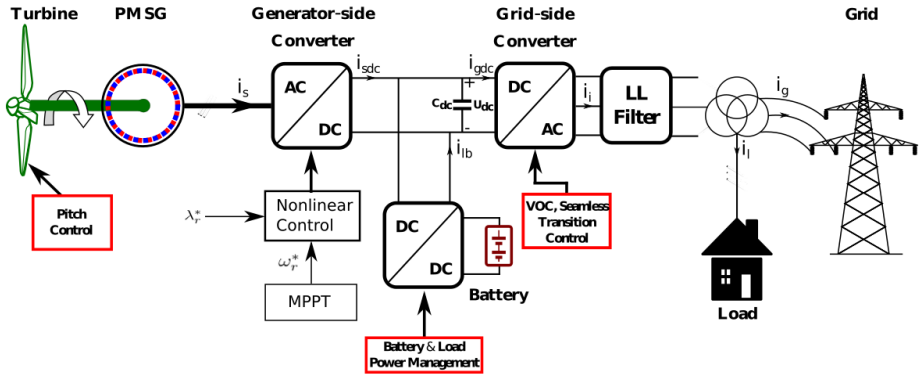


FIGURE 5.1: WECS setup [1]

The wind turbine will turn a shaft that is the rotor of the SCIG. The SCIG stator is connected to the generator-converter. Note that the controller designed in this thesis will only control the generator-side converter. The controller for voltage on the grid side will be a different control design which is not the topic of this thesis.

The method of showing the effectiveness of the proposed control algorithm is to compare with conventional methods. It is preferred to compare non-linear adaptive control to several different control methods such as Direct Torque Control and Field Oriented Control to see the pros and cons of adaptive control. In order to do the comparison a simulation model of the controller has to be implemented using the same induction machine model with the same parameters. Due to the limited time and resources available, only one conventional controller will be used in comparison,

namely Field Oriented Control. Field Oriented Control is chosen because it is the most popular controller used in industry to drive induction machines for both motor and generator applications. Furthermore, FOC uses the field orientation component which will be necessary for non-linear adaptive control as well.

TABLE 5.1: System Specifications [2]

| | |
|---|---|
| Rated Output Power | 2.30 MW |
| Rated Mechanical Power | 2.3339 MW |
| Rated Apparent Power | 2.59 MVA |
| Rated Line to line Voltage | 690 V (rms) |
| Rated Phase Voltage | 398.4 V (rms) |
| Rated Stator Current | 2169 A |
| Rated Stator Frequency | 50 Hz |
| Rated Power Factor | 0.888 |
| Rated Rotor Speed | 1512 rpm |
| Rated Slip | -0.008 |
| Number of Pole Pair | 2 |
| Rated Mechanical Torque | 14.74 kN·m |
| Rated Stator Flux Linkage | 1.2748 Wb (rms) |
| Rated Rotor Flux Linkage | 1.2096 Wb (rms) |
| Stator Winding Resistance, $R_s$ | 1.102 $m\Omega$ |
| Rotor Winding Resistance, $R_r$ | 1.497 $m\Omega$ |
| Stator Leakage Inductance, $L_{ls}$ | 0.06492 mH |
| Rotor Leakage Inductance, $L_{lr}$ | 0.06492 mH |
| Magnetizing Inductance, $L_m$ | 2.13461 mH |
| Moment of Inertia, $J$ | 1200 $kg \cdot m^2$ |
| Inertia Time Constant, $H$ | 5.8078 sec |
| Base Flux Linkage, $\Lambda_B$ | 1.2681 Wb (rms) |
| Base Impedance, $Z_B$ | 0.1838 $\Omega$ |
| Base Inductance, $L_B$ | 0.58513 mH |
| Base Capacitance, $C_B$ | 17316.17 $\mu F$ |

The parameters for the induction machine is given in the table above. These parameters are very standard parameters used in many WECS simulation models.

There're different modes to control a SCIG, one can control the torque or the speed. For the algorithm proposed previously, the controller will be controlling the speed. The electrical torque will be kept constant at the rated mechanical torque of the generator.

The states of the induction machine block given the inputs is generated by the state space equations given in equation (4.7). The initial conditions of the state variable are set as the steady states of the states at equilibrium. The steady state initial condition is a realistic initial condition because most wind energy systems are brought to operating speed by an external motor. The steady state values are found by setting the derivative of the state equations to zero. Moreover, the terms containing the inputs ought to be taken out of the equation. This can be demonstrated in equation (5.1)

$$\begin{aligned}
0 &= a_1 I_{ds} + a_3 \lambda_{dr} - a_4 \omega_r \lambda_{qr} \\
0 &= a_1 I_{qs} - a_4 \omega_r \lambda_{dr} + a_3 \lambda_{qr} \\
0 &= a_8 \lambda_{dr} - \omega_r \lambda_{qr} + a_6 I_{ds} \\
0 &= a_8 \lambda_{qr} + \omega_r \lambda_{dr} + a_6 I_{qs} \\
0 &= a_7 I_{qs} \lambda_{dr} - a_7 I_{ds} \lambda_{qr} - a_2
\end{aligned} \tag{5.1}$$

The initial conditions of the induction machine model are used to begin the simulation is set to the steady-state values in order to simplify the calculation at the beginning of the simulation before any perturbations are introduced. In order to calculate the state variables at steady-state, the parameters of the induction machine has to be taken from the specifications of the generator.

Given in equation (4.8), the parameter of the system can be calculated using the values of table 5.1 the system parameters can be calculated in equation (5.2).

$$\begin{aligned}
L_s &= L_{ls} + L_m \\
L_r &= L_{Lr} + L_m \\
D &= 1/(L_r L_s - L_m^2) \\
a_1 &= D(-L_r R_s - R_r L_m^2 / L_r) = -19.6362 \\
a_2 &= P T_m / J = 24.5667 \\
a_3 &= R_r L_s D^2 L_m - R_r L_m^3 D^2 / L_r = 5.1633 \times 10^3 \\
a_4 &= D L_m = 7.5864 \times 10^3 \\
a_5 &= D L_r = 7.8171 \times 10^3 \\
a_6 &= R_r L_m / L_r = 0.0015 \\
a_7 &= 3P^2 L_m / (2 J L_r) = 0.0049 \\
a_8 &= -R_r L_s D + R_r L_m^2 D / L_r = -0.6806
\end{aligned} \tag{5.2}$$

Once the coefficients have been calculated in equation (5.2), one can start calculating some of the steady-state variables. Some state variable values at steady-state are already known. Since the objective is to control $\lambda_{dr}$ such that it approaches the reference flux value $\lambda_r^*$, and $\lambda_{qr}$ such that it approaches zero. The electrical rotor speed at equilibrium will be $N^* = 1512rpm$ which is equivalent to $158rads/s$. Therefore $\lambda_{dr-equilibrium} = 1.711Wb$, and $\lambda_{qr-equilibrium} = 0$. Setting the initial conditions of the SCIG to these steady-state is a reasonable assumption because in many cases a wind turbine is brought to operating speed by a separate motor.

## 5.1 FOC Model Setup

The FOC model will be based on one that is shown in figure 2.4. The field orientation portion will be omitted for the present, all simulations will be conducted in the $dq$ reference frame to simplify the simulation.

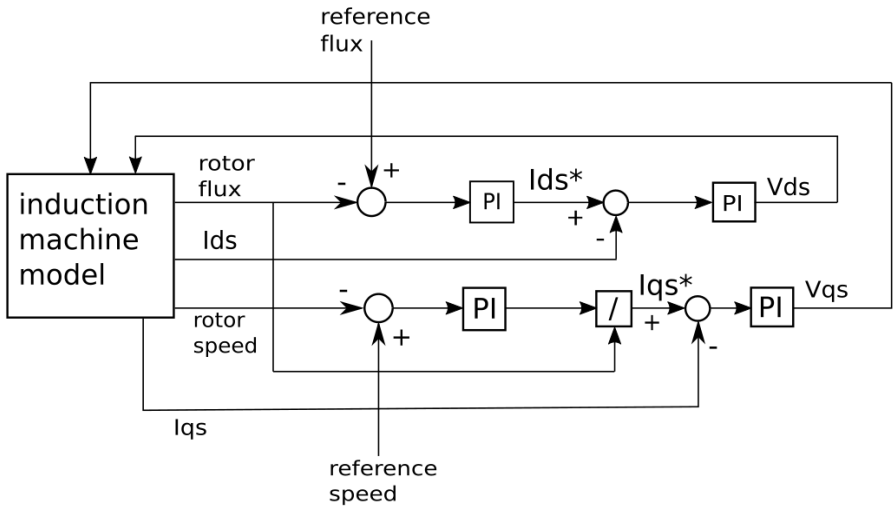


FIGURE 5.2: DFOC Simulation Model

Shown in figure 5.2 is the simulation model of FOC. The model is based on figure 2.4 which was discussed previously in the literature review section. Induction Machine block is the same block used in building the adaptive control model in figure 4.4 using the same system parameters.

The synchronous speed $\omega_s$ is kept constant at the rated stator frequency $50Hz$. The inputs to the induction machine is the stator voltage in $dq$ reference frame. The PID controller block labeled PID Controller 1 regulates the the rotor flux $\lambda_r$ which produces the reference for $I^*_{ds}$. PID controller 2 regulates the difference between $I^*_{ds}$ and $I_{ds}$ to produced the input $V_{ds}$. PID controller 4 regulates the difference between the reference rotor speed $\omega^*_r$ and the actual rotor speed $\omega_r$ which produces the reference $I^*_{qs}$. PID Controller 2 regulates the difference between $I^*_{qs}$ and $I_{qs}$ to produce the input $V_{qs}$.

## 5.2 Method of Comparison

The performance of adaptive control must have realistic application advantages. As discuss previously in section 3, there are two limitations of FOC which the proposed nonlinear adpative control will improve upon. One issue is the range of stability is limited for FOC, since PID controllers only optimally tuned for a certain operating point. The second limitation of FOC is the uncertainty of stability when the parameters are unknown or changes during operation. The goal of testing the adaptive control method is two fold:

1. To test the performance of adaptive control for wide operation ranges.
2. To test the performance of adaptive control when the parameters of a machine are unknown or varying with time.

To test the performance of adaptive control, that performance has to be compared with a standard, in this case the standard will be FOC. To assess the first criteria one can already see some difficulties with FOC. Typically FOC utilizing PID controllers works optimally for a certain operating point. In the case of WECS, the generator is required to function in a wide range of speeds. The PID controllers in FOC will deteriorate in performance as the reference output strays away from the operating point which the controller is tuned.

The second point of contention is also obvious for FOC. Most of the time parameter identification is impossible or economically not viable for generators already installed. Therefore FOC controllers are tuned according to similar machines off-line. The problem with this approach is that no two machine are identical, therefore error in tuning of the controller will be the result.

The direct adaptive control technique proposed will in theory solve both of the difficulties present for FOC. The input-output linearization control will stabilize the system in all operating ranges, the adaptive component will resolve the issue of uncertain or time varying system parameters.

Let us test the first hypothesis, that the system parameters are known. Let's assume that the FOC controller is tuned based on an induction machine with idea parameters. The gains for the PID controllers are the following:

TABLE 5.2: PID controller gains

| | |
|---|---|
| PID Controller 1 | P=1, I=0, D=0 |
| PID Controller 2 | P=1, I=1, D=0 |
| PID Controller 3 | P=1, I=0, D=0 |
| PID Controller 4 | P=100, I=2, D=10 |

The controller gains shown above are obtained using trial and error, it is very difficult to derive a systematic way to find the good tuning of a drive that is based on PID controllers. It is also difficult to simulate the actual reference rotor speed because the reference speed is derived from the Maximum Power Point Tracking (MPPT) scheme discussed on page 53. The MPPT scheme provides an optimal rotor speed reference based on the wind speed. However the wind speed is unpredictable and random, therefore the reference rotor speed is unpredictable and random; which makes the prediction of how the system parameters will vary almost impossible.

As for the nonlinear adaptive control simulation, the poles are chosen to be $p = [-100, -100, -100, -20, -20]$. The signs of the poles has to be negative real, the magnitude of the poles are chosen via trial and error. Some intuition can be applied when choosing the poles of the system, base on which states has faster response than other states, but very often when adaptive control is applied in conjunction with input-output linearization, the system is very complex and the system poles may affect the adaptive control. It becomes difficult to use any theory to chose the poles, therefore trial and error is generally used.

Given the poles of the system and the system matrix $A$ and the input matrix $B$ given in equation (4.37), the feedback gain matrix $K$ can be obtained using matlab:

$$[K] = \begin{bmatrix} 2000 & 120 & 0 & 0 & 0 \\ 0 & 0 & 2000 & 120 & 0 \\ 0 & 0 & 0 & 0 & 100 \end{bmatrix} \tag{5.3}$$

It would suffice for the purpose of testing to assume a rotor reference speed within the limit of the rated speed and provide a step change to a different rotor reference speed. The reference signal will cover the entire range of the generator operating speeds. The stability of the two controllers will be compared and analysed.

The second objective is to compare the performance of the two controller when the parameters are unknown or time varying. The problem here is that the simulation in both cases requires a functioning model which would require the system parameters, thus lies the problem because the parameters are supposedly unknown. If the parameters are time varying, there no way to know how they vary, and by how much. One way to conduct this simulation is to tune the two controllers according to ideal parameters, then alter the parameters of the machine one by one and compare the performance of the two controllers.

## 5.3 Range of Stability for FOC

The plan to tackle the parameter uncertainty problem is as follow. Both controllers will be tuned to the ideal parameters. The same controllers will be tested on an induction machine with slightly different parameters.

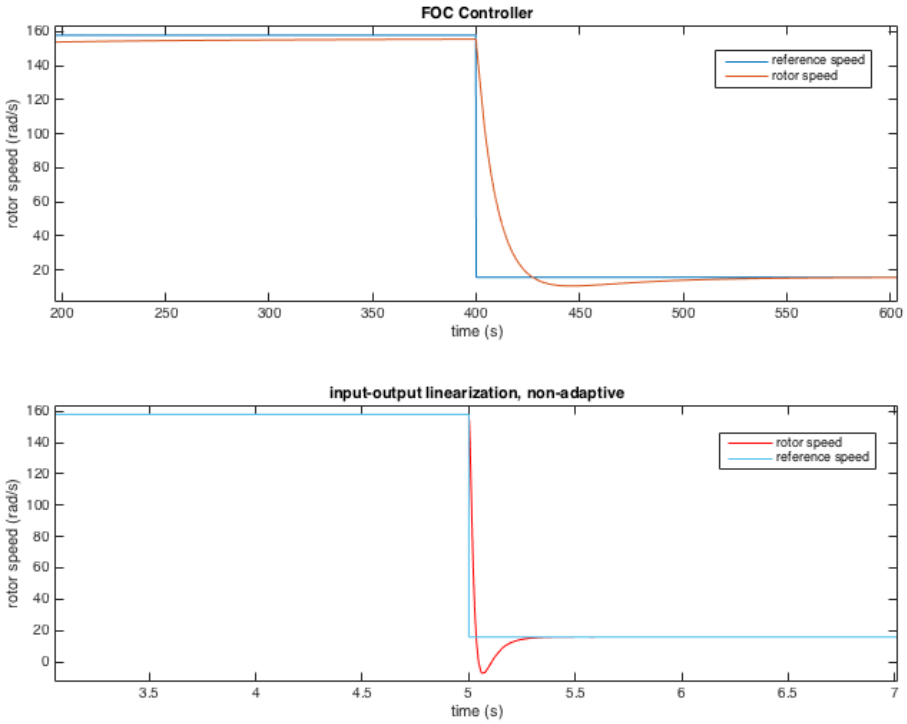


FIGURE 5.3: FOC and input-output linearization performance with ideal parameters, from 100% rated speed to 10% rated speed

Shown in figure 5.3 are the performance of FOC and nonlinear adaptive control. Both controllers are tuned to ideal parameters. The adaptive portion of the nonlinear adaptive control is turned off, this is to demonstrate the range of stability of input-output linearization technique. The reference speed which the generator will track starts at 100% operating speed, then the step decrease will be to 10% operating speed. This covers the full operating range of the generator.

The two simulations are done for different times. For FOC, the simulation is conducted over 800s with the step change at t=400s. The nonlinear adaptive control simulation is conducted over 10s with the step change

occurring at t=5s. This is to show the quickness in response of the non-linear controller. With input-output lineariztion, the transient response is a fraction of a second. Where as in FOC, the transient can last over 100s. The conclusion is that both controllers are able to stabilize the generator with operating speeds from 100% to 10% rated speeds, however the response of the input-output linearization is far superior to that of FOC.

One must know that sometimes a system can be simulated to produce a result when in reality it is impossible. In this example the speed tracking performance for the input-output linearization occurs in a matter of milliseconds when the reference speed changes. The generator in reality cannot change speed as fast as in the simulation. In this case, the discrepancy between real performance and simulation is not an issue because the difference of performance between FOC and input-output linearization is so vast. Even if the input-output linearization control cannot track the speed as fast as the simulation, it is still definitely faster than FOC.

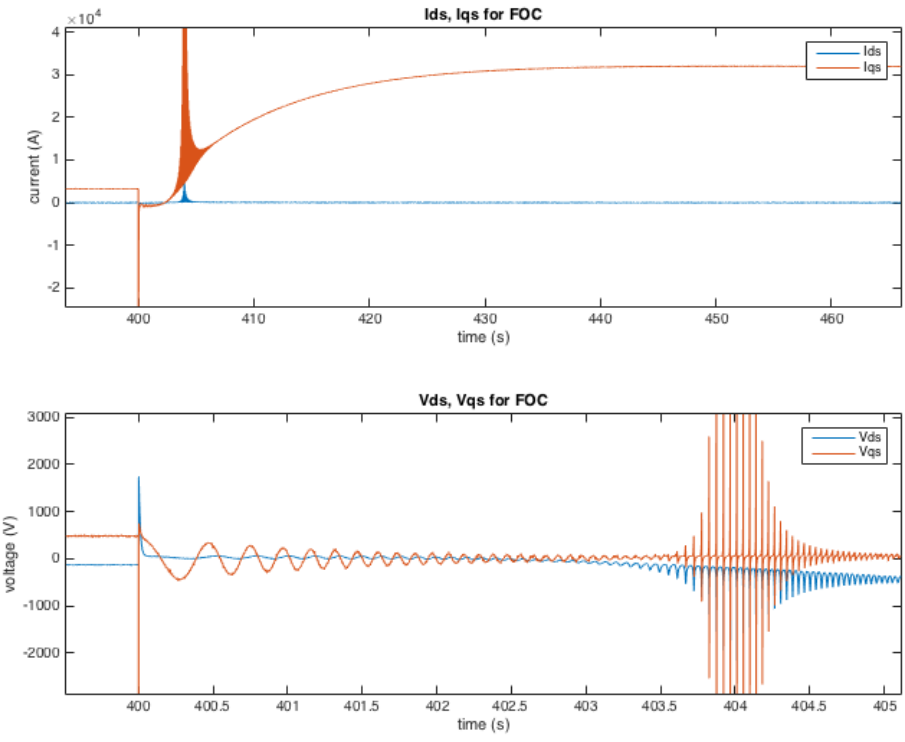


FIGURE 5.4: Current (Ids, Iqs) and Voltage (Vds, Vqs) for FOC

Shown in figure 5.4 are the current in $dq$ coordinate system $I_{ds}$ and $I_{qs}$ and the voltage in $dq$ coordinate system $V_{ds}$ and $V_{qs}$. The speed change occurs at $t = 400s$, as one would expect there is a transient phase for current and voltage right after $t = 400s$. One has to be cautious that the current does not spike to high than the rated current. The increase in current is more damaging on the hardware if it is prolonged period of time, however spikes in current should still be considered when designing a controller.

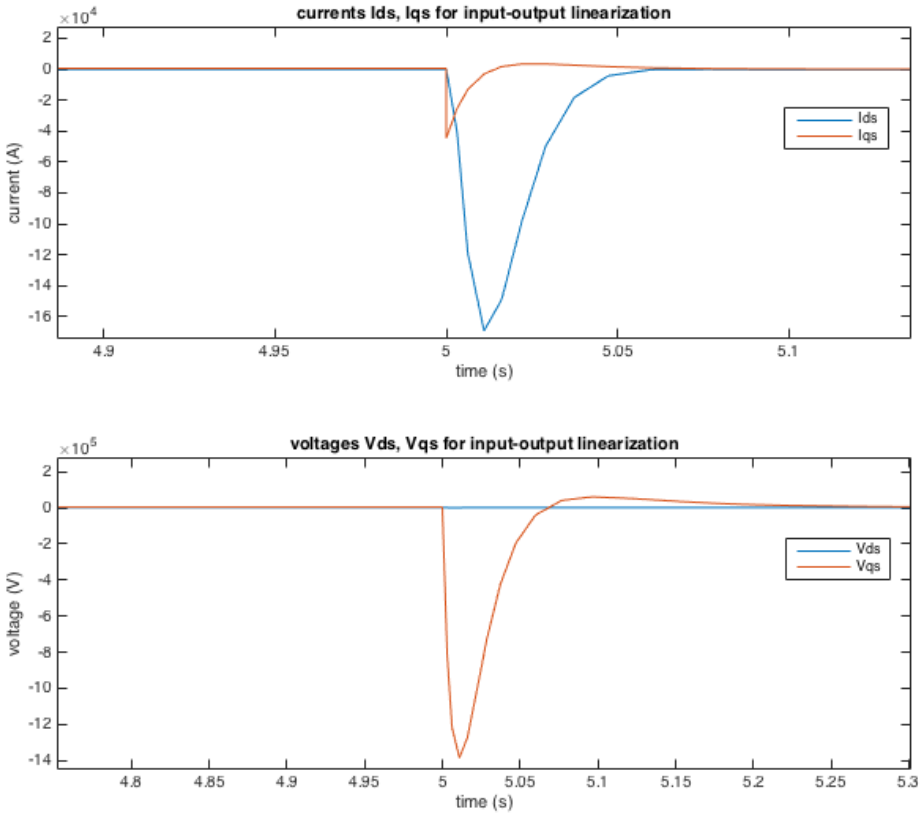


FIGURE 5.5: Current (Ids, Iqs) and Voltage (Vds, Vqs) for input-output linearization

Shown in figure 5.5, a similar behavior is observed, there is an increase voltage and current at $t = 5s$. The increase in current is fairly large, similar to the FOC controller. The difference is that there is no ripples in the current and voltage transient phase.

In summary the performance of FOC and non-adaptive input-output linearization control was conducted using ideal parameters. The tunning for FOC is done by trial and error and far from guaranteed to be ideal. However ideal tunning is not required to prove the central idea of this thesis. The full range of operating speed is tested. Both controller were able to stabilize the generator system. The performance of input-output linearization is superior to that of FOC. The transient phase of input-output linearization is much faster than FOC. The current and voltage for both FOC and input-output linearization exhibited a spike during the speed change. The current spike for both controllers are similar in magnitude.

## 5.4 Speed and Torque Behavior

In previous section the range of stability has been tested for FOC and nonlinear control. It was discovered that nonlinear control has a greater stability than FOC. In this section the speed and torque behaviors of FOC and nonlinear adaptive control will be analysed. The reference speed will be starting at 50% rated speed and increased to 70% rated speed in a step change fashion. The simulations will be done using ideal parameters. The time span for adaptive control will be 10s, the speed change will occur at t=5s. The time span for FOC will be 800s and the speed change will occur at t=400s. The reason for the difference in time span is due to the difference in transient response between the two controllers. Nonlinear adaptive control has a much faster response than FOC, therefore the simulation can be done in shorter time than FOC.

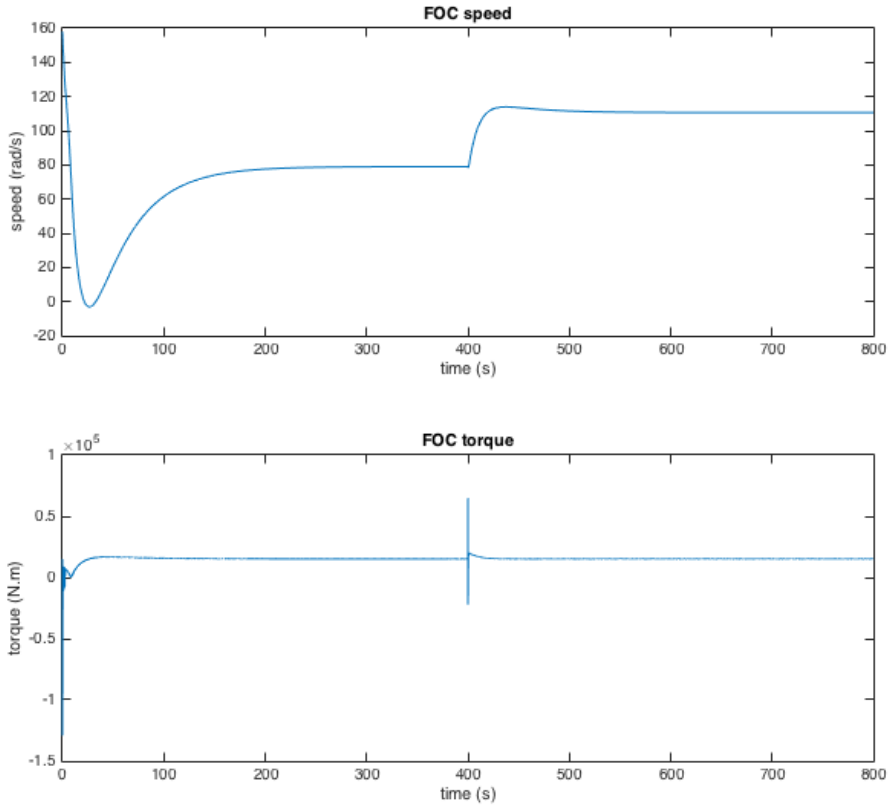


FIGURE 5.6: field oriented control speed and torque comparison

In figure 5.6, the behavior of speed and torque give the simulation parameters mentioned above have been displayed for FOC. As one would expect there is a spike in torque at t=400s due to the change is speed reference. One can observe a transient phase after t=400s between it converges to a steady state phase. The details of the transient behavior will be discussed subsequently.

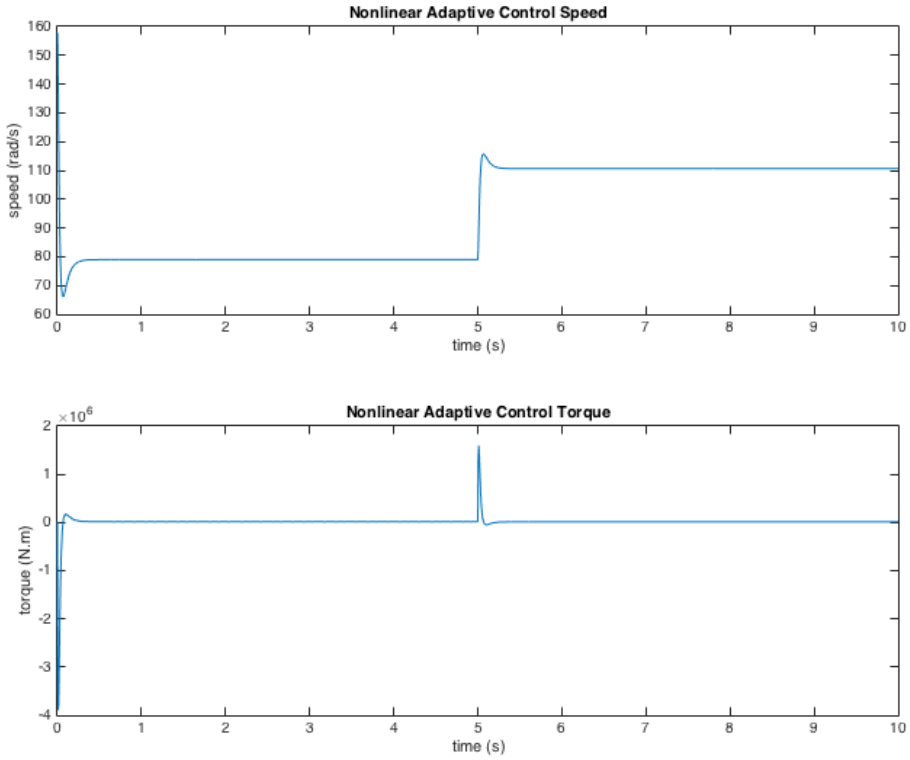


FIGURE 5.7: nonlinear adaptive control speed and torque comparison

In figure 5.7, the behavior of speed and torque given the simulation parameters mentioned above have been displayed for nonlinear adaptive control. As one would expect there is a spike in torque at t=5s due to the change is speed reference. One can observe a transient phase after t=5s before it converges to a steady state phase. The details of the transient behavior will be discussed subsequently.

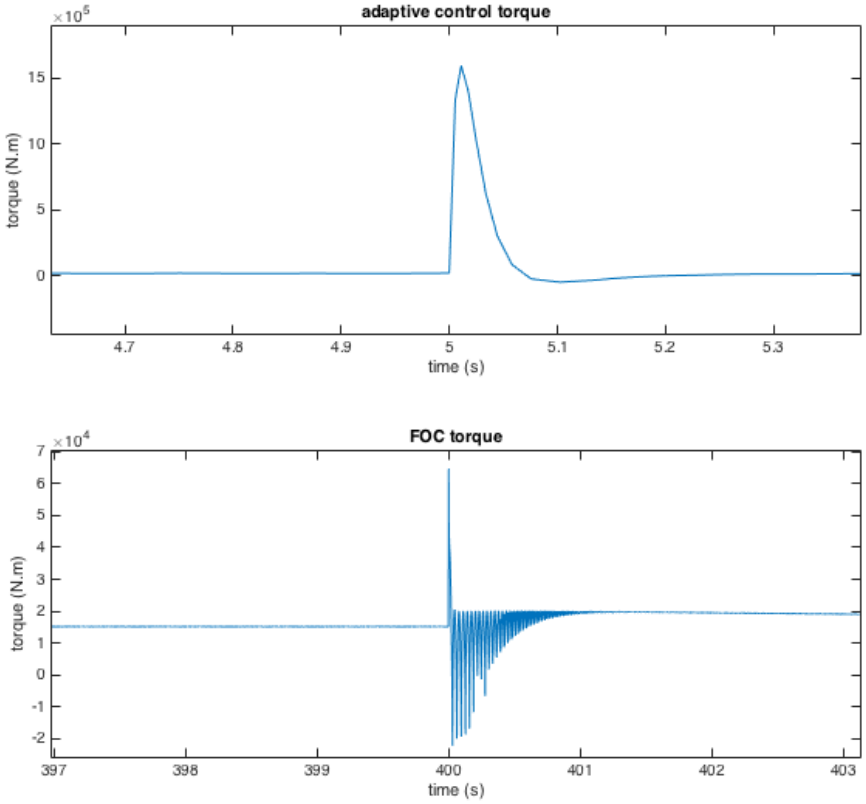


FIGURE 5.8: torque comparison between FOC and nonlinear adaptive control

In figure 5.8 the transient behavior for the generator torque for both the FOC and nonlinear adaptive control is displayed. There is no significance in the differences of the torque behavior for both adaptive control and FOC. The overshoot for adaptive control is slightly greater than the FOC torque spike, however the peak overshoot happens very quickly (less than 0.1s). For FOC, there are some torque ripples in the transient phase. Torque ripples are generally not desireable, but since the duration of the torque ripples are so short (less than 1s), its effect is of no significance.

In summary, the torque behavior between nonlinear adaptive control system and FOC system behaved as expected given the change in reference speed. There is a transient phase beginning with the change in reference speed, after which the torque for both simulations converges to a steady state phase. The transient phase for both simulations is very short,

therefore the slight difference in transient behavior of the torque is of no significance for both control systems.

## 5.5 Uncertain or Time Varying Parameters

During this section of the results, the ability of non-linear adaptive control to stabilize the system when the parameters is either uncertain or varying with respect to time is test against FOC. The approach to this test is to systematically turn on the adaptive component of the controller to adapt one parameter at a time. The way to test for controller performance for uncertain or time varying parameters is to tune the controller for ideal parameters and test the controller on an induction machine with drastically different parameters. If the controller is able to stabilize such system, then the controller is able to stabilize the system when the parameters are different during operation.

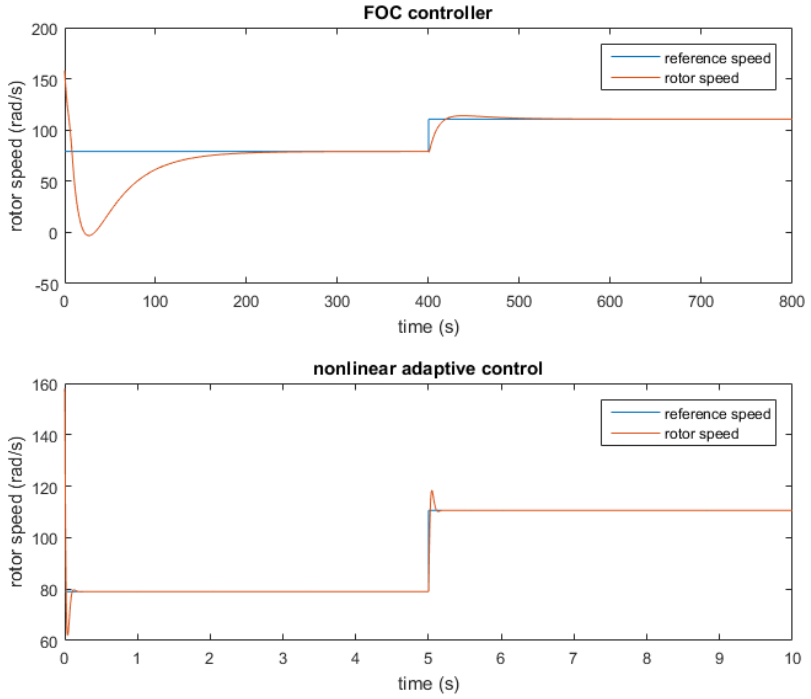


FIGURE 5.9: performance of FOC and nonlinear adaptive control when $R_r$ is uncertain

Typically the parameter that is of concern the most is the rotor resistance $R_r$, the temperature increase in the rotor will cause the resistance to increase to a magnitude of 100%. As matter of fact, there have been similar controllers built with adaptive control for only $R_r$ parameters. The

first simulation will be to test how the proposed nonlinear adaptive controller deals with the most common parameter variation.

Refer to equation (5.2) the parameters that involve $R_r$ are $a_1$, $a_3$, $a_6$ and $a_8$. The way to simulate the uncertain parameter of $R_r$ is to tune the controllers to ideal parameters and use them to control a machine with $R_r$ that is twice the ideal parameter. The adaptive control gains for $a_1$, $a_3$, $a_6$ and $a_8$ are turned on. In figure 5.9 are the results for FOC controller and nonlinear adaptive controller. Both simulations are done with the reference speed going from 50% to 70% reference speed. One can see right away the advantages of the nonlinear adaptive controller. FOC takes way longer to converge to a steady state in the beginning, approximately 200s, where nonlinear adaptive control takes milliseconds. Also when the reference speed is increased from 50% to 70%, at t=400s for FOC and t=5s for nonlinear adaptive control, simliar behavior for the transient response is observed. FOC takes approximately 100s to reach the new steady state compared to a matter of milliseconds for nonlinear adaptive control.

The next parameter to test the controllers on is $R_s$. $R_s$ does not vary as much as $R_r$ but it is next on the list in terms of variations with respect to temperature. Referring to equation (5.2), the parameters that involve $R_s$ are contained in the $a_1$. The parameter $a_1$ is already set to adaptive previously, however the value for $R_s$ was set to ideal value. For this simulation the value of $R_s$ in the induction machine is set to twice the ideal value for $R_s$.

The results for both $R_r$ and $R_s$ adaptive is shown on figure 5.10. The performance of both controllers seems to be unaffected by the additional uncertainty of $R_s$. The transient behavior for both controllers are almost identical to the simulation in figure 5.9. Needless to say that the adaptive control out performs the FOC controller.

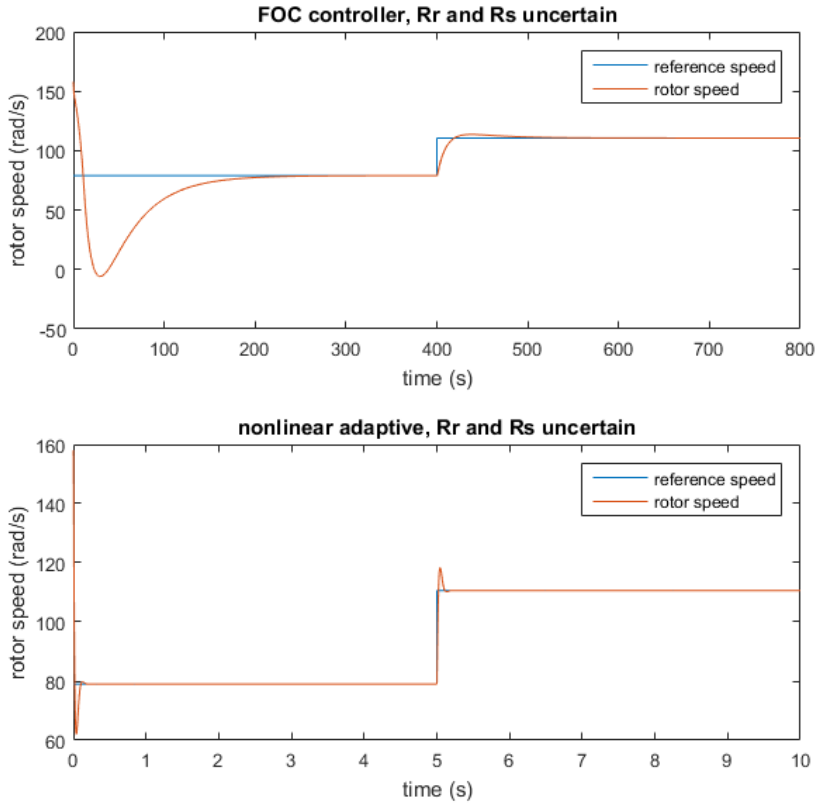


FIGURE 5.10: performance of FOC and nonlinear adaptive control when $R_r$ and $R_s$ are uncertain

The next simulation is to add the additional uncertainty of $L_{ls}$. According to equation (5.2), in addition to $a_1$, $a_3$, $a_6$ and $a_8$ being uncertain, $a_4$ and $a_5$ are also adaptive. The initial condition of the adaptive control will be set to the ideal value of $L_{ls}$, the induction machine however will adopt a value of $L_{ls}$ twice that of it ideal value.

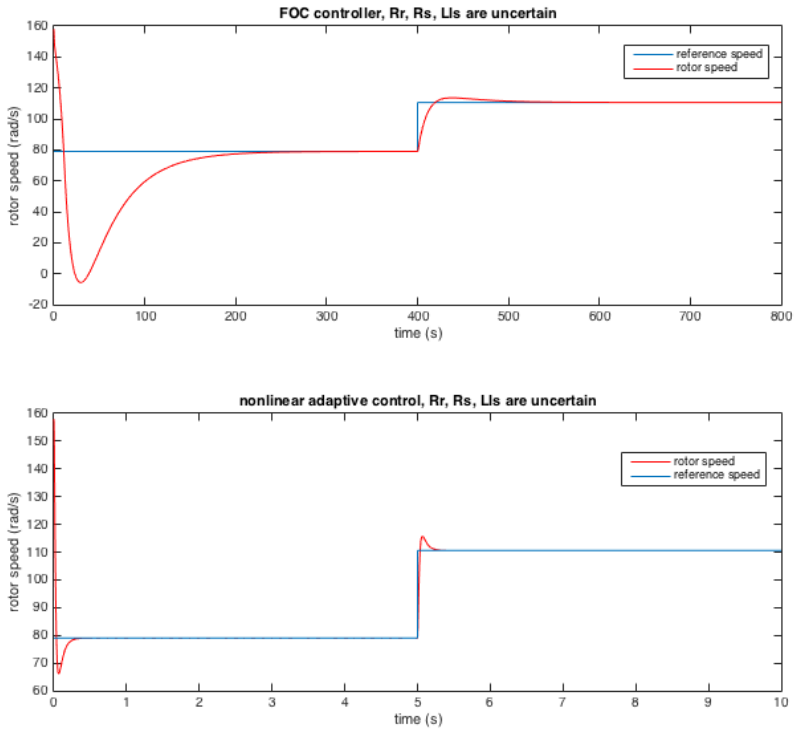


FIGURE 5.11: performance of FOC and nonlinear adaptive control when $R_r$, $R_s$ and $L_{ls}$ are uncertain

Shown in figure 5.11 are the results for FOC and nonlinear adaptive control when $R_r$, $R_s$ and $L_{ls}$ are uncertain. Again there is little difference in performance compared to the last three simulations. Both controllers are able to stabilize the system. Nonlinear control has better performance in terms of speed of response and transient response.

Shown in figure 5.12 are the estimated parameters calculated by the adaptive law for the simulation where $R_r$, $R_s$ and $L_{ls}$ are uncertain. As expected $a_2$ and $a_7$ are constant therefore non adaptive. There rest of the estimations are changing at the right now (t=5s) to control the system output. Note that the values of $\hat{a}$ are merely manipulated by the control law such that the output will be stable, such is the nature of direct adaptive control. The values of $\hat{a}$ are necessarily equal to the values of $a$ which is the case for the parameter estimation based indirect adaptive control.

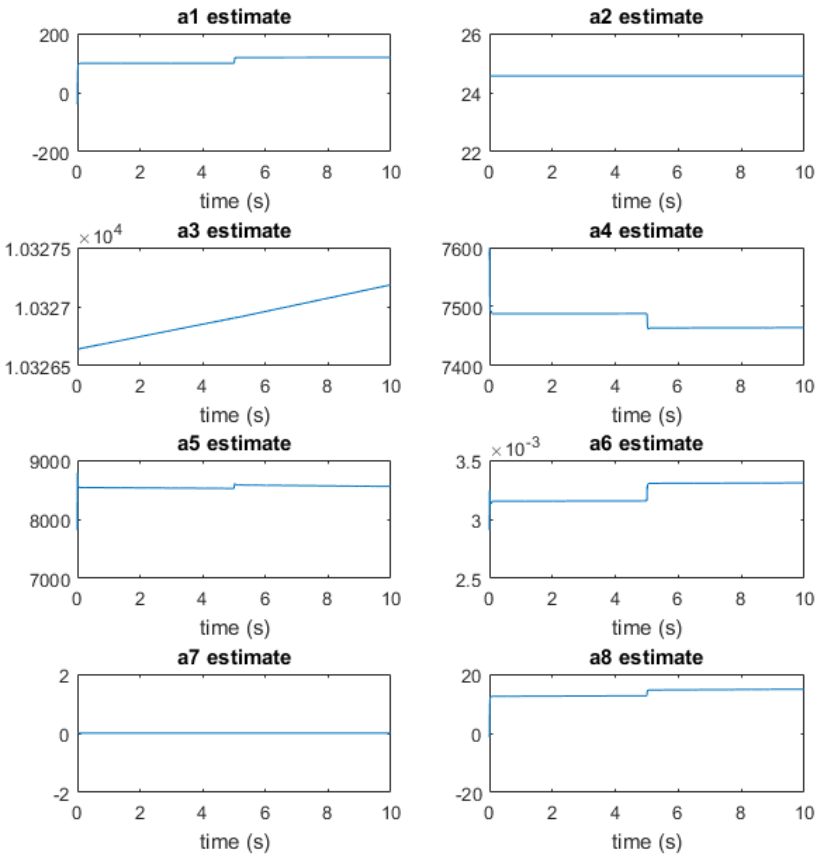


FIGURE 5.12: parameter estimates $a_1$ to $a_8$ for when $R_r$, $R_s$ and $L_{ls}$ are uncertain

The next parameter to add to the list of uncertain parameters is $L_{lr}$. $a_7$ would now be adaptive and the value of $L_{ls}$ in the induction model will be set to twice the ideal value of $L_{lr}$.

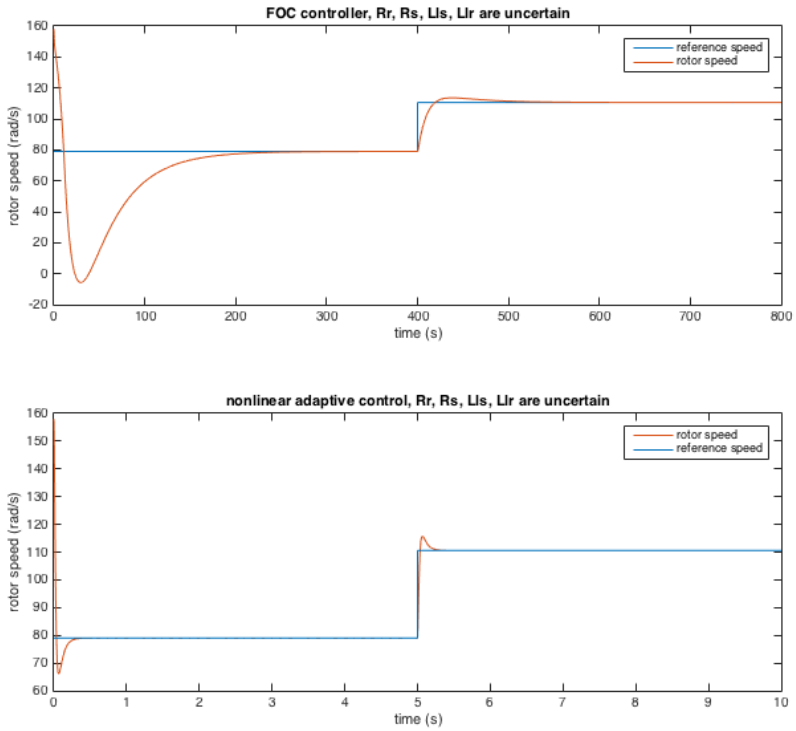


FIGURE 5.13: performance of FOC and nonlinear adaptive control when $R_r$, $R_s$, $L_{ls}$ and $L_{lr}$are uncertain

Shown in figure 5.13 are the results for FOC and nonlinear adaptive control when $R_r$, $R_s$, $L_{ls}$ and $L_{lr}$ are uncertain. Again there is little difference in performance compared to the last four simulations. Both controllers are able to stabilize the system. Nonlinear control has better performance in terms of speed of response and transient response.

Shown in figure 5.12 are the estimated parameters calculated by the adaptive law for the simulation where $R_r$, $R_s$ and $L_{ls}$ are uncertain. As expected $a_2$ and $a_7$ are constant therefore non adaptive. There rest of the estimations are changing at the right now (t=5s) to control the system output.

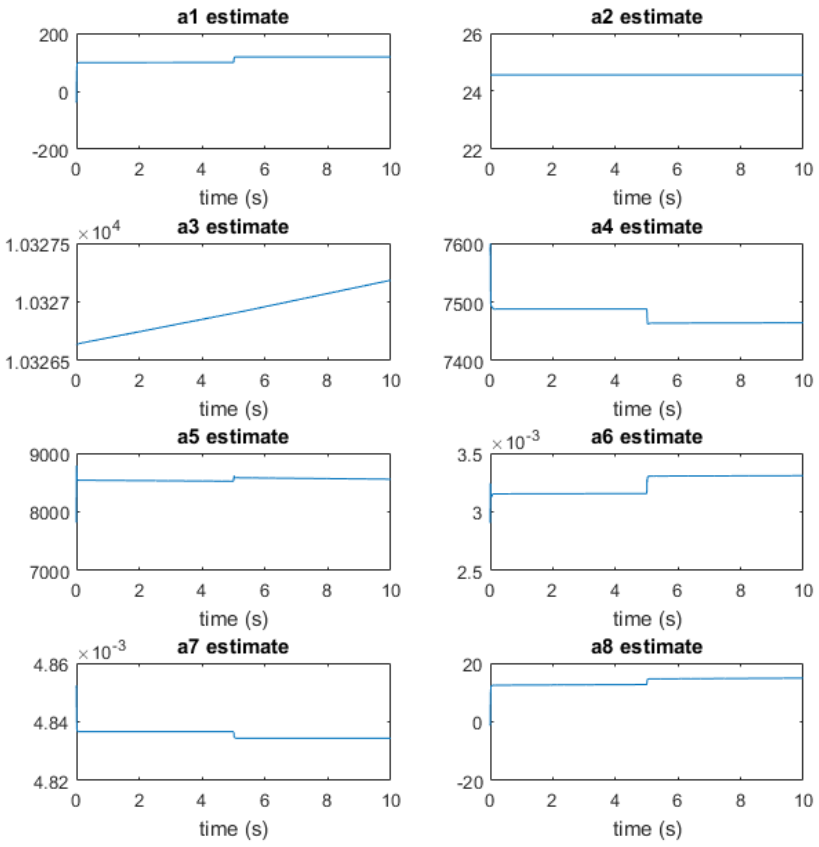


FIGURE 5.14: parameter estimates $a_1$ to $a_8$ for when $R_r$, $R_s$, $L_{ls}$ and $L_{lr}$ are uncertain

Shown in figure 5.16 are the estimated parameters calculated by the adaptive law for the simulation where $R_r$, $R_s$, $L_{ls}$ and $L_{lr}$ are uncertain. As expected $a_7$ is constant therefore non adaptive. The rest of the estimations are changing at t=5s to control the system output.

The next parameter to test is the magnetizing inductance $L_m$. The value of $L_m$ is to be made 1.2 times the ideal value. The difference between the actual parameter value and the ideal parameter value is to be made smaller than other previous parameters because the simulation is too slow to yield any results otherwise. With the value of $L_m$ being uncertain, only $a_7$ is non-adaptive, the rest of the coefficients are adaptive.

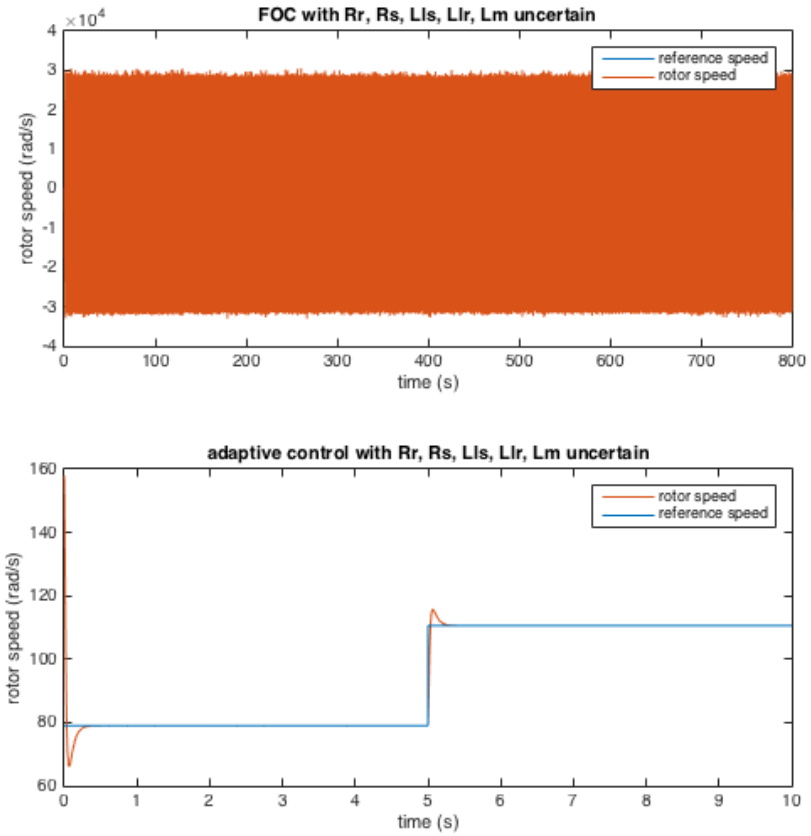


FIGURE 5.15: performance of FOC and nonlinear adaptive control when $R_r$, $R_s$, $L_{ls}$, $L_{lr}$ and $L_m$ are uncertain

One can observe in figure 5.15 the simulation results of $R_r$, $R_s$, $L_{ls}$, $L_{lr}$ and $L_m$ being uncertain. The limitations of FOC can be observed, the FOC controller is not able to stabilize the system to track the reference speed. The adaptive control however remains consistant in performance. There is virtually no different in tracking performance compared with the previous simulations.

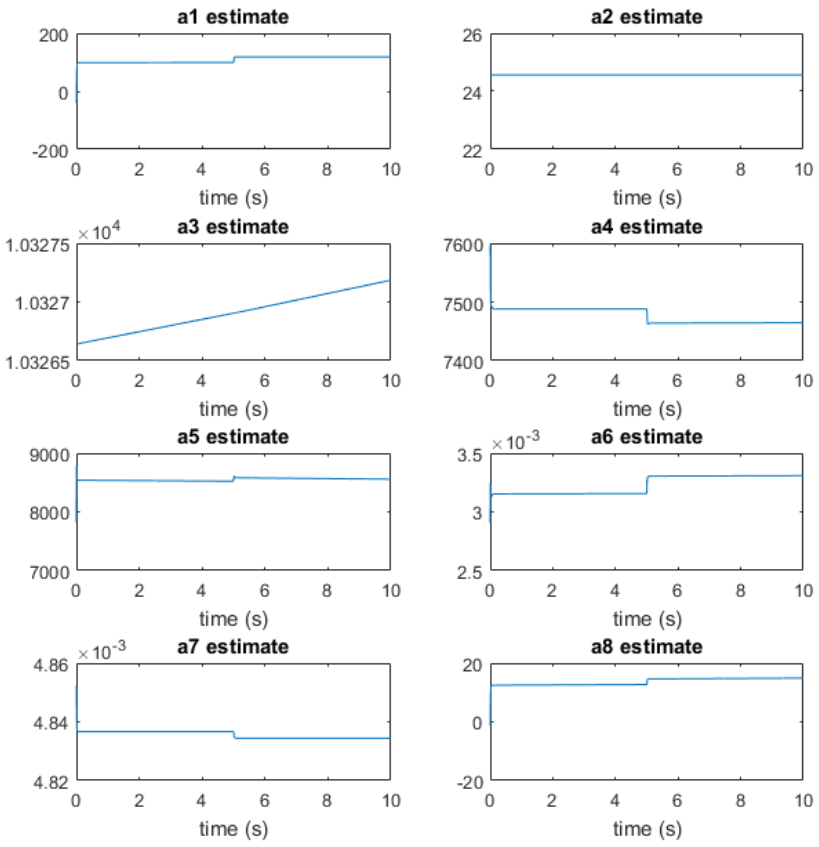


FIGURE 5.16: parameter estimates $a_1$ to $a_8$ for when $R_r$, $R_s$, $L_{ls}$, $L_{lr}$ and $L_m$ are uncertain

The estimated parameter are shown in figure 5.16. As expected all estimated parameters are adaptive except for $a_2$. The next step is to make the value of the rotor moment of inertia $J$ uncertain. The calculation of $J$ is dependent upon the physical dimensions of the rotor and its density distribution, the exact values for these factors are unknown. Most of the time the value of $J$ are approximated using a simplified shape and know dimensions. The density distribution are assume to be uniform. For the next simulation, assume the value of $J$ is twice the ideal parameter value, then test the two controller for their tracking capability.

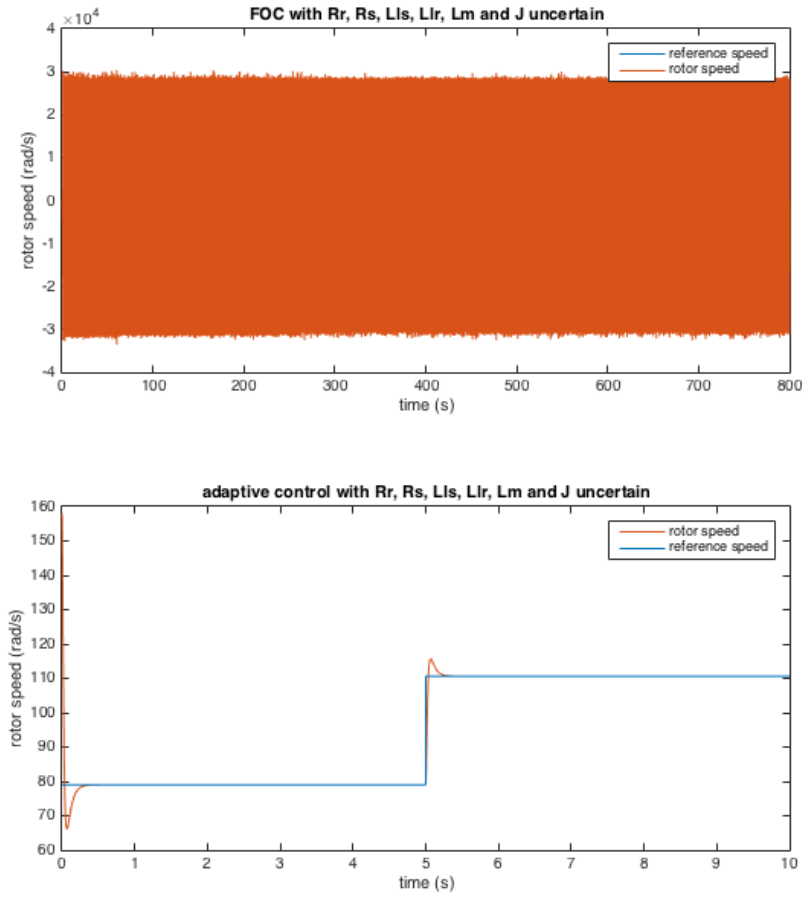


FIGURE 5.17: performance of FOC and nonlinear adaptive control when $R_r$, $R_s$, $L_{ls}$, $L_{lr}$, $L_m$ and J are uncertain

The results shown in figure 5.17 is the simulation done with all the parameters are uncertain. The results in figure 5.17 are almost identical to figure 5.15. The value of $J$ being uncertain has little affect on the outcome of the simulation. FOC controller is unable to control the system. The performance of nonlinear adaptive control remains consistant, the transient behavior is virtually identical to the non-adaptive and system remains stable despite the uncertainty of all parameters.

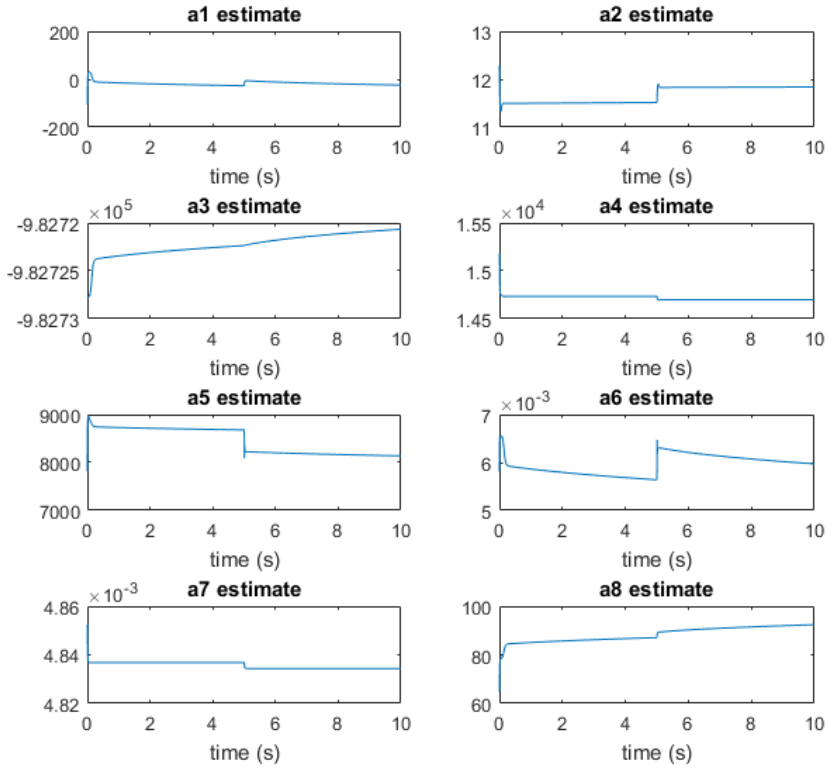


FIGURE 5.18: parameter estimates $a_1$ to $a_8$ for when $R_r$, $R_s$, $L_{ls}$, $L_{lr}$, $L_m$ and $J$ are uncertain

Shown in figure 5.18 are the parameter estimates for all eight adaptive control coefficients $a_1$ to $a_8$. The behavior are exactly as expected, when the simulation first begins there is a transient phase starting at t=0s. The estimated value from the adaptive law slows down to a steady-state value. Then at t=5s, there is another transient because the reference speed changes at t=5s. After the second transient phase, the estimated values of all the parameters settles again to a steady-state.

## 5.6 Comparison of Currents and Voltages

Although it is not the intension of this thesis to investigate the effects of abnormal voltage and current on the health of the machinery, it is worth noting the behavior of the generator currents and voltages. In the context of power generator the second most devastating economic loss is from premature generator failures next to the cost of unscheduled shutdowns of process. Abnormal voltage behaviors that can cause deterioration of a generator is overvoltage. Overvoltage as the name suggests is when the voltage input to the generator is over the rated voltages.

When the voltage is below the rated voltage, a greater current is drawn to provide the same amount of power. The danger of increased stator current is due to the heat build up in the stator windings. Depending on the duration of the heat build up, damage and deterioration of the winds can occur. The longer the windings are exposed to this temperature increase, the greater the damage.

In the case of high voltage, the electromagnetic aspect of the generator can approach saturation which will cause more current to be drawn in order to magnetize the ferrous material beyond saturation. The excessive current will cause overheating of the windings, thus damaging the generator. Essentially both overvoltage and undervoltage have the same outcome, and is to be avoided as much as possible.

In this section, a set of ideal parameters will be used such that both adaptive control and FOC will be able to stabilize. There will be a reference speed step change from 50% rated speed to 70% rated speed. Typically the voltage and current will under go a transient phase as the reference speed change occurs. The voltage and currents will be analyzed to determine which controller will cause the least heating to the stator windings thus better for the longevity of the generator.

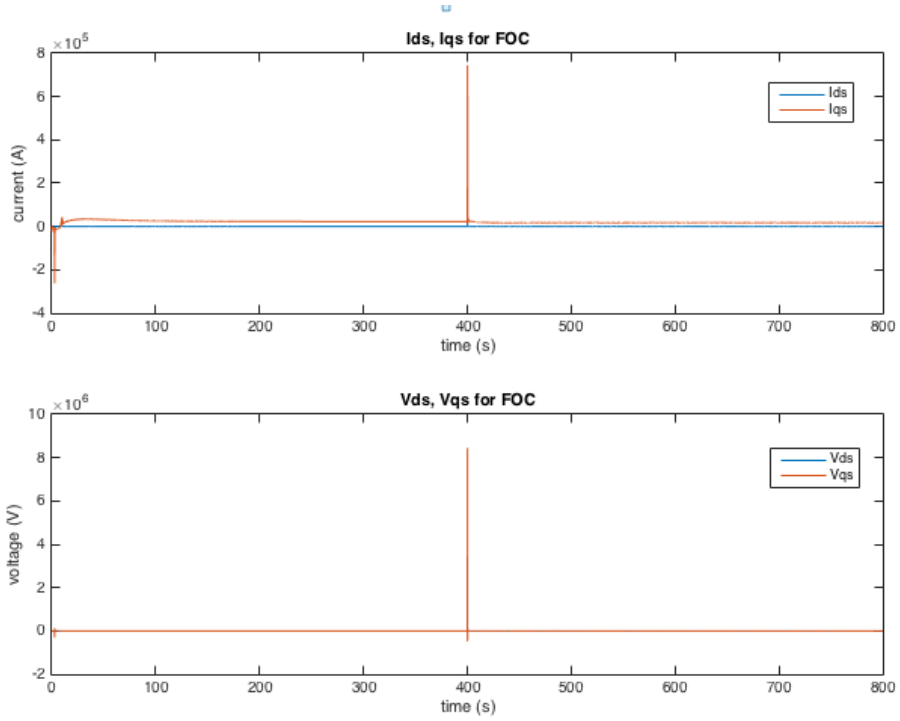


FIGURE 5.19: FOC voltage and current analysis

Shown in figure 5.19 are the currents and voltages in dq $dq$ reference frame for FOC. As one might expect at the time of the step change t=400s there is a change in current and voltage is the form of a spike. Generally a spike in current is not a major concern in terms of hardware damage. The heating of the wiring and windings are due to prolonged over current. If the current quickly settles to nominal values, it should not present problems for hardware longevity.

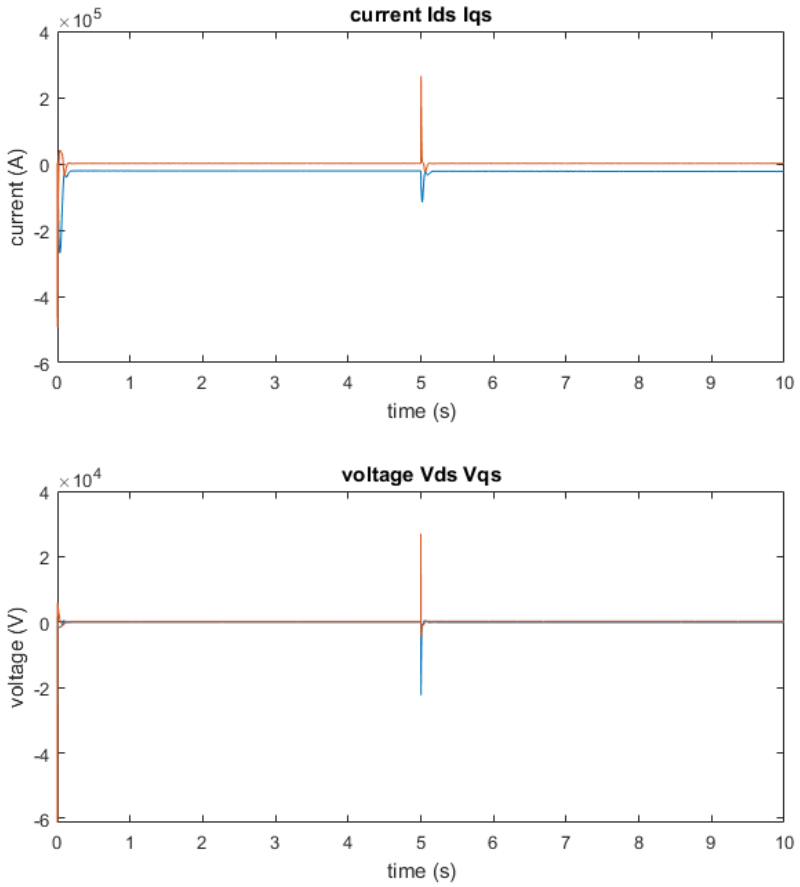


FIGURE 5.20: nonlinear adaptive control voltage and current analysis

Shown in figure 5.20 are the currents and voltages in $dq$ reference frame for adaptive control. As one might expect at the time of the step change t=5s there is a change in current and voltage is the form of a spike. As mentioned previously a spike in current is not a major concern in terms of hardware damage. The heating of the wiring and windings are due to prolonged over-current. The current quickly settles to nominal values within milliseconds after the t=5s, it should not present problems for hardware longevity.

## 5.7 Power and Efficiency

In this section the power and efficiency of the generator performance as result of the two controllers FOC and nonlinear adaptive control will be discussed. The efficiency of a generator in steady state is inherent of the generator. The power efficiency is simply:

$$\eta_{power} = P_e/P_m \tag{5.4}$$

$P_m$ being the mechanical power and $P_e$ being the electrical power. The respect equations for $P_m$ and $P_e$ are:

$$\begin{aligned} P_e &= 3/2(V_{ds}I_{ds} + V_{qs}I_{qs}) \\ P_m &= T_m \cdot \omega_r \end{aligned} \tag{5.5}$$

The efficiency of a generator has to do with the construction of the generator. A generator will operate more efficiently in some certain speed ranges. a controller will not change the steady-state efficiency of a generator. However, during a transient phase when there is a disturbance to the system, one controller can stabilize the system more efficiently than the other.

In the following simulations, the generators will adopt ideal parameters. The speed reference will begin at $50\%$ rated speed and increase to $70\%$ rated speed. The speed increase will take form of a step change. The step change for FOC will occur at $t = 400s$, for nonlinear adaptive controll at $t = 5s$. The simulation for FOC will run for $800s$, and for nonlinear adaptive control $10s$. The reason for the difference in simulation time is that FOC requires much longer to settle to a steady-state after a change in speed than nonlinear adaptive control.

**Power Analysis of FOC system**

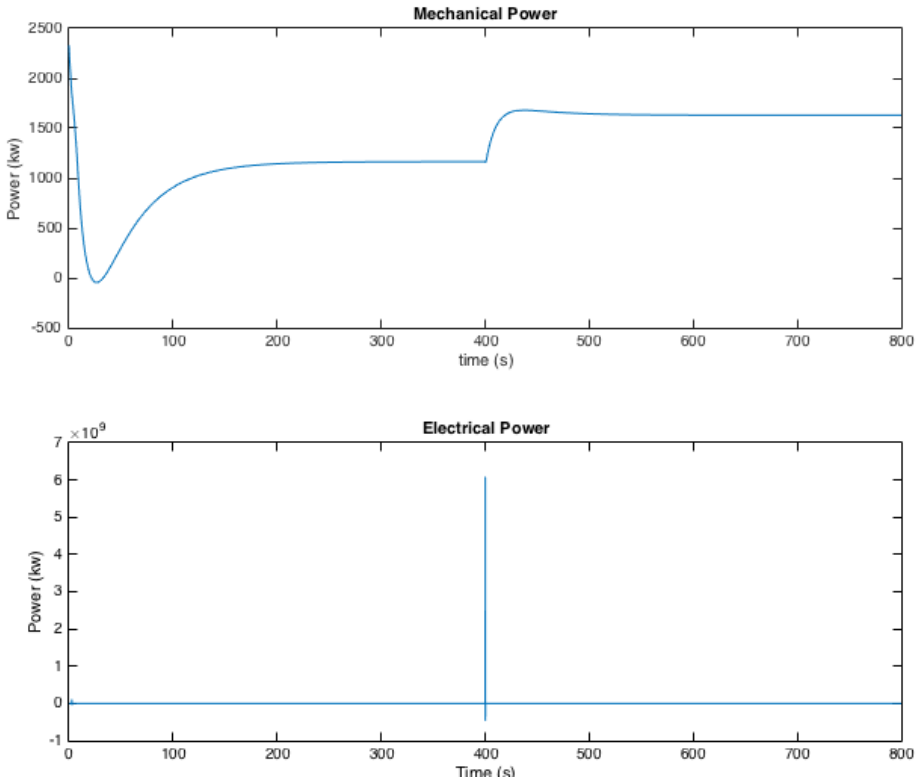


FIGURE 5.21: Mechanical Power and Electrical Power for FOC

In figure 5.21, the mechanical power and the electrical power for FOC is illustrated. Since the mechanical torque is kept constant, the mechanical power behaves very much like the mechanical speed, which is expected. The second graph for electrical power however, illustrates a huge spike during the speed change, which is also expected since the voltage and current behaves the same way, and electrical power is a function of the stator voltage and current.

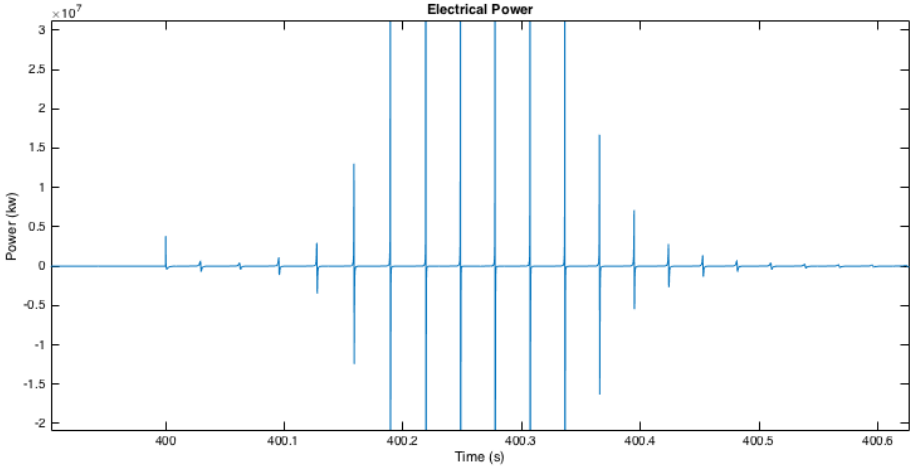


FIGURE 5.22: Close-up of Electrical Power for FOC during transient phase

Illustrated in figure 5.22 is a close-up of the electrical power graph shortly after the speed change at $t = 400s$. It would be really difficult to conclude what effects of electrical power during the transient phase on the efficiency.

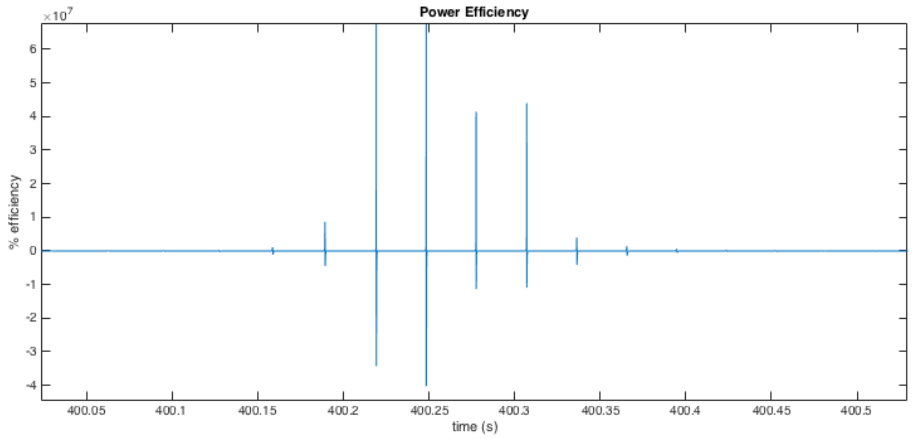


FIGURE 5.23: close-up of power efficiency of FOC system during transient phase

Figure 5.23 shows the power efficiency during the transient phase shortly after $t = 400s$. One can see that due to the spikes in electrical

power, the efficiency data is not very useful for analysis.

### Power Analysis of Nonlinear Adaptive system

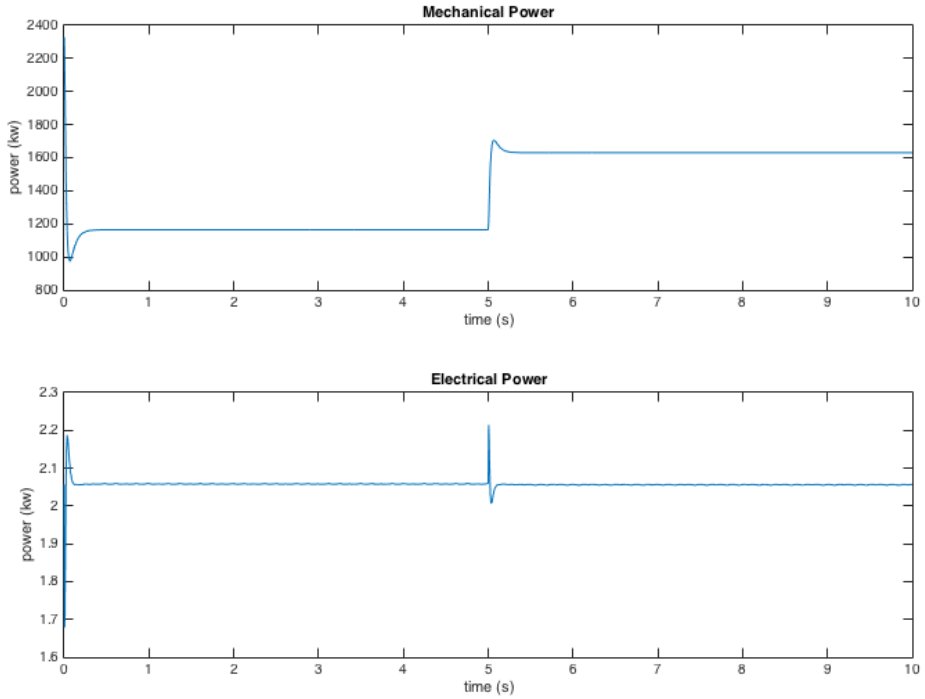


FIGURE 5.24: Mechanical Power and Electrial Power for nonlinear adaptive system

Figure 5.24 shows the mechanical power and electrical power behavior for nonlinear adaptive control system. As one can observe the transient phase at $t = 5s$ is much quicker than that of FOC. The mechanical power behaves much like the speed tracking, which is expected, since the mechanical torque is kept constant.

The behavior of the electrical torque has much less overshoot during the transient phase than FOC system. This is due to the low current and voltage spikes at $t = 5s$.

**Rotor Flux Estimator**

The central theme of this thesis is based on the adaptive algorithm to control the speed of the SCIG. There is however another issue not directly related to the controlling of the generator speed that needs to be addressed. In the adaptive algorithm propose in the previous section, it is assumed that the rotor flux values are known. The rotor flux in reality cannot be measured, they are typically obtained through a manipulation of the machine equations.

However, the motivation of the topic of this thesis is that the parameters are uncertain, and this uncertainty will undoubtedly produce error when calculating the rotor flux, and will further deteriorate the performance of the SCIG system. What is warranted is an adaptive rotor flux observer to estimate the rotor flux in order to perform the field orientation.

There has been research in the past which addresses the issue of flux estimation inaccuracy through online tuning or compensation techniques [35–42]. There re several popular techniques that deserves mentioning, one such technique is model reference adaptive control (MRAC) which is an online estimation technique that is widely used to estimate the machine parameters [35]. The difficulty with MRAC is that it assumes the parameters in the reference model are constant [36], where in reality the parameters vary during operation some parameter vary to great extents (greater than 100% in the case of rotor resistance).

Another common flux estimators is the Luenberger oberserver which utilizes an adaptive law to estimate the machine parameters and speed simultaneously [34], one downside of the Luenberger observer is that the complexity of the algorithm will significantly increase the computation burden [34]. In addition to the computation burden, a superimposed AC component must be injected into the reference command [37–39], which can result in torque ripples [34]. In terms of calculation demands, compensation techniques involves relatively simple algorithms, however addition information such as slip frequency and electrical frequency are required [34].

Sliding mode control techniques has becoming popular in recent years due to its parameter insensitivity [41, 42], many rotor flux observers has been designed using sliding mode techniques [41, 42]. The advantage of

sliding mode observers is that they are robust and produce good performances, however they require detailed knowledge of the rotor time constant for flux estimations [34]. As a result, any error in the estimation of the rotor time constant will effect the observer estimation accuracy [34]. Other techniques like neural network artificial intelligence observers also provides robust solutions for the issue of parameter variation and measurement noise [43, 44], these techniques also involves complexed algorithms which require high computation time.

One adaptive flux observer has been proposed in [34] which uses adaptive control theory very similar to the concept proposed in this thesis to control the speed of the SCIG. The algorithm such as the one proposed in [34] maybe used to estimate for the rotor flux values. If time permits for further research, the rotor flux estimator proposed in [34] can be used to estimate for the rotor flux values to simulate a more realistic control system.

# Chapter 6

# Summary and Conclusion

During the development of this thesis, it was identified that SCIG has many economical advantages over other generator types such as PMSG or DFIG. SCIG has a simplicity and robustness that renders it much cheaper in terms of production and maintenance. However, SCIG has a very nonlinear structure which makes control design more challenging than other generator types. Furthermore, the parameters of the system in most cases cannot be identified, even when the parameters are known, they could vary in operation. The uncertainties of the system parameters introduces more limitations for existing controllers.

The most common controllers in use in industry was analyzed to expose some of their inadequacies. The two controllers analyzed in detail as part of the literature review are FOC and DTC. It was found that in both of these controllers it is assumed that the system parameters are constant. The controller's ability to stabilize the generator output cannot be guaranteed given the uncertainties of the parameters in operation. The limitation of FOC was that it uses PID controllers. PID controllers are designed for linear systems, for a nonlinear system such as SCIG, the structure has to be linearize in order to apply FOC. The problem with this approach is that as soon as the operating point leans away from the point of linearization, stability cannot be guaranteed. This uncertainty to stabilize the system magnifies when the system parameters are varying with respect to time.

The proposed control algorithm must improve on the two limitations of FOC and DTC if it is to be of a contribution to this area of research. It most provide a greater range of stability. Also, it must provide guarantee of system stability given time varying parameters. Given these design criteria, input-output linearization with adaptive control was proposed. The input-output linearization will guarantee system stability in all operating ranges. The adaptive control will guarantee stability given time varying

or uncertain system parameters.

The method of input-output linearization is based on the principle that a non-linear system can be transformed into a new coordinate system through input feedback. In the new coordinate system the structure appears to be linear. Once the system structure is linearized, pole placement technique can be used. The pole placement technique ensures the system has negative poles thus guaranteeing its stability. The adaptive control component of the controllers postulates the parameters in a way that it is represented in terms of the estimated parameter and the parameter error. Once the system expression is obtained containing the estimated parameter and the parameter error, the state equations can be divided into two sections; a section containing the parameter estimate, and a section containing the parameter error. Since the parameter error represents the difference between the actual system parameter and the estimated parameter, the goal is to design an adaptive law to manipulate the parameter estimate in order to stabilize the output of the generator; this was achieve via Lyapunovs theory. Once the expressions of Lypunov's candidate function is obtained, by finding its derivative, the adaptive law is obtained.

Once the full control algorithm is implemented in Simulink, the controller is compared with FOC controller which is also implemented in Simulink. FOC is chosen due to crossover components between FOC and adaptive control; namely the field orientation aspect of the simulation. Both FOC and adaptive control require field orientation to convert 3 phase system to 2 phase, thus field orientation portion of the simulation can be omitted, both simulations can be done in $dq$ reference frame. The tuning of both the FOC PID controllers and adaptive control gains are done by trial and error. Because trial and error is used, the gains are not guaranteed to be optimal; the comparison of performance is set up in ways than the effect of less that optimal tuning is minimized.

Once both simulations are implemented, several experiments were conducted to test the different aspect of their performance. First, the range of stability is tested for both controllers. In this first experiment the parameters are assumed to be constant and known. As expected, FOC had a range of stability, when the operating point falls outside of that range, the controller can no longer stabilize the system. Nonlinear adaptive control on the contrary was able to stabilize the system in its full range of operating conditions even beyond that of the rated operating speed. From the results obtained in this section of the simulation, the first objective was

obtained, which is that the nonlinear adaptive controller was able to stabilize the system in operating points that FOC cannot. Not only is the stability range of nonlinear adaptive control greater than FOC, the transient response of nonlinear adaptive control outperforms FOC interms of quickness of response and the settling time. FOC control has greater overshoot and far longer settling time than nonlinear adaptive control

The second objective is to test the performance of the two controllers with when the parameters are unknown. This is very hard to test in a simulation, because its very difficult to know exactly how the parameters change in a SCIG used in wind energy system. The experiment was postulated in a way that best mimics the uncertainty of the parameters. Both controllers were tuned to ideal parameters, the parameters of the SCIG were set to be different than the ideal parameters to which the controllers were tuned. The difference in parameters were done one at a time. The order to which the parameters are set to adaptive is determined by which parameters typically vary the most during operation. In the case of SCIG, the parameters that vary the most are the resistances due to temperature change, then the inductance followed by possibility of the error when calculating the moment of inertia.

It was found that the performance of nonlinear adaptive is virtually identical even with all the uncertainty of the parameters. The adaptive law has a very fast response in estimating the appropriate parameter to control the output. For FOC however, the controller was able to stabilize the generator with some parameters being uncertain. When the uncertainty of the magnetizing inductance $L_m$ and the moment of inertia $J$ was introduced, FOC was not able to stabilize the generator. When FOC was able to stabilize the system with some of the parameters being uncertain, adaptive control has far superior performance than FOC in terms of quickness of response and low overshoot during transient phases.

The overall results confirms the prediction when nonlinear adaptive control was introduced, the range of stability is far greater when compared with FOC. In the case of uncertain system parameters the adaptive control algorithm again outperformed the FOC controller by providing greater stability even when all the parameters are uncertain. Furthermore, nonlinear adaptive control performance is consistent and virtually identical regardless of parameter variation, which is not the case for FOC.

One component that is indirectly related to this thesis is the design of

adaptive flux observer. The rotor flux values are used for the adaptive control algorithm. However, in reality the rotor flux cannot be measured. Conventionally the rotor flux is calculated by manipulating the generator equations which involves the use of system parameters. The motivation of this thesis is that the parameters are uncertain; therefore the problem of having accurate values of the rotor flux must be mentioned. There have been research done in creating such adaptive flux observer. Due to time restraints the observer was not implemented as part of the simulation.

# Bibliography

[1] B. Housseini, F. A. Okou, and R. Beguenane, "A unified nonlinear controller design for on-grid/off-grid wind energy battery-storage system," *IECON 2015-41st Annual Conference of the IEEE*, 2015.

[2] N. Z. S. K. Bin Wu, Yongqiang Lang, *Power Conversion and Control of Wind Energy Systems*. IEEE Press, 2011.

[3] L. Ioan Dore, "Adaptive Control." http://www.landau-adaptivecontrol.org.

[4] S. D. U. A.E.Fitzgerald, Charles Kingsley Jr, *Electric Machinery*. McGraw-Hill, sixth ed.

[5] F. A. F. M. Godoy Simoes, *Modeling and Analysis with Induction Generators*. Power Electronics and Applications Series, CRC Press, third ed.

[6] B. N. Watthana Suebkinorn, "An implementation of field oriented controlled scig for variable speed wind turbine," *IEEE Conference Publications*, no. 12170164, 04 August 2011.

[7] D.-Y. F. Faa-Jeng Lin, Kuang-Hsiung Tan, "Squirrel-cage induction generator system using intelligent control for wind power applications," *IEEE Conference Publications*, 08 October 2013.

[8] N. M. Anissia Beainy, Chantal Maatouk, "Comparison of different types of generator for wind energy conversion system topologies," *IEEE Conference Publications*, 2016.

[9] R. C. C. M. A. M. Marios C. Sousounis, Jonathan K.H. Shek, "Comparison of permanent magnet synchronous and induction generator for a tidal current conversion system with onshore converters," *IEEE Conference Publications*, 2015.

[10] H. A. A. S. Manaullah, Arvind Kumar Sharma, "Performance comparison of dfig and scig based wind energy conversion systems," *IEEE Conference Publications*, 2014.

[11] A. J. S. F. Michael A. Hernández Navas, José L. Azcue Puma, "Direct torque control for squirrel cage induction generator based on wind energy conversion system with battery energy storage system," *IEEE Conference Publications*, 30 July 2015.

[12] M. S. B. Hussam M. El-kafrawi, "Torque control of squirrel-cage induction generator using stator oriented field control," *IEEE Conference Publications*, 21 May 2015.

[13] B. S. M. E. K. Miloud Rezkallah, Ambrish Chandra, "Vector control of squirrel-cage induction generator for stand-alone wind power generation," *IEEE Conference Publications*, 24 December 2012.

[14] L. T.-R. A. J.-F. José Luis Domínguez-García, Oriol Gomis-Bellmunt, "Vector control of squirrel cage induction generator for wind power," *IEEE Conference Publications*, 25 October 2010.

[15] S. N. Vishal D Dhareppagol, "Modelling and simulation of wecs for maximum power extration and optimal efficincy control using squirrel cage induction generator," *IEEE Conference Publications*, 2015.

[16] A. B. M.M. Ismail, H.A. Abdel Fattah, "Adaptive input-output linearization of induction motors with magnetic saturation," *IEEE Conference Publications*, November 2003.

[17] C.-H. C. Wen-Jieh Wang, Chun-Chieh Wang, "High-performance adaptive speed controller for induction motor with input-output linearization," *IEEE Conference Publications*, April 2002.

[18] S. E. Enev, "Input-output linearization control of current-fed induction motors with rotor resistance and load torque identification," *IEEE Trans. Ind. Electron*, pp. 132–139, 2006.

[19] M. K. Saïd Boubzizi, Hafedh Abid, "Comparison of adaptive input-output linearization and fuzzy sliding-mode control for induction motor," *IEEE Conference Publications*, December 2015.

[20] A. I. Hamdi Echeikh, Ramzi Trabelsi, "Comparative study between the rotor flux oriented control and non-linear backstepping control of a five-phase induction motor drive – an experimental validation," *IET Journals  Magazines*, December 2016.

[21] A. G. L. Alma Y. Alanis, Edgar N. Sanchez, "Discrete-time backstepping induction motor control using a sensorless recurrent neural observer," *IEEE Conference Publications*, December 2007.

[22] H. C. S. Issaouni, A. Boulkroune, "Adaptive fuzzy backstepping controller of induction machine," *IEEE Conference Publications*, December 2015.

[23] H. L. Xianglong Jiang, Jin Zhao, "Neural network speed controller of induction motor drive based on direct mrac method," *IEEE Conference Publications*, November 2003.

[24] Z. W. Yue Wang, Jun Yang, "A novel mrac of induction motor," *IEEE Conference Publications*, January 2005.

[25] H. A. G. Rodrigo Padilha Vieira, Rodrigo Zelir Azzolin, "A sensorless single-phase induction motor drive with a mrac controller," *IEEE Conference Publications*, November 2009.

[26] H. A. G. R. Z. Azzolin, "A mrac parameter identification algorithm for three-phase induction motors," *IEEE Conference Publications*, June 2009.

[27] Z. M. A. P. Carlos Henrique Silva de Vasconcelos, "A sensitivity analysis of the ifoc and mrac induction machine drives including a robust parameter estimation method," *IEEE Conference Publications*, December 2009.

[28] E. M. Committee, *IEEE Standard Test Procedure for Polyphase Induction Motors and Generators*, May 2004.

[29] C. A. I. Zubia, A. Zatarain, "In situ electrical parameter identification method for induction wind generators," *IEEE Conference Publications*, vol. 5, 2011.

[30] F. W. F. Sonke Thomsen, Kai Rothenhagen, "Online parameter identification methods for doubly fed induction generators," *IEEE Conference Publications*, pp. 2735–2741, 2008.

[31] S. P. R. Marino, P. Tomei, "Output feedback control of current-fed induction motors with unknown rotor resistance," *IEEE Transactions on Control Systems Technology*, vol. 4, pp. 336–347, July 1996.

[32] J. X. Xiaoyu Wang, MIEEE, "Parameter identification of doubly-fed induction generator by the levenberg-marquardt-fletcher method," *IEEE Conference Publications*, pp. 1–5, 2013.

[33] R. B. Boubacar Housseini, Aime Francis Okou, "Robust nonlinear controller design for on-grid/off-grid wind energy battery-storage system," *IEEE Early Access Article*, 2017.

[34] S. L. H. Z. S. Wang, "Adaptive rotor flux position observer in the absence of machine parameter information for vector controlled induction motor drives," vol. 33, pp. 801–818, November 2014.

[35] T. M. R. R. J. Kerkman, B. J. Seibel and D. Schlegel, "A new flux and stator resistance identifier for ac drive systems," *Conf. Rec. IEEE-IAS Annu. Meeting*, pp. 310–318, 1995.

[36] G. G. M. P. T. G. Habetler, F. Profumo and A. Bettini, "Stator resistance tuning in a stator-flux field-oriented drive using an instantaneous hybrid flux estimator," *IEEE Trans. Power Electron*, vol. 13, pp. 125–133, Jan 1998.

[37] T. Du and M. A. Brdrys, "Shaft speed, load torque and rotor flux estimation of induction motor drive using extended luenberger observer," *Proc. IEE EMD*, pp. 179–184, 1993.

[38] K. M. H. Kubota and T. Nakano, "Dsp-based speed adaptive flux observer of induction motor," *IEEE. Trans. Ind. Application*, vol. 29, pp. 344–348, March 1993.

[39] H. Kubota and K. Matsuse, "Speed sensorless field-oriented control of induction motor with ro- tor resistance adaptation," *IEEE Trans. Ind. Application*, vol. 30, pp. 1219–1224, Sept/Oct 1994.

[40] B. K. Bose and M. G. Silmoes, "Speed sensorless hybrid vector controlled induction motor drive," *Industry Applications Conference, Proc. IEEE, IAS '95*, pp. 137–143, 1995.

[41] H. R. N. I. A. Derdiyok, M. K. Güven and L. Xu, "Design and implementation of a new sliding-mode observer for speed-sensorless control of induction machine," *IEEE Trans. Industrial Electronics*, vol. 49, pp. 1177–1182, October 2002.

[42] C. J. Z. Yan and V. I. Utkin, "Sensorless sliding-mode control of induction motors," *IEEE Trans. Ind. Electron*, vol. 47, pp. 1286–1297, Dec 2000.

[43] P. Vas, *Artificial-Intelligence-Based Electrical Machines and Drivers-Application of Fuzzy, Neural, Fuzzy-Neural and Genetic-Algorithm-Based Techniques*. Oxford Univ. Press, 1999.

[44] M. F. R. B. Karanayil and C. Grantham, "On-line stator and rotor resistance estimation scheme for vector-controlled induction motor drive using artificial neural networks," *Industry Applications Conference, 38th IAS Annual Meeting*, pp. 132–139, 2003.

### 6.0.1 Annex

$$
\begin{aligned}
\dot{\hat{z}}_1 =& 2\hat{a}_8\lambda_{dr}^2 + 2\tilde{a}_8\lambda_{dr}^2 + 2\hat{a}_6 I_{ds}\lambda_{dr} + 2\tilde{a}_6 I_{ds}\lambda_{dr} + 2\hat{a}_8\lambda_{qr}^2 \\
&+ 2\tilde{a}_8\lambda_{qr}^2 + 2\hat{a}_6 I_{qs}\lambda_{qr} + 2\tilde{a}_6 I_{qs}\lambda_{qr} \\
\dot{\hat{z}}_2 =& [4\hat{a}_8^2(\lambda_{dr}^2 + \lambda_{qr}^2) + 2\hat{a}_3\hat{a}_6(\lambda_{dr}^2 + \lambda_{qr}^2) + 6\hat{a}_6\hat{a}_8(I_{ds}\lambda_{dr} + I_{qs}\lambda_{qr}) \\
&+ 2\hat{a}_1\hat{a}_6(I_{ds}\lambda_{dr} + I_{qs}\lambda_{qr}) + 2\hat{a}_6^2 I_{ds}^2 + 2\hat{a}_6^2 I_{qs}^2 + 2\hat{a}_6 I_{qs}\omega_r\lambda_{dr} \\
&- 2\hat{a}_6 I_{ds}\omega_r\lambda_{qr} - 4\hat{a}_4\hat{a}_6\omega_r\lambda_{dr}\lambda_{qr}] \\
&+ [2(\lambda_{dr}^2 + \lambda_{qr}^2)\dot{\hat{a}}_8 + 2(I_{ds}\lambda_{dr} + I_{qs}\lambda_{qr})\dot{\hat{a}}_6] \\
&+ [4\hat{a}_8(\lambda_{dr}^2 + \lambda_{qr}^2)\tilde{a}_8 + 4\hat{a}_8(I_{ds}\lambda_{dr} + I_{qs}\lambda_{qr})\tilde{a}_6 \\
&+ 2\hat{a}_6(I_{ds}\lambda_{dr} + I_{qs}\lambda_{qr})\tilde{a}_1 + 2\hat{a}_6(\lambda_{dr}^2 + \lambda_{qr}^2)\tilde{a}_3 + 2\hat{a}_6\lambda_{dr}\lambda_{qr}\omega_s\hat{a}_4 \\
&+ 2\hat{a}_6(I_{ds}^2 + I_{qs}^2)\tilde{a}_6 + 2\hat{a}_6(I_{ds}\lambda_{dr} + I_{qs}\lambda_{qr})\tilde{a}_8 + 2\hat{a}_6(V_{ds}\lambda_{dr} + V_{qs}\lambda_{qr})\hat{a}_5 \\
&- 4\hat{a}_6\lambda_{dr}\lambda_{qr}\omega_r\tilde{a}_4 + 2\hat{a}_6\lambda_{dr}\lambda_{qr}\omega_s\tilde{a}_4 + 2\hat{a}_6\lambda_{dr}V_{ds}\tilde{a}_5 + 2\hat{a}_6\lambda_{qr}V_{qs}\tilde{a}_5] \\
&+ [-\hat{a}_4\hat{a}_7\lambda_{qr}^2\omega_s - \hat{a}_7\hat{a}_7\lambda_{qr}V_{ds} + \hat{a}_5\hat{a}_7\lambda_{dr}V_{qs}] \\
\dot{\hat{z}}_3 =& \hat{a}_7 I_{qs}\lambda_{dr} - \hat{a}_7 I_{ds}\lambda_{qr} - \hat{a}_2 + \tilde{a}_7 I_{qs}\lambda_{dr} - \tilde{a}_7 I_{ds}\lambda_{qr} - \tilde{a}_2 \\
\dot{\hat{z}}_4 =& [\hat{a}_1\hat{a}_7 I_{qs}\lambda_{dr} - \hat{a}_7\hat{a}_4\omega_r\lambda_{dr}^2 + \hat{a}_7\hat{a}_8 I_{qs}\lambda_{dr} - \hat{a}_7\omega_r I_{qs}\lambda_{qr} - \hat{a}_1\hat{a}_7 I_{ds}\lambda_{qr} \\
&+ \hat{a}_4\hat{a}_7\omega_r\lambda_{qr}^2 - \hat{a}_7\hat{a}_8 I_{ds}\lambda_{qr} - \hat{a}_7\omega_r I_{ds}\lambda_{dr}] \\
&+ [I_{qs}\lambda_{dr}\dot{\hat{a}}_7 - I_{ds}\lambda_{qr}\dot{\hat{a}}_7 - \dot{\hat{a}}_2] \\
&+ [\hat{a}_7 I_{qs}\lambda_{dr}\tilde{a}_1 - \hat{a}_7\omega_r\lambda_{dr}^2\tilde{a}_4 + \hat{a}_7\lambda_{dr}V_{qs}\tilde{a}_5 + \hat{a}_7 I_{qs}\lambda_{dr}\tilde{a}_8 - \hat{a}_7 I_{ds}\lambda_{qr}\tilde{a}_1 \\
&- \hat{a}_7\lambda_{qr}^2\omega_s\tilde{a}_4 + \hat{a}_7\omega_r\lambda_{qr}^2\tilde{a}_4 - \hat{a}_7\lambda_{qr}V_{ds}\tilde{a}_5 - \hat{a}_7 I_{ds}\lambda_{qr}\tilde{a}_8] \\
&+ [\hat{a}_5\hat{a}_7\lambda_{dr}V_{qs} - \hat{a}_5\hat{a}_7\lambda_{qr}V_{ds} - \hat{a}_4\hat{a}_7\lambda_{qr}^2\omega_s] \\
\dot{\hat{z}}_5 =& [\hat{a}_8\lambda_{qr} + \omega_r\lambda_{dr} + \hat{a}_6 I_{qs}] + [\tilde{a}_8\lambda_{qr} + \tilde{a}_6 I_{qs} - \lambda_{dr}\omega_s]
\end{aligned}
\tag{6.1}
$$

The above equations can be written in a form that separates the input-output linearization and adaptive control shown in equation (6.2).

$$
\begin{aligned}
\dot{\hat{z}}_1 =& f_{z_1}(x,\hat{a}) + g_{z_1}(x,\hat{a},u) + \Omega_{z_1}(x,\dot{\hat{a}}) + \Psi_{z_1}(x,\tilde{a}) \\
& f_{z_1} = \hat{z}_2 \\
& g_{z_1}(x,\hat{a},u) = 0 \\
& \Omega_{z_1}(x,\dot{\hat{a}}) = 0 \\
& \Psi_{z_1}(x,\tilde{a}) = 2(\lambda_{dr}^2 + \lambda_{qr}^2)\tilde{a}_8 + 2(I_{ds}\lambda_{dr} + I_{qs}\lambda_{qr})\tilde{a}_6 \\
\dot{\hat{z}}_2 =& f_{z_2}(x,\hat{a}) + g_{z_2}(x,\hat{a},u) + \Omega_{z_2}(x,\dot{\hat{a}}) + \Psi_{z_2}(x,\tilde{a}) \\
& f_{z_2}(x,\hat{a}) = 4\hat{a}_8^2(\lambda_{dr}^2 + \lambda_{qr}^2) + 2\hat{a}_3\hat{a}_6(\lambda_{dr}^2 + \lambda_{qr}^2) + 6\hat{a}_6\hat{a}_8(I_{ds}\lambda_{dr} + I_{qs}\lambda_{qr}) \\
& \quad + 2\hat{a}_1\hat{a}_6(I_{ds}\lambda_{dr} + I_{qs}\lambda_{qr}) + 2\hat{a}_6^2 I_{ds}^2 + 2\hat{a}_6^2 I_{qs}^2 + 2\hat{a}_6 I_{qs}\omega_r\lambda_{dr} \\
& \quad - 2\hat{a}_6 I_{ds}\omega_r\lambda_{qr} - 4\hat{a}_4\hat{a}_6\omega_r\lambda_{dr}\lambda_{qr} \\
& g_{z_2}(x,\hat{a},u) = 2\hat{a}_6\hat{a}_4\lambda_{dr}\lambda_{qr}\omega_s + 2\hat{a}_6\hat{a}_5\lambda_{dr}V_{ds} + 2\hat{a}_6\hat{a}_5\lambda_{dr}V_{qs} \\
& \Omega_{z_2}(x,\dot{\hat{a}}) = 2(\lambda_{dr}^2 + \lambda_{qr}^2)\dot{\hat{a}}_8 + 2(I_{ds}\lambda_{dr} + I_{qs}\lambda_{qr})\dot{\hat{a}}_6 \\
& \Psi_{z_2}(x,\tilde{a}) = 4\hat{a}_8(\lambda_{dr}^2 + \lambda_{qr}^2)\tilde{a}_8 + 4\hat{a}_8(I_{ds}\lambda_{dr} + I_{qs}\lambda_{qr})\tilde{a}_6 \\
& \quad + 2\hat{a}_6(I_{ds}\lambda_{dr} + I_{qs}\lambda_{qr})\tilde{a}_1 + 2\hat{a}_6(\lambda_{dr}^2 + \lambda_{qr}^2)\tilde{a}_3 \\
& \quad + 2\hat{a}_6(I_{ds}^2 + I_{qs}^2)\tilde{a}_6 + 2\hat{a}_6(I_{ds}\lambda_{dr} + I_{qs}\lambda_{qr})\tilde{a}_8 \\
& \quad - 4\hat{a}_6\lambda_{dr}\lambda_{qr}\omega_r\tilde{a}_4 + 2\hat{a}_6\lambda_{dr}\lambda_{qr}\omega_s\tilde{a}_4 + 2\hat{a}_6\lambda_{dr}V_{ds}\tilde{a}_5 + 2\hat{a}_6\lambda_{qr}V_{qs}\tilde{a}_5 \\
\dot{\hat{z}}_3 =& f_{z_3}(x,\hat{a}) + g_{z_3}(x,\hat{a},u) + \Omega_{z_3}(x,\dot{\hat{a}}) + \Psi_{z_3}(x,\tilde{a}) \\
& f_{z_3}(x,\hat{a}) = \hat{z}_4 \\
& g_{z_3}(x,\hat{a},u) = 0 \\
& \Omega_{z_3}(x,\dot{\hat{a}}) = 0 \\
& \Psi_{z_3}(x,\tilde{a}) = \tilde{a}_7 I_{qs}\lambda_{dr} - \tilde{a}_7 I_{ds}\lambda_{qr} - \tilde{a}_2 \\
\dot{\hat{z}}_4 =& f_{z_4}(x,\hat{a}) + g_{z_4}(x,\hat{a},u) + \Omega_{z_4}(x,\dot{\hat{a}}) + \Psi_{z_4}(x,\tilde{a}) \\
& f_{z_4}(x,\hat{a}) = \hat{a}_1\hat{a}_7 I_{qs}\lambda_{dr} - \hat{a}_7\hat{a}_4\omega_r\lambda_{dr}^2 + \hat{a}_7\hat{a}_8 I_{qs}\lambda_{dr} - \hat{a}_7\omega_r I_{qs}\lambda_{qr} - \hat{a}_1\hat{a}_7 I_{ds}\lambda_{qr} \\
& \quad + \hat{a}_4\hat{a}_7\omega_r\lambda_{qr}^2 - \hat{a}_7\hat{a}_8 I_{ds}\lambda_{qr} - \hat{a}_7\omega_r I_{ds}\lambda_{dr} \\
& g_{z_4}(x,\hat{a},u) = \hat{a}_5\hat{a}_7\lambda_{dr}V_{qs} - \hat{a}_5\hat{a}_7\lambda_{qr}V_{ds} - \hat{a}_4\hat{a}_7\lambda_{qr}^2\omega_s \\
& \Omega_{z_4}(x,\dot{\hat{a}}) = I_{qs}\lambda_{dr}\dot{\hat{a}}_7 - I_{ds}\lambda_{qr}\dot{\hat{a}}_7 - \dot{\hat{a}}_2 \\
& \Psi_{z_4}(x,\tilde{a}) = \hat{a}_7 I_{qs}\lambda_{dr}\tilde{a}_1 - \hat{a}_7\omega_r\lambda_{dr}^2\tilde{a}_4 + \hat{a}_7\lambda_{dr}V_{qs}\tilde{a}_5 + \hat{a}_7 I_{qs}\lambda_{dr}\tilde{a}_8 - \hat{a}_7 I_{ds}\lambda_{qr}\tilde{a}_1 \\
& \quad - \hat{a}_7\lambda_{qr}^2\omega_s\tilde{a}_4 + \hat{a}_7\omega_r\lambda_{qr}^2\tilde{a}_4 - \hat{a}_7\lambda_{qr}V_{ds}\tilde{a}_5 - \hat{a}_7 I_{ds}\lambda_{qr}\tilde{a}_8 \\
\dot{\hat{z}}_5 =& f_{z_5}(x,\hat{a}) + g_{z_5}(x,\hat{a},u) + \Omega_{z_5}(x,\dot{\hat{a}}) + \Psi_{z_5}(x,\tilde{a}) \\
& f_{z_5}(x,\hat{a}) = \hat{a}_8\lambda_{qr} + \omega_r\lambda_{dr} + \hat{a}_6 I_{qs} \\
& g_{z_5}(x,\hat{a},u) = -\lambda_{dr}\omega_s \\
& \Omega_{z_5}(x,\dot{\hat{a}}) = 0 \\
& \Psi_{z_5}(x,\tilde{a}) = \tilde{a}_8\lambda_{qr} + \tilde{a}_6 I_{qs}
\end{aligned}
\tag{6.2}
$$